Home based formulation of personalised medicines by means of inkjet printing technique

Nikolaos Scoutaris, MSc

Thesis submitted to the University of Nottingham for the degree of Doctor of Philosophy

September 2010

Acknowledgments

There are a lot of people I would like to thank. However, I am really grateful to my supervisors Prof. Clive Roberts and Prof. Morgan Alexander and Dr. Paul Gellert without their patience and encouragement, the thesis would not have finished and my family without their efforts this thesis would not have started.

Also, special thanks to Dr. Chen for his help with AFM, NTA and SThM and Dr. Andrew Hook for preparing for me the microarrays samples.

Finally, I would like to thank AstraZeneca and EPSRC for funding and LBSA group in general for the professional and well equipped environment they provide.

Abstract

The potential application of inkjet printing technology to produce precisely dosage care is demonstrated in this thesis. Inkjet printing technology as it offers the opportunity to deliver quantities with high accuracy can produce medicines tailored for each patient.

The viability of this method was first demonstrated by using Felodipine as an active pharmaceutical ingredient polyvinyl pirrolidone (PVP) as an excipient. Felodipine is an antihypertensive drug which is poorly soluble in water and PVP is a highly soluble polymer commonly used to improve drugs' bioavailability. These were dissolved at various ratios in a mixture of ethanol and DMSO (95/5). Using a piezoelectric driven dispenser, picolitre size droplets of the solutions were dispensed onto suitable hydrophobic substrates. The dried products were characterized using AFM, localized nano-thermal analysis and high resolution vibrational spectroscopy (ATR-IR and Raman). Results indicate intimate mixing of the micro-dot API and excipient mixtures. Specifically, ATR-IR confirmed the interaction of felodipine and PVP by means of hydrogen bonding. Nanothermal analysis indicates a single glass transition point which is lowered as the API concentration increases. Finally, confocal Raman microscopy mapping on single droplets allows the visualization of the homogeneous distribution of the drug.

Also, capozide has been used as a model therapeutic system which could be produced rapidly as a viable formulation using the inkjet printing technology. Capozide consists of captopril, an angiotensin converting enzyme (ACE) inhibitor and hydrochlorothiazide, a thiazide diuretic drug, in varying ratios. These active pharmaceutical ingredients (APIs) and poly(lactic-co-glycolic acid) (PLGA) were dissolved in appropriate solvents and using a piezoelectric driven dispenser and pipetting, picolitre and microlitre size droplets respectively were deposited onto hydrophobic coated glass slides. Captopril and PLGA were dissolved in chloroform, ethanol and DMSO (75/18/7). Hydrochlorothiazide (HCT) and PLGA were dissolved in acetone and DMSO (93/7). The dried products where characterised using AFM and

high resolution Raman microscopy. The results showed that both capropril and HCT are phase separated with the PLGA. Also, the dissolution profiles of the final products were measured using HPLC where it has been shown that PLGA can control the release of the drug from the formulation. These results are a promising first step to produce pharmaceutical by means of inkjet printing.

Abbreviations

3DP	three dimensional printing
ADE	Acoustic Droplet Ejection
AFM	Atomic Force Microscopy
API	Active Pharmaceutical Ingredient
ATR	Attenuated Total Reflectance
CAP	Captopril
CCD	Charge Couple Device
CRDDS	Controlled Release Drug Delivery Systems
CRM	Con-Focal Raman Microscopy
DCLS	Direct Classical Least Squares
DMA	Dynamic Mechanical Analysis
DMSO	Dimethyl Sulfoxide
DNA	Deoxyribonucleic acid
DSC	Differential Scanning Calorimetry
HCT	Hydrochlorothiazide
HPC	hydroxylpropyl cellulose
HPMC	hydroxypropyl methyl cellulose
HPMCP	hydroxylpropyl methyl cellulose phthalate
LED	Light-emitting diode
LTA	Localised Thermal Analysis
MCR	Multivariate Curve Analysis
NTA	Nanothermal Analysis
OSSM	oily semisolid matrix
PC	Principal Component
PCA	Principal Component Analysis
PCL	poly(e-caprolactone)
PE	polyethylene
PEG	Polyethylene Glycol
PET	polyethylenetelephalate
PLGA	poly(lactic-co-glycolic acid)
PLS	Partial Least Square
PVA	Polyvinyl alcohol
PVP	Polyvinypirrolidone
SCC	squamous cell carcinoma
SThM	Scanning Thermal Microscopy
T_g	Glass transition temperature
TMA	Thermo Mechanical Analysis

Contents

Figures

1. Introduction

1.1 Current trends in oral dosage drug formulation production

Nowadays the most popular drug delivery systems are tablets and intravenous solutions. The advantages that they can offer are the greater stability, pain avoidance, versatility, patient compliance accurate dosage and easy production [1-2].

Tablets are compressed powders. The main aim of these compressed powders is to be easily dissolved in the gastrointestinal tract and aid in the complete absorption of API. The tablet manufacture process can be classified as granulation (wet and dry) and direct compression. Direct compression is the term used to define the process where powder blends of the drug substance and excipients are compressed on a tablet machine. There is no mechanical treatment of the powder apart from a mixing process. Granulation is a generic term for particle enlargement, whereby powders are formed into permanent aggregates. In granulation, the particles are agglomerated to improve the flow, density and compressibility of particulate material by size enlargement. The agglomeration can be achieved by using a dry binder (dry granulation) or a binder solution (wet granulation) which stick the individual particles together.

More specifically in dry granulation, the powder blends are compacted through roller or slugging compactions. Slugging involves the manufacture of a large compressed tablet, whereas roller compaction pushes powder blends through two counter-rotating rolls, producing a sheet of agglomerated material [3-4]. The main advantage of dry granulation is that the powders are not exposed to moisture and dry process. However, the applied mechanical stresses during processing may lead to phase

transformation via the solid-state or melt mechanisms [5]. Also, the tablets produced when materials possess a low bulk density may be too thin after compression. Finally, dry granulation is not suited for poorly flowing drug compounds [2].

Wet granulation provides better control of drug content uniformity at low drug concentrations, as well as control of product bulk density and ultimately compactibility (brittle fracture), even for high drug contents. Wet granulation involves two types of processing; fluid bed granulators or high-shear mixers. Wet granulation typically involves wet massing a blend of API and excipients in a wet granulator followed by subsequent sieving and finally drying [3-4]. However, during wet granulation process different crystalline polymorphs of the API can be formed [6-7]. Other limitations of wet granulation are the expensive equipment and the solvent recovery when it is not used as water as a solvent.

In direct compression the powder blends of APIs and excipients are compressed on a tablet machine. The advantages over the granulation process are the lower cost as it is much simpler not requiring many operations granulations. However, the inherent physical properties of the individual filler materials are highly critical, and minor variations can alter flow and compression characteristics, so as to make them unsuitable for direct compression [3-4]. Armstrong described the requirements for direct compression fillers which must have good flow properties, possess good compaction properties, have appropriate particle size to avoid segregation and have high bulk density [8]. Various excipients are available now that allow tablet production without granulation process intervenes such as microcrystalline cellulose, starch 1500 and lactose [2].

From all the above it is clear that the first choice as a tablet manufacture method is the direct compression due to its low cost. However, this method is not always applicable as it requires specific properties from the compounds and also it cannot be used for drug loading more than 30% [4]. Hence, the manufacture part of a formulation requires a considerable amount of cost and time. Consequently, a simpler generic method to produce solid drug dosages would revolutionize the pharmaceutical industry. Inkjet printing is a well established method for transferring quantities with high accuracy and perfectly localised [9-11]. In this case, the active compound can be dissolved with excipients depending on the properties of the final

formulation product. By implementing, inkjet printing in drug formulation many of the excipients required in manufacture such as lubricants, binders, fillers etc. will not be necessary. Also, properties of the compounds that affect the tablet's properties such as compactability, bulk density, particle size, melting points cannot be considered as the most important properties will be taken into account are the solubility of the compounds and the viscosity of the solution that will occur. A more thorough analysis of inkjet printing is represented in chapter 1.5.

1.2 Stability in drug formulations

One of the major concerns in pharmaceutical industry is the long term stability of the formulation product. There have been drugs with the best therapeutic properties but failed to come to the market due to lack of physical and chemical stability. For instance ritonavir was marketed by Abbott in 1996, however two years later lots of capsules failed the dissolution experiments due to the formation of another polymorph of the drug [12]. The main factors that affect the stability of product are heat, humidity, oxidation and light.

Humidity can have a significant effect on solid drug substances or drug products. First of all, humidity can alter the adhesion properties of API with excipient. Price *et al.* found that the adhesion interactions between lactose and drug probes of salbutamol sulphate and budesonide were shown to be significantly increased with each incremental rise in humidity. This could result to a reduction of the dispersion and deaggregation properties of a DPI formulation, influencing the aerolisation efficiency and therapeutic efficacy of the irrespirable drugs to the respiratory tract [13]. Also, uptake of moisture can have a plasticization effect to any of the compounds in the formulation reducing the glass transition temperature [14]. For instance, the glass transition temperature of sucrose can range between 60 – 75°C depending on the water uptake from each sample [15]. The high mobility that molecules have on glass transition temperature can lead to crystallization of the product which in turn can affect dramatically the therapeutic properties of the drug.

Hydrolysis is a common phenomenon that happens to pharmaceuticals. This happens when the compound comes into contact with water. Hydrolysis is often the main degradation pathway for drug substances having ester and amide functional groups within their structure [16]. Example can be hydrochlorothiazide, a drug substance with excellent solid-state stability, can undergo hydrolysis to form formaldehyde and 4-amino-6-chloro-1,3-benzenedisulphonamide. Desai *et al.* have shown that the inclusion of povidone K-30 NF (PVP) as binder and poloxamer 188 NF (Pluronic F68) as a wetting agent significantly increases drug hydrolysis during storage [17].

Oxidation is a well-known degradation pathway for pharmaceuticals. Compounds can be oxidised by the atmospheric oxygen. Hydrocortisone, meth-otrexate, adinazolam, hydroxyl group directly bonded to an aromatic ring (eg, phenol derivatives such as catecholamines and morphine), conjugated dienes (eg, vitamin A and unsaturated free fatty acids), heterocyclic aromatic rings are some of the compounds that can be subjected to oxidative degradation [16].

Light can also affect the stability of the formulation leading to changes in the physico-chemical properties of the product. Light-sensitive drugs can be affected either by sunlight (especially ultraviolet irradiation) or artificial light sources (e.g. fluorescent light). This may not only lead to photodegradation of the active pharmaceutical ingredient but also to a change in the physico-chemical properties of the product, e.g. the product becomes discolored or cloudy in appearance, a loss in viscosity or a change in dissolution rate is observed or a precipitate is formed [18].

From all the aforementioned it is clear that stability's investigation can be a big part of the research to bring a medicine to the market. Consequently, the ability to produce optimized formulations immediately prior to use can be the key to address the huge amount of research to achieve the long term formulation stability. Inkjet printing has the potential to produce precise amount of medicine which are preordained for instant consumption. A controller connected with the patient's personal doctor, can control the delivery of one or more drugs and/or change the drug regimens in response to a changing in medical conditions of the patient. The formulation can be prepared directly and consumed instantly.

1.3 Poorly soluble drugs; challenges and prospects

Solubility is one of the most important factors that influence bioavailability of the drugs. The drug is first released from the formulation and through the gastrointestinal wall, it is transferred to the circulation system [19].

Various approaches have been used to improve solubility and enhance the dissolution rate of poorly soluble drugs involving both physical and chemical modification [20]. The physical modification aims to increase the surface area and wettability of the API. This approach focuses on particle size reduction [21] and the generation of amorphous state [22]. The particle size reduction by milling aims at increasing the surface area of the particles and thus increasing the solubility. This technique has been applied to a variety of poorly soluble drugs [23-26]. Other approaches to increase the solubility involves the solubilization with surfactants and complexation with cyclodextrins [27].

One of the most promising strategies to increase the solubility of the drug is the dispersion of it into a hydrophilic inert polymer matrix. The two major methods to produce solid dispersion products are the melting and the solvent evaporation method. The melting process was first applied by Sekiguchi and Obi when they found that the administration of a fused mixture of the poorly water-soluble drug sulphathiazole and the water-soluble carrier urea produced an enhanced absorption of the drug in rabbits [28]. In the melting method the active compounds are suspended in a previously melted carrier with subsequently cooling and solidify the mixture. The main disadvantage of this method is the degradation of the drug or the carrier can be caused by the heat [29].

The solvent evaporation method consists of the solubilisation of the drug and a polymer into a volatile solvent that is later evaporated. The final product will be an amorphous carrier in which the drug is molecularly distributed. This type of solid solution will be homogenous. Also, the product can be an amorphous carrier where the drug is dispersed in the form of amorphous clusters. This type is not homogenous on a molecular level and consists of two phases [20]. The most common polymers have been used are Polyvinyl Pyrrolidone (PVP) [30], Polyethylene Glycols (PEGs) [30-31], Polyvinyl Alcohol (PVA) [32] and cellulose derivatives such as HydroxyPropyl

Methylcellulose (HPMC) [30] and HydroxyPropylCellulose (HPC) [33]. Common characteristics of these polymers are that they are water soluble, soluble in most common organic solvents and they can interact with API by forming bonds such as hydrogen bonding.

Despite the growing interest of solid dispersion, its commercial value is still limited. The main reason for this is the poor stability. The physical instability of the product can come from the recrystallization of the API. However, different polymers, which are used to solid dispersion, have been shown that inhibit the crystallization of the drug [34]. In particular PVP has been found to have significance inhibitory effects of the drugs crystallization [35-38]. The mechanism of inhibition of PVP involves the antiplasticising effect of PVP as well as specific interaction with the API [37]. However due to their chemistry and polarity, these polymers are highly hygroscopic which by absorbing water can promote the crystallization [22] which in turn can causes phase separation. For instance, Rumodor *et al* by investigating the phase behaviour of amorphous solid dispersions found that although the drug and the polymer were completely miscible immediately after the manufacture, they exhibited phase separation during storage and in elevated humidity [39]. Additionally, changes in the dissolution rate during storage have been observed [40-41].

Other issues which limits the commercial application of solid dispersion are referred by Serajuddin [29] and these can involve any residual solvent that can not be removed from the solid dispersions, the scale up of the manufacturing process, and the dosage form development. The manufacture issues come from that the texture of the product is soft and tacky and therefore difficult to pulverize. Other issues are the poor flow, mixing properties of powders and poor compressibility.

Inkjet printing can be the key technology to overcome the aforementioned issues and the solid dispersion technology becomes a commercial reality. In inkjet printing, as in the solvent evaporation method, both the API and the excipients will be dissolved in an appropriate solvent. The solvent will be evaporated leaving the product onto an appropriate substrate. As it was mentioned in the previous section, inkjet printing is preordained to produce drug for instant consumption and hence the long term stability is not necessary. An application of this is represented in chapter 3

where the poorly soluble felodipine dissolves with PVP in ethanol and ejected using an inkjet printer. However, it is worth mentioning that the compounds must remain stable when they are dissolved in the solvents before they are sprayed. Also, the phenomenon of polymorphism must be taken into account as depending on the solvent used different crystalline forms of the API can be grown [42]

1.4 Technologies in Controlled drug delivery systems

Conventional dosage forms are not able to control the rate of drug delivery or the target area and provide an immediate of drug release. As a result, drug concentration in the blood and tissue fluctuates widely. In controlled release drug dosage forms (CRDDS), the drug is at maintained the necessary therapeutic levels with narrow fluctuations reducing the frequency of drug administration and improving the treatment efficiency (Figure 1.1).

Generally, natural and synthetic polymers are used as the structural backbone for controlled release drug delivery system. Among all, the CRDDS the monolithic matrix is the simplest and least expensive used. The polymer is homogenously distributed with the drug by blending the drug with the polymer and then molding, extruding, or casting them together. The dissolution profile of the drug from the polymer matrix can follow various mathematical models [43-44]. For instance pharmaceutical dosage forms which contains water soluble drugs in porous matrices for which the Fick's low governs the release of the drug, follow the first order mathematical model [44].

The disadvantage of this diffusion controlled system is the decreasing amount of the drug with time. Therefore, various approaches employing release mechanisms other than diffusion control have been developed to achieve constant release rates in polymer matrix devices, for example, swelling controlled delivery systems based on hydrogels [45-47], erosion polymers [48] and osmotic pressure pumps .

Hydrogels are three-dimensional crosslinked polymeric structures that are able to swell in an aqueous environment. During the dissolution of the hydrogel two phenomena take place; swelling and true dissolution of the polymer. In the early stage of drug delivery, matrix thickness increases due to polymer swelling. The

successive polymeric chain disentanglement (true polymer dissolution), and the dissolution of the drug or fillers used, counteracts this increase in thickness, producing a diminution of the volume of the matrix. Finally, the matrix disappears when all the polymer is swollen [45]. Examples of polymers are used as hydrogels are ethylene glycol dimethacrylate, Methoxyethoxyethyl methacrylate, Methacrylic acid etc. All the common polymers are mentioned in the excellent review of Hamidi *et al.* [46].

In terms of polymer erosion, there are two mechanisms can be identified; surface and bulk erosion. Bulk erosion occurs when water molecules are able to permeate into the bulk of the polymer matrix at a quicker rate than erosion. The surface erosion occurs when the polymer degradation is much faster than the water intrusion (Figure 1.2). Polyanhydrides are examples of bulk erosion materials whereas poly(lactide) and poly(lactide-co-glycolide) are surface erosion materials [48-49].

Osmotic systems utilize the principle of osmotic pressure to deliver drugs. When the dosage form comes into contact with water, imbibes water at a rate dependent on the fluid permeability of the membrane and osmotic pressure of the core formulation. This osmotic imbibition of the water causes a saturated drug inside the core which is dispensed at a controlled rate (Figure 1.3) [50]. Various types of osmotic pumps are in the market nowadays [51].

A final approach can be applied to control the drug release is the utilization of polymers as film coatings. Different types of polymers can be used as coatings. For instance cellulose derivatives, poly(vinyl acetates) and polymethacrylates. Also, blends of enteric and gastro-intestinal-tract (GIT)-insoluble polymers are particularly interesting for the coating of solid dosage forms, being able to provide large ranges of drug release profiles at low as well as at high pH [52]. Hence, as ethyl cellulose is poorly permeable from the drugs, it is usually added with PEG [53], PVP [54], and hydrophilic cellulose ethers [55-56]. These hydrophilic additives are dissolved and leach out from the polymeric membranes resulting in a more permeable films and increased drug release rates.

Apart from the polymer coating technology systems, matrix systems made of swellable and non swellable polymers and osmotically controlled devices discussed

above, more sophisticated CRDDS are still being developed. These systems are based on microparticulate systems which involves polymeric biodegradable nanoparticles which aim at the uptake the drug particles intact. This approach is promising in the case of delivering peptides and other macromolecules which normally cannot be administered orally [57-58].

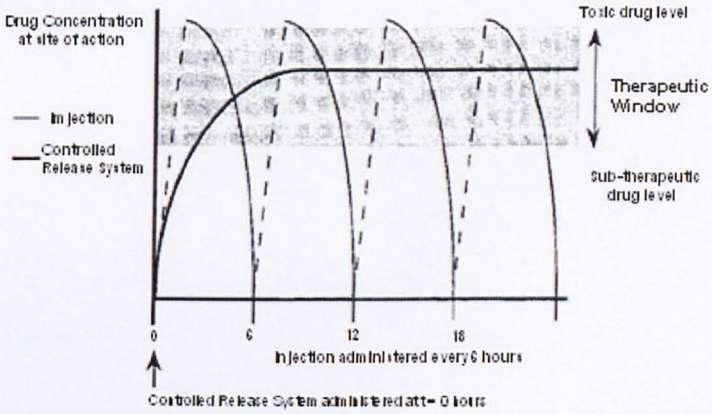

Figure 1.1: Drug concentration at the site of therapeutic action after delivery as a conventional injection (thin line) and as a temporal controlled release system (bold line) [49].

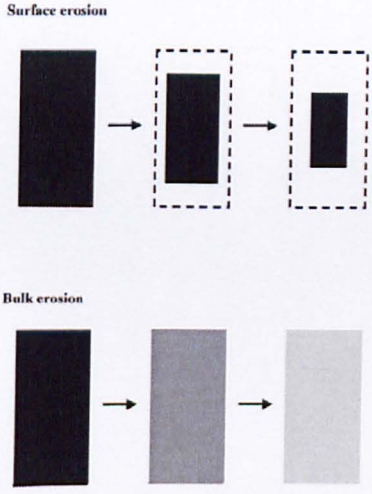

Figure 1.2: schematic illustration of surface and bulk erosion [48].

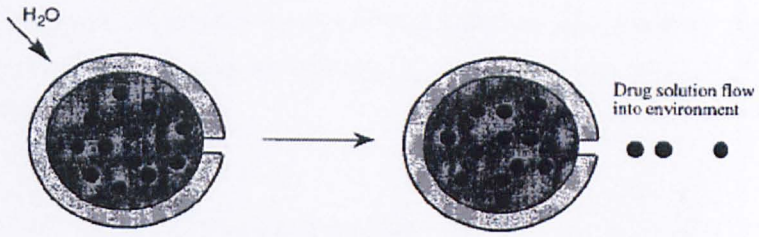

Figure 1.3: Schematic diagram of the drug release due to the osmotic gradient [49].

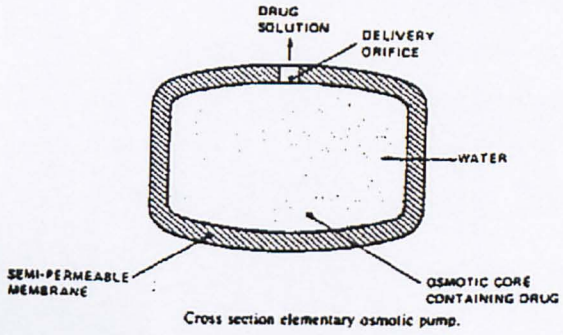

Figure 1.4: Schematic diagram of the osmotic drug controlled release systems [51].

1.5 Inkjet printing

1.5.1 Introduction

Inkjet printing can be defined as the deposition of functional materials in the form of a liquid onto a specific substrate. The most common application is the transfer of electronic data to paper. However, nowadays more and more applications demands of the accurate transferring materials with specific electrical, biological or optical properties on substrates. Inkjet printing is one of the most promising technologies on that matter [59-60]

The main advantage of this method is that it offers high accuracy and throughput of fluids. Nano or even pico quantities of materials can be transferred and perfectly localized. Also, the high uniformity and small size of the droplet generating renders this technique capable of producing precise micro features. Exploiting this capability, microelectromechanical systems (MEMS) has been improved by localized features

which were not possible by photolithography and also, transistor made by injected semiconductive organic thin film have been fabricated [61-62].

1.5.2 Inkjet printing technology

Inkjet printing is fundamentally divided into continuous and drop on demand mode. In continuous mode the liquid is pressurised to form a jet through a nozzle. By imposing a periodic perturbation, uniform droplets are formed (Figure 1.5). Continuous mode is used for high speed graphical applications such as textile printing and labelling. In drop on demand mode the liquid is held and pressurised creating a droplet only when needed (Figure 1.6) [63].

Depending on the technology implemented, inkjet printing is categorised into thermal, piezoelectric, electrostatic and acoustic inkjet. An excellent paper was published by Hue which describes each technology [64]. Thermal and piezoelectric are the most widespread technologies, whereas the latter ones are still in the development stages. In thermal inkjet, the ink is heated creating a rapid expanded vapour bubble which ejects from the nozzle. Depending on its configuration, a thermal ink-jet can be a roof-shooter (Figure 1.7a) with an orifice located on top of the heater, or a side-shooter (Figure 1.7b) with an orifice on a side located nearby the heater. The roof-shooter design is used in the printheads from Hewlett-Packard, Lexmark, and Olivetti. The side-shooter design is implemented in the Canon and Xerox printheads [64].

Piezoelectric dispensers rely on the deformation of a piezoelectric material. When voltage applied the piezo material changed its shape to a preordained direction, causing a sudden volume change creating pressure waves which results in a drop being ejected from the orifice. Depending on the deformation of the piezoelectric material, the technology can be classified into four main categories; squeeze mode where radially polarised tubes are used, bend and push mode design where the electric field is generated between the electrodes parallel to the polarization of the piezo electric material and finally shear mode where the electric field is perpendicular to the polarization of the piezoceramic (Figure 1.8) [9, 65-66].

In the electrostatic dispensers, an electric voltage is applied in the form of a signal between two electrodes. Due to the applied voltage, an intense electric field is generated between the two electrodes which induce the liquid meniscus at the interface. When this electrostatic force is greater than the surface tension at the liquid meniscus, the liquid breaks up and droplets are ejected (Figure 1.9) [67].

Acoustic droplet ejection (ADE) uses a pulse of ultrasound to move low volumes of fluids (typically nanoliters or picoliters) without any physical contact. This technology focuses acoustic energy into a fluid sample in order to eject picolitter size of droplets. The acoustic droplet ejection process (Figure 1.10) transfers nanoliter or picoliter droplets from a conventional flat-bottom microplate (A) using acoustic energy (B) from the transducer (C). The energy is focused on the surface of the liquid in the lower well, causing a droplet of precise volume to be ejected without any physical contact between the transducer and the liquid being dispensed [68].

The most important properties of liquid in dispensers that implement a piezoelectric response are viscosity, surface tension and density. These fluid properties influence the drop formation mechanism and subsequent drop size at a given voltage. Also, these properties can provide information about the impact of the droplet into the substrate. Schiaffino and Sonin classified the drop impact into four different regimes according to Weber ($We = \frac{\rho D U^2}{\sigma}$) and Ohnesorge ($Oh = \eta / \sqrt{D\rho\sigma}$) numbers, where ρ is the density of the liquid, D is the diameter of the drop before impact, U is the impact velocity, σ is surface tension, and η is the viscosity of the liquid. In regime I, where We >>1 and Oh <<1, kinetic energy dominant motion prevails, and fluid behaves almost like an in viscid fluid; in regime II, where We >> 1 and Oh >> 1, capillarity drives the motion of in viscid fluids; in regime III, where We << 1 and Oh >>1, capillary effect is dominant, and the viscosity of the fluid is important; finally, in regime IV, where We >>1 and Oh >> 1, kinetic energy dominates the capillarity, and the viscous force is also important [69]. Jang *et al* investigated the printability of the fluids by applying the inverse (Z) of the Ohnesorge number (Oh) which relates to the viscosity, surface tension, and density of the fluid. They have experimentally defined the printable range as $4 < Z < 14$ by considering characteristics such as single droplet formability, positional accuracy, and maximum allowable jetting frequency. This

range of Z corresponds to low viscosity fluid [70]. Yang *et al* showed that a smaller value of surface tension represents a weaker cohesive which leads to a slender liquid ligament with a relatively longer break up length. The shapes of the liquid and tail droplet tend to be round for the cases of high surface tension. It also takes more time for contraction of a spherical droplet for the liquid with lower surface tension [71].

Finally, the volume of the droplet is directly dependent on the voltage and the duration of the signal that is applied. Hence, the droplet velocity and volume are found to show a linear relation with driving voltage, but show a more complicated and periodic behaviour with changing frequency and pulse width. Derby *et al* showed that droplet velocity exhibits a maximum as a function of pulse width, which remains unchanged when driving voltage amplitude increased [72].

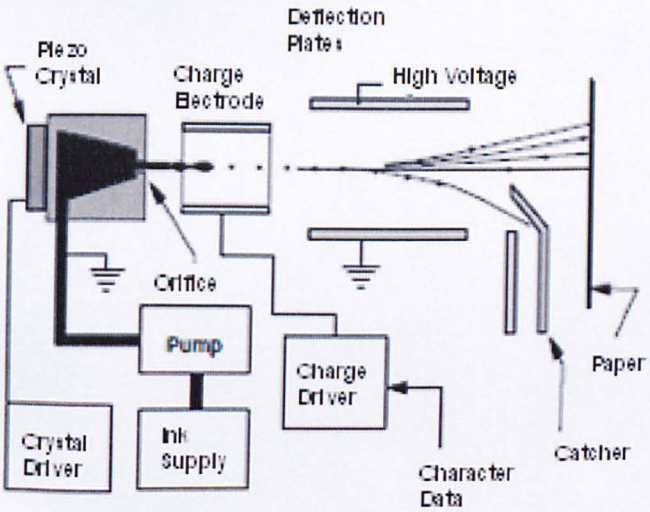

Figure 1.5: Schematic diagram of continuous inkjet printing system [9].

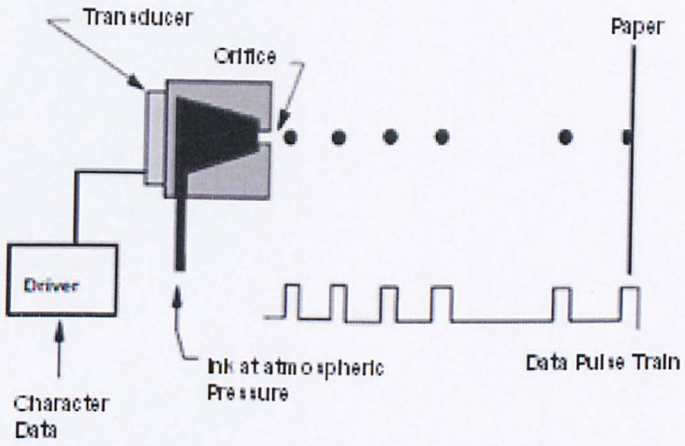

Figure 1.6: Schematic diagram of drop on demand inkjet printing system [9].

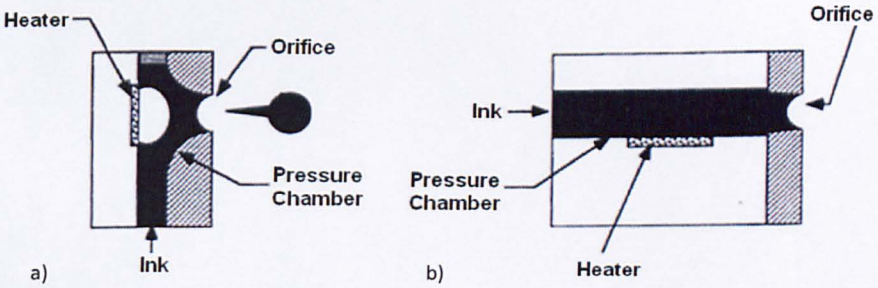

Figure 1.7: a) schematic diagram of a roof-shooter thermal inkjet dispenser b) a side shooter thermal inkjet dispenser [64].

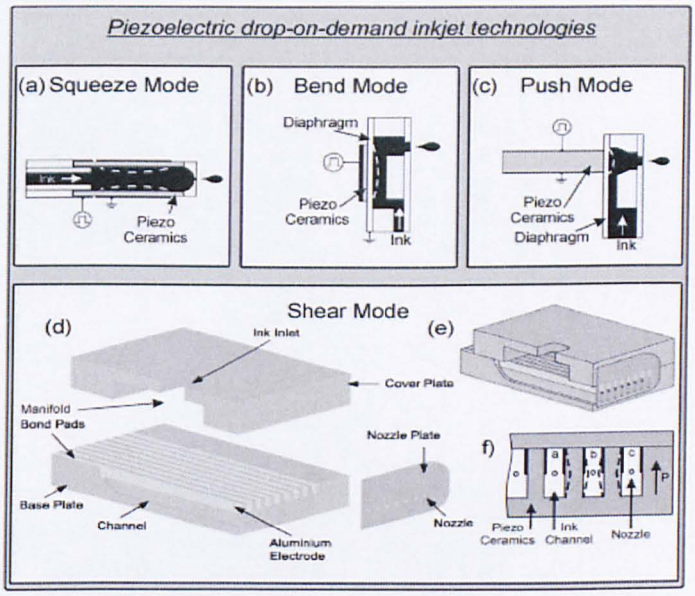

Figure 1.8: piezoelectric inkjet technologies [65]

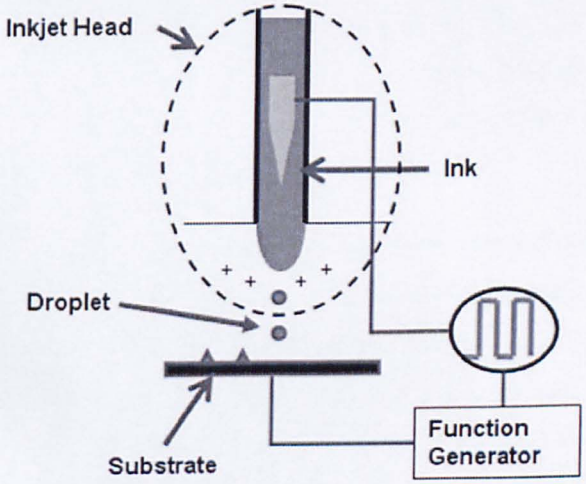

Figure 1.9: schematic diagram of electrostatic inkjet dispenser [67]

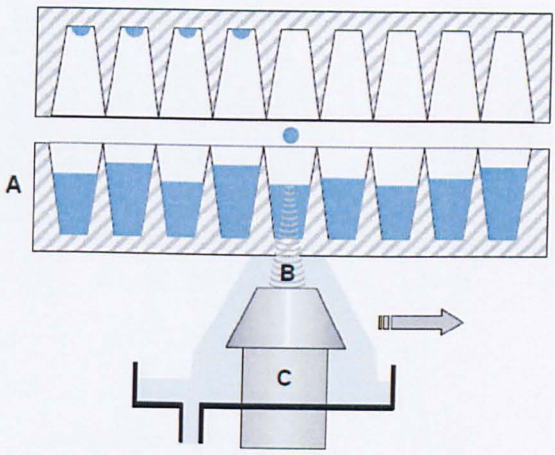

Figure 1.10: schematic diagram of acoustic drop on demand dispenser [68].

1.5.3 Inkjet Printing in life sciences

In life sciences inkjet printing has been proved a key technology. Compound synthesis, genomics, drug screening, drug delivery and biomaterials are some of the areas where this technique is or can be applied offering unique capabilities. All of these applications are driven by the desire to miniaturize process in order to achieve higher cost efficiencies and better detail.

In high throughput screening, higher density well plates have started being used to reduce reagent costs and to obtain more information from each plate run through the screening process. The first step in HTS is to transfer a small quantity of compound from the master plate to the assay plate. By applying microdispensing technology the compound can be transferred in well-plates in various concentrations even in nanolitters, avoiding the intermediate dilution step. After the assay is prepared, it is conducted by a series of reagent additions and incubations followed by a read-out of the results [10-11].

In genomics, the basic application involves the dispensing DNA or synthetic oligonucleotides onto substrates and probing for complementary base-pair binding. Yamamoto et al managed to fabricate DNA microarrays by means of a bubble jet ink device to eject oligonucleotides to a glass surface. In that case, the dispenser, ejecting pico litter solution, was able to achieve highly densed spots per cm^2. These

were screened with a fluorescently labeled synthetic 18-mer oligonucleotide derived from the *p53* gene, or segments of the *p53* gene that had been PCR amplified from genomic DNA of two cell lines of human oral squamous cell carcinoma (SCC). This allowed us to discriminate between matched hybrids and 1 bp-mismatched hybrids [73].

Apart from the well-established applications of inkjet printing in genomics and HTS, inkjet printing is a novel technique with respect to the biomaterial fabrication. An interesting study comes from the Barralet *et al* group. In this study, implants based on calcium 3D phosphate structures involving hydroxyapatite and brushite ceramics were printed by spraying calcium phosphates powders [74]. Also, for medical devices such as drug-containing stents, ink-jet technology due to the controllable and reproducible nature of the droplets in the jet stream and the ability to direct the stream to exact locations on the device surfaces can offer a boost to the cost of the procedure. Tarcha *et al* programmed target deliveries of 100 μg of drug, a typical dose for a small stent, into cuvettes which gave a standard deviation (SD) of dose of 0.6 μg. Jetting on coated, uncut stent tubes exhibited 100% capture efficiency with a 1.8 μg SD for a 137 μg dose. In preliminary studies, continuous jetting on stents can yield efficiencies up to 91% and coefficients of variation as low as 2%. These results indicate that ink-jet technology may provide significant improvement in drug loading efficiency over conventional coating methods [75].

1.5.4 Inkjet printing in drug formulation

Inkjet printing as a drug formulation method is a novel technique. To date, the literature concerning this issue is limited. Thermal inkjet technology has been utilized by the Hewlett Packard's laboratories to prepare solid dosage forms of drugs. This group promoted this method as an alternative technique for low water soluble active pharmaceutical ingredients (APIs). Therefore, they chose prednisolone as a test molecule due to its low solubility in water [76].

Inkjet printing has been applied as an alternative technique to fabricate therapeutic agents with the appropriate size and shape. By applying the current inkjet technology, amphiphiles, dissolved in ethanol solution, were sprayed into water forming small unilamellar vesicles with diameter 50-200 nm which can be used as

drugs' carriers. The group demonstrated this method as one that allows excellent control and reproducibility of particle size and shape, together with efficient encapsulation [77]. Furthermore, Radulescu *et al* by using inkjet technology and simple emulsion-solvent evaporation technique prepared PLGA microcapsules loaded with paclitaxel. Paclitaxel and PLGA were dissolved in DCM and sprayed in PVA solution. After the solvent removal, the product was PLGA spheres having encapsulated paclitaxel with 66.7% efficiency [78]. A similar work has been accomplished by Xie *et al*, where PLGA biodegradable nanoparticles produced to encapsulate protein based drug using a co-axial electrospray technique [79]. Moreover, Chan *et al* using inkjet printing technology, they deposited mixtures of ibuprofen and PEG 6000. Subsequently, by using ATR properly modified, they characterized the samples by investigating the distribution of ibuprofen in the mixture [80]. Finally, Kastra *el at* by using three dimensional printing technique (3DP), they prepared erosion mechanism delayed-release tablets with varying polymer content [81]. In 3DP technique, layers are created by adding layers of powders at the top of a piston using inkjet printing. The powder layers are selectively joined each other where the where the part is to be formed by 'ink-jet' printing of a binder material [82].

The benefits of inkjet printing in drug formulation can be various. As it was mentioned earlier, a drug formulation consists of the API and several other polymers which are used during the manufacture process. The implementation of inkjet printing in drug formulation will render these polymers unnecessary and a big part of the manufacture process avoidable.

Also, this technique has the potential to produce medicines for instant consumption. APIs along with the necessary excipients and the appropriate solvents can be sold and ejected through an inkjet printing device. At this point, it is worth mentioning that the consequently, long term stability issues will be avoided.

Another potential application of this technique deals with the recent advances in pharmacology. In the future, the therapy will be determined by the specific genotype for each patient. Hence, it is possible that each patient will be provided with his own cartridges of drug, to print each own drug with the right dosage.

1.6 Aims and objectives of thesis

So far the reader has been introduced to various issues that need to be overcome during the tablet manufacture. These can be related to the cost of manufacture due to the use of various excipients to give to the processed compounds the appropriate compressibility, stability and release profile and the long term stability studies must take place.

The aim of this thesis is to introduce inkjet printing as a novel drug formulations technique which could produce medicine preordained for instant consumption and hence avoiding any manufacture and stability issue. Also, since the inkjet printing technology offers high fluid delivery accuracy, a successful implementation of this technology can offer the ability to produced precise amounts of medicine, tailored to individual patients.

The feasibility and efficiency of inkjet printing to produce proper drug formulation product is investigated in this thesis by spraying various APIs with excipients and characterising them with micro- and nano- analytical methods.

Hence, in the third chapter, the nano-scale production of drug formulations by means of inkjet printing technology is described. The formulations consisted by felodipine and hydrochlorothiazide with PVP and Captopril with Hydrochorothiazide with PLGA in various ratios.

In Chapter 4, the release of the felodipine from the felodipine/PVP drug formulation produced by inkjet printing in microscale is investigated be means of confocal Raman microscopy.

Chapter 5 attempts to increase the production scale of felodipine/PVP drug formulation so that the felodipine to be in the therapeutic amount by producing a microarray of the formulation.

Finally, chapter 6 investigates the feasibility of inkjet printing to produce capozide as a model therapy. As Capozide tablet consists of captopril and HCT, inkjet printing can produce the tablet by preparing individual formulations of each API onto a single

substrate to consists a therapy. Also, the feasibility of PLGA to control the drug release from the formulation has been investigated.

2. Instrumentation

2.1 Pico-litre dispenser

The dispenser used in this thesis is a piezo-driven dispenser (GeSim, Germany) (Figure 2.1a) mounted on a Kruss Drop shape Analysis system (DSA 100, Kruss, Germany) (Figure 2.1d). The microdispenser was created from microstructured silicon and glass chips, tightly connected. The piezoelectric material is glued outside of the thin silicon wafer (Figure 2.1b). By applying a voltage, the piezoelectric material goes out of shape in a specific direction. This distortion is transferred to the solution causing the formation of a small droplet (Figure 2.1c).

The overall volume of the droplets is determined by the dispenser type (mainly by the size of the orifice). However, the droplet volume can be tuned by adjusting piezo parameters (amplitude, pulse width, excitation frequency); increasing amplitude or pulse duration will produce larger droplets.

Apart from the dispenser, the DSA system consists of a camera to record the droplet at the side, a mechanical stage which can move automatically in x- and y- directions accordingly and a light source (Figure 2.1d).

a)

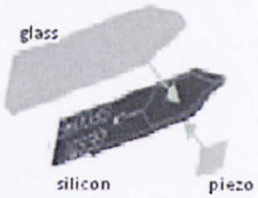

b)

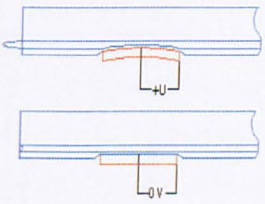

c)

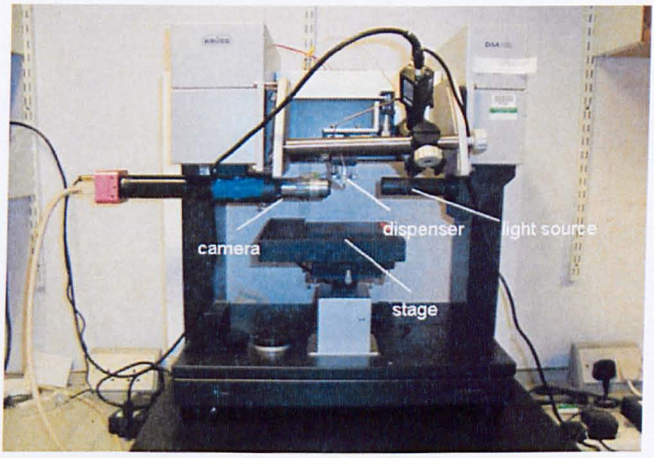

d)

Figure 2.1: a) Photo of the dispenser used in the experiments, b) schematic diagram of the piezoelectric dispenser manufacture c) schematic graph of the operation principle of piezo-driven dispenser d) DSA 100 system.

2.2 Micro array printer

A Scienion sciFLEXARRAYER piezo system (BioDot, Germany) was used in this work, is a non contact liquid handling and spotting system. The technology dispenses with a high dynamic volume range (picolitre to microlitre) and can accurately aspirate and dispense aqueous and organic solutions. Using the piezo-elements, spot volume can be changed as well as dispensing reagents on top of each other without contamination.

This configuration uses a solenoid nozzle that is synchronized with a positive displacement of the syringe to dispense drops at frequencies in the range of 20-1000

Hz to dispense non-contact drops on a continuous base. This quantitative non contact technology couples the BioDot "drop-on-demand" valve with a high resolution syringe pump to meter precise amounts of reagent.

The system consists of the liquid handling station, wash station, the dispenser and the dispense control system. The liquid handling station pumps the solution to the capillaries (nozzles) by a syringe pump using Teflon or PEEK tubes (Figure 2.2). The flow of the liquid system is controlled via the 3/2 way valve. For aspiration the valve is in the first position and the syringe pump is moving down. After taking up a certain volume the valve switches to position 3 to push the aspirated volume into the system liquid bottle. For flushing the tubes with the system liquid the valve switches to position 3 first and the syringe pump soaks up the system liquid. The valve is changed to position 2 and the syringe pumps the liquid out of the dispenser capillary.

The sample can be taken up by positioning the nozzle is in the sample solution, the 3/2 way valve is switched to position 2 and the syringe pump starts aspiration. After the required uptake volume is completed, the valve will be switched to position 3 and the syringe pump will move to the default position which is in the middle of the syringe. The uptake will be stopped by changing the valve to position 1 and lifting the nozzle above the sample solution.

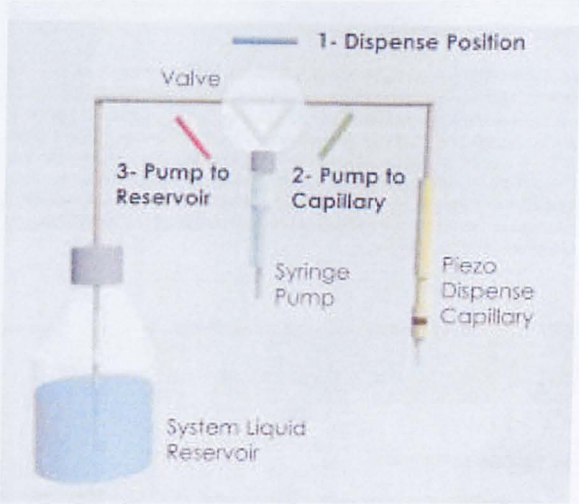

Figure 2.2: Schematic diagram of the liquid handling [83].

The wash station comprises one independent, chemically inert wash channel for each dispenser nozzle, supplied by a peristaltic pump using separate, chemically inert

tubes. The inside of the nozzle is automatically cleaned with the system liquid when flushed. The outside of the nozzle is additionally cleaned in the wash station via a wash command. During the wash, the piezoelectric elements ultrasonicate each dispense capillary individually, for maximum wash efficiency. The wash station is also served by a two channel peristaltic pumps. The wash solution is put in a large flask and a filter is placed before the uptake tube. This tube can be split into several tubes depending on the number of nozzles installed. After the wash procedure, the waste from all channels is combined in one single pass through the wash station and taken away by one wash out tube, connected to the waste container.

The dispense head can accommodate up to eight piezo dispense nozzles which each controlled individually. The dispense control station includes high resolution optical measurements, a stroboscopic LED for image illumination and a video camera. The camera is situated closed to the nozzle for visual inspection of the drop formation (Figure 2.3). The selected nozzle dispenses drops with its fixed frequency. The LED for image illumination is triggered by the piezo frequency, but it flashes at a user definable delay and hence the image can be captured at any point of the trajectory. This allows monitoring and optimization of drop size, drop velocity and drop trajectory.

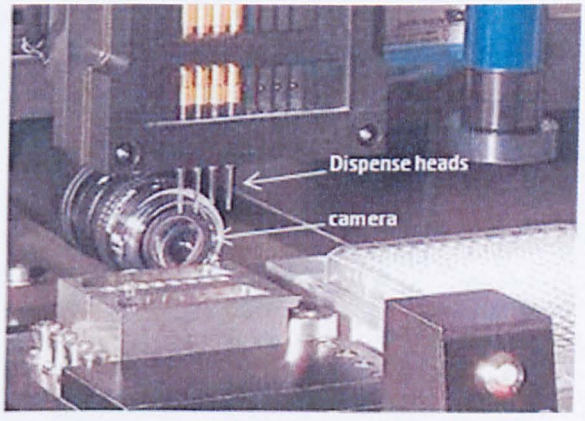

Figure 2.3: Photo of the dispense head and the camera [83].

The nozzle consists of a glass capillary with an outer diameter of 1 mm. This glass capillary is embedded into a piezo ceramic material, which is cemented onto the capillary. Most of the inner and outer surface of this piezo ceramic tube is an electrode to which a rectangular voltage pulse is applied. The ceramic contracts

while the voltage is applied initiating a pressure wave towards the glass capillary and towards the system liquid within the capillary.

The stage comprises two magnetic linear servo drives (Figure 2.4). A high resolution optical encoder continuously controls the motion of each driver.

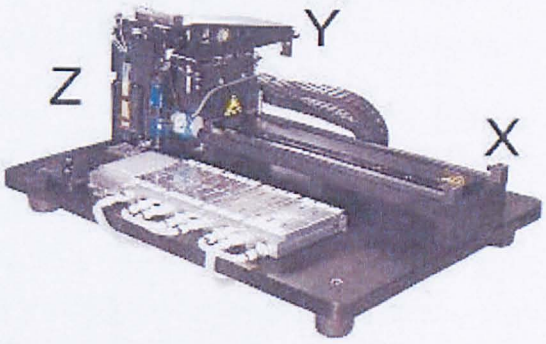

Figure 2.4: Photo of the stage showing translation axes [83].

2.3 Atomic Force Microscopy

AFM is an imaging and force measurment technique which can visualise surfaces to the micrometre and nanometre scale. Figure 2.5 illustrates a schematic diagram of an AFM. It consists of a sharp tip which is scanned over a surface with a feedback mechanisms that enables the piezo-electric scanners to maintain the tip at a constant force (to obtain height information), or height (to obtain force information) above the sample surface [84]. As the tip scans the surface of the sample, moving up and down with the contours of the surface, the laser beam is deflected off the attached cantilever into a quadrant element photodiode. The photodetector measures the difference in light intensities between the upper and lower photodetector quadrants to determine the degree of cantilever flexure. Feedback from the photodiode difference signal, through software control from the computer, enables the tip to be maintained at either a constant force or constant height above the sample. In the constant force mode the piezo-electric transducer monitors real time height deviation. In the constant height mode the deflection force on the sample is recorded. The latter mode of operation requires calibration parameters of the scanning tip to be inserted in the sensitivity of the AFM head during force calibration of the microscope.

AFM can obtain topographical images in either contact mode (as described) or in tapping mode. In tapping mode the cantilever oscillates at its resonant frequency making intermittent contact with the surface. As the oscillating cantilever contacts the surface, the cantilever oscillation is necessarily reduced due to energy loss caused by the tip to the surface. The reduction in oscillation amplitude is used to identify and measure surface features. Typically, tapping mode is operated in a constant amplitude mode, whereby the feedback signal controls the height of the cantilever to maintain a constant user-set amplitude [85-86].

Apart from topographical information, AFM can provide details on the local compositions of the sample. There are many modes that can be used to achieve this [87-89], but the most common is to monitor the phase shift of the oscillating cantilever in tapping mode [90]. Such 'Phase imaging' can be used to detect nanoscale variation in composition, adhesion, friction, viscoelasticity, and other properties of the materials [86, 91]. Changes in the phase lag often indicate changes in the properties of the sample surface. Phase imaging has been proved an extremely useful tool for pharmaceutical characterization. Phase imaging has been used to reveal polymeric forms from single crystal measurements [92], to confirm phase separation of two copolymers for drug delivery [93] and to identify formation of amorphous domains during miling of crystalline salbutamol [94]. Other applications of AFM in pharmaceuticals concern the surface morphology [95-96], porosity [97], hardness [98] and surface energy [98-99] of drugs and excipients.

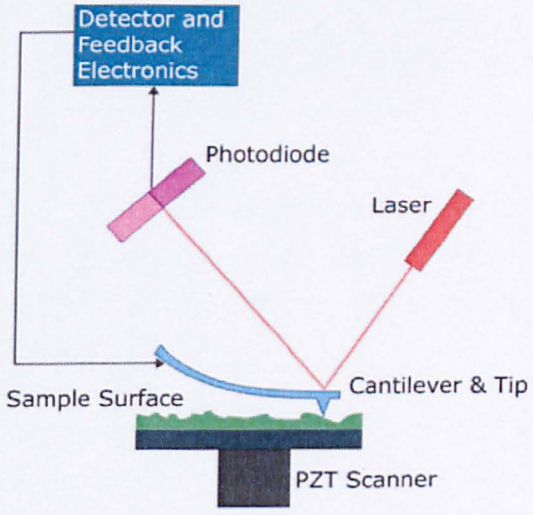

Figure 2.5: Schematic diagram of the main components of an Atomic Force Microscope.

2.4 Localised Thermal Analysis

In localised thermal analysis (LTA), the sample is heated locally with a thermally active probe providing information about the glass transition temperature and the melting point of the sample at this location. LTA has proved useful for thin layers or coatings where bulk methods such as DSC, TMA and DMA cannot be applied [100]. Bulk methods measure the mean thermal properties of a sample, whereas LTA can provide information about the spatial distribution of the thermal properties of a material surface which can be useful to design materials with the desired properties.

When the thermal probe is placed on the sample, the temperature of the tip is ramped linearly with time at a pre-defined rate while the degree of bending is monitored. At the point of phase transition, the material beneath the tip softens and the probe penetrates into the sample. This is reflected as reduction of the deflection whereby phase transition temperatures of the sample such as glass transition temperature or melting point can be determined.

In this thesis, two different LTA methods scanning thermal analysis (SThM) and nanothermal analysis (NTA) were used. The main difference between these methods is the size of the probe. In SThM, the tip has a terminal radius of ca. 500nm, whereas an NTA tip can be below 100nm. In SThM a Wollaston wire probe is used. It consists of a silver wire with a fine platinum core which is bent into a sharp loop and etched to expose the core (Figure 2.6) [101]. This probe is relatively stiff and can be used in contact mode only.

The NTA probes are fabricated from doped silicon by Anasys instruments (Santa Clara, CA) (Figure 2.7). These probes have a heater integrated into the end of the cantilever which allows them to be heated by the application of a current to around 400° C at very rapid heating rates. Their advantages against the Wollaston probes are that they can achieve better spatial resolution and also they can image in both contact and tapping AFM modes and hence are more suitable for softer easily damaged samples.

LTA has been successfully applied to many aspects of the industry, such as in electronics, polymer and biology science. Moreover, this technique has been gained significant interest in pharmaceuticals. The main advantage of this technique is that

can distinguish different components in a drug dosage forms *in situ* with minimal sample preparation and high spatial resolution. Hence, SThM has proved to be a useful tool to discriminate polymorphic forms of drug [102] and the coating of a tablet and its core [103] whereas NTA has been implemented to characterise nano-dispersed pharmaceutical systems to confirm their heterogeneity [104-105].

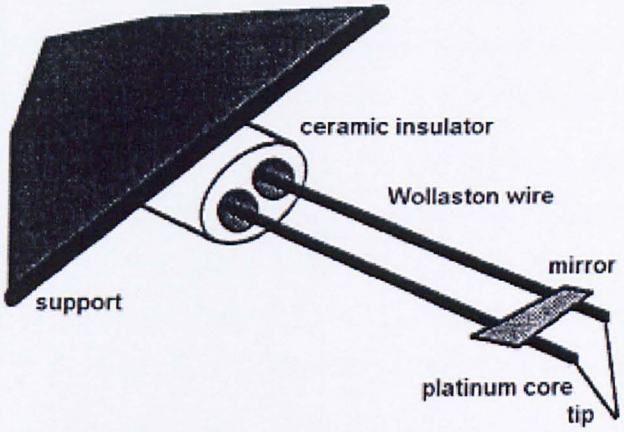

Figure 2.6: Schematic diagram of an SThM Wollaston tip [101].

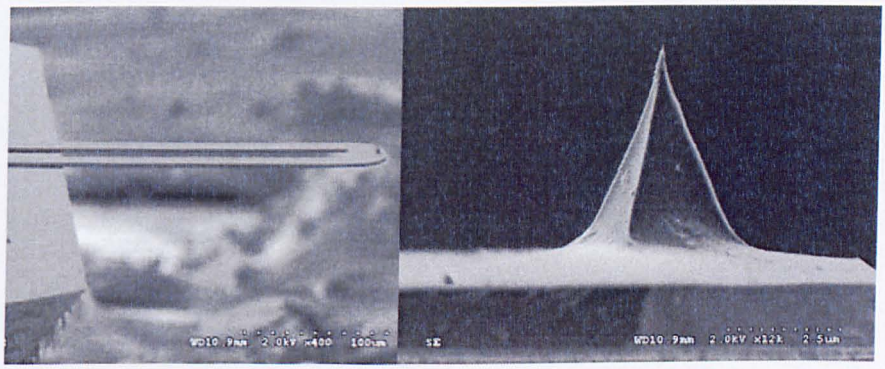

Figure 2.7: SEM images of the nanothermal cantilever (left) and its probe [106].

2.5 Confocal Raman Microscopy

2.5.1 Theory

When monochromatic radiation is incident upon a sample then this light depending on its interaction with the sample may be reflected, absorbed or scattered in some manner. In the Raman technique, the scattering of the radiation is considered to extract information about the molecular structure of the samples.

Raman scattering is an inelastic scattering of photons. The scattered light consists of two types; one called Rayleigh scatter which is strong and has the same intensity with the incident beam, and the other called Raman scattering which is very weak (10^{-5} of the incident beam). There are two types of Raman scattering; Stokes and anti-Stokes scattering. In Stokes scattering, photons are scattered at low energy. Since at room temperature the population state of a molecule is principally in its ground vibrational state, this is the larger Raman scattering effect. In anti-Stokes scattering, the scattered photon are scattered at a higher energy.

The incident photons will thus interact with the sample molecules, and the amount of energy change (either lost or gained) by a photon will be characteristic of the nature of each bond (vibration) present. However, not all vibrations will be detectable with Raman spectroscopy, since if the vibration of the molecule does not change its polarizability the Raman band will be very low or zero.

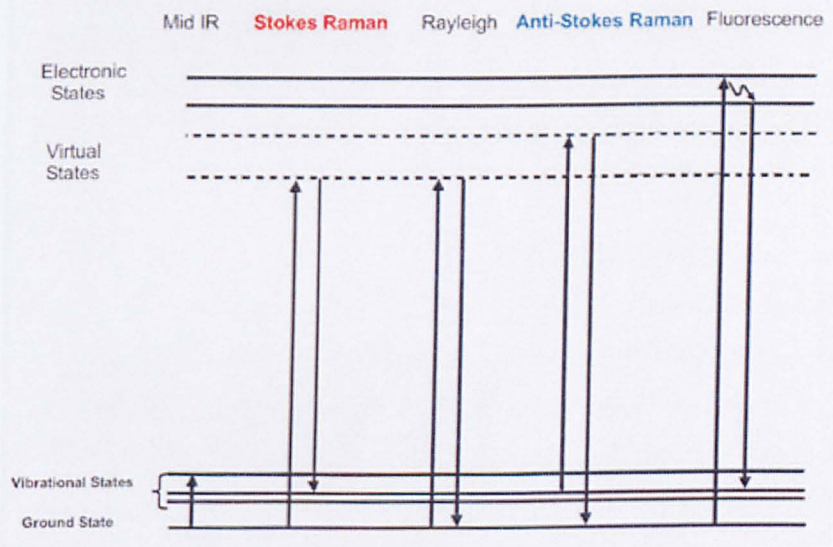

Figure 2.8: Schematic diagram of the different energetic levels of photons for Raman scattering.

2.5.2 Raman microscopy

A Raman microscope can offer a powerful non-destructive and non-contact method of spatially resolved sample analysis.

A standard Raman microspectrometer consists of an excitation source, a microscope, a spectrometer and a detector. Raman microscopy can use various radiation sources

which can be applied from ultra violet to near infra-red. The spectrometer is used to narrow the pass bands. The most common detectors that have been used are CCDs. In a confocal Raman microscope, there are additional pinhole apertures, to reject the out of focus light. One aperture is placed between the laser and the objective and the other is placed at the image plane of the objective. The apertures block the light scattered from regions outside the focal plane of the objective. A schematic diagram of a confocal microscope is illustrated in Figure 2.9 [107]. The main advantage of the confocal Raman is that it enables a very small sample area or volume to be analysed – down to the micron scale.

One of the most important applications that confocal Raman spectroscopy offers is the opportunity to chemically map and image of a sample. In this case, images are recorded point by point and line by line while scanning the sample through the excitation focus. Chemical imaging as an analytical tool has been favoured as a non-destructive, non-contact and non-invasive technique. Chemical imaging offers the ability to simultaneously identify and quantify several substances within samples. There are a plethora of publications related to this issue [108-114]. For instance, Raman mapping gave the opportunity to investigate the distribution of ibuprofen in PVP [115] and Alprazolam to Xanax [113].

One of the main challenges we need to face is that this technique can be time consuming, especially for samples with low Raman scatter that are mapped with high spatial resolution. Moreover, mapping an area with a point laser source may be very time consuming, subject to the desired spatial resolution, because of the small size of the laser spot (typically 1–10 μm). The problem of long acquisition time has been resolved by employing Principal Component Analysis (PCA) to analyse experimental Raman mapping spectra [112]. Other techniques have been used to reduce the acquisition time are line imaging [116] where the detector analyses the spatial and spectral dimensions simultaneously and a focal plane array where optical detectors are composed of several thousand elements forming a matrix of pixel. They enable thousands of spectra to be obtained simultaneously [117].

Another factor which increases the time to plot a chemical map and was a significant factor here is the loss of focus of the laser beam. Samples with increased roughness can contribute to this effect (Figure 2.10). This can be resolved by using autofocus

technology where during the scan of the sample surface the focal point microscope objective is moving up and down to focus exactly at the sample surface [118]. Autofocus considers that at the maximum light reflection, the refractive intensity from the laser is also at a maximum. In practise, this may not be true and usually an offset must be set. When autofocus is employed the acquisition time per spectra increased to around 4 seconds.

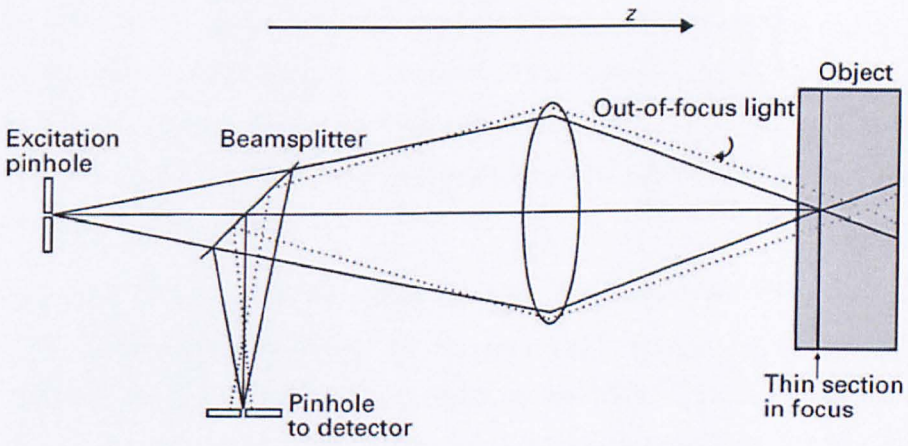

Figure 2.9: A schematic diagram of Confocal microscopy.

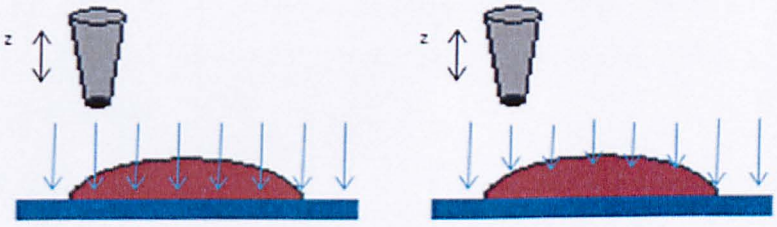

Figure 2.10: Schematic image of the principle of autofocus where the end of the arrows indicate where the focus location. The left image represent the system working without autofocus where the laser only at the edge of the spot is focused. The right image represents the autofocus system where the laser beams are focused along the surface of the spot.

2.5.3 Extraction of distribution maps

Chemical images can be produced from the acquired spectra (with tagged spatial coordinates) in various ways. The simplest option is to follow the intensity or the area under a certain peak which is characteristic for a compound. This so-called

univariate approach is used whenever possible because it is the simplest and most understandable way to produce chemical images, one for each component. However, the condition that all the components of the imaged sample have uniquely assignable wave numbers with satisfactory signal-to-noise (s/n) ratio is not always fulfilled. Additionally, mapping an area may be demanding because of the small size of the laser spot (typically between 1-10μm) and also because of the high acquisition time required to increase the s/n ratio [111]. Moreover, in more complex systems where the specific peaks can be overlapped or a constituent compound is at a low concentration then univariate analysis cannot extract reliable distribution maps, and hence more advanced data analysis tools are used. Multivariate curve resolution has been shown to be very effective for unravelling complex spectral data from mapping (or imaging) Raman data.

Multivariate analysis takes into account all the spectrum information. The most common multivariate methods for imaging data analysis include principal component analysis (PCA), and partial least square (PLS). These methods aim to unravel the pure spectra of the compounds and their concentrations from mixed spectra. They are based on the assumptions that the signal collected is linearly related to the concentration of the components. Thus, the mixed spectra can be expressed as the sum of each pure material spectrum plus the experimental noise. The spectrum set of a mixture containing k compounds can be mathematically expressed, if the interactions among the constituents are negligible, with the following equation.

$$X = CS^T + E \tag{2.1}$$

Where S^T (k×λ) is the pure spectra matrix, consisting of λ wavenumbers, k is the number of samples. X (p×λ) is the matrix containing the mapping spectra which is equal to the numbers of samples × number of wavenumbers and C (p×k) is the concentration matrix of the components (number of samples × number of components). The matrix E represents the residual noise. In effect, PCA decomposes the data into sections of signal and noise. By removing the noise, the signal to noise ratio (s/n) can be significantly improved. The major results that PCA provide are the number of components that have detectable signal, the features that are related to the signal and the features that are related to the concentration [119]. It should be

noted that the data is originally acquired in a three-dimensional hypercube form (n×m×λ), thus, the data has to be unfolded into a two dimensional matrix beforehand. Every mapping data set is a 3D data structure (two spatial dimensions and one spectral) which can be temporarily rearranged by appending two spatial coordinates to produce a 2D data structure (one spatial and with mixed with x- and y- coordinates and one spectral dimension (Figure 2.11). PCA is applied to this 2D data structure and, after completion of the 2D results, scores are folded back into the original 3D data sets from which then chemical images are then produced. All the procedure mentioned before is employed to all multivariate studies of Raman spectra.

If the pure spectra matrix is available, the direct classical least square (DCLS) can be used. In this case the spectral concentrations are estimated by:

$$C = XS(S^T S)^{-1} \qquad (2.2)$$

Other techniques involve clustering techniques, and multivariate curve resolution (MCR) [108].

Zhang *et al.* described theoretical multivariate methods of analysis applied to a model a pharmaceutical tablet. From all the techniques, DCSL was considered to provide the most reliable results since it is based on reference spectra. PCA was described as an exploratory data analysis technique. In general, there is not a one to one correspondence between a principal component and a chemical compound but in some formulations it is possible that a PCA loading matches a pure reference spectrum. Cluster analysis has been shown that it is a useful tool to segment a data set into regions of similar chemical composition or physical form. It is a useful tool to characterize a product with distinct spatial distribution character. Finally, MCR provided similar results with the DCLS. However, its interpretation should be with caution as a particular component spectra may have the signature of the other [108].

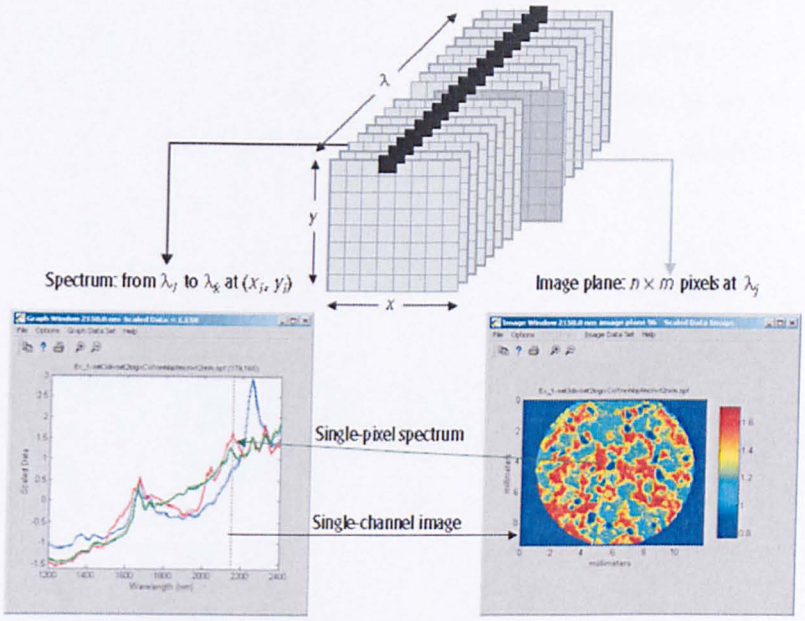

Figure 2.11: Schematic representation of a spectral imaging hypercube showing the relationship between spatial and spectral dimensions [117].

2.6 Attenuated Total Reflectance Spectroscopy (ATR)

ATR-FTIR is a method of performing spectroscopy on a solid sample to detect the frequencies of IR radiation absorbed by the material. In ATR spectroscopy, an infrared beam is directed onto an optically dense crystal with a high refractive index at an angle greater than the critical angle to internal reflection. This internal reflectance creates an evanescence wave that extends beyond the surface of the crystal into the sample held in contact with the crystal. This evanescent wave protrudes only a few microns (0.5 μ - 5 μ) beyond the crystal surface and into the sample. Consequently, there must be good contact between the sample and the crystal surface. In regions of the infrared spectrum where the sample absorbs energy, the evanescent wave will be attenuated or altered. The attenuated energy from each evanescent wave is passed back to the IR beam, which then exits the opposite end of the crystal and is to a detector in the IR spectrometer. The system then generates an infrared spectrum.

The most popular ATR crystal analysis materials are zinc selenide (ZnSe) and diamond. Both of these crystals have a refractive index of 2.4. A typical polymer refractive index is 1.5. At 45 degrees angle of incidence and at a wave number of

1000 cm^{-1} the ATR depth of penetration would be about 2 microns. The most likely differentiation for use of ZnSe or diamond is the form and hardness of the polymer sample. The Knoop hardness (kg/mm^2) of diamond is 8820 whereas that of ZnSe is 120.5. In practical terms this means that for softer or for flat polymer samples a ZnSe ATR crystal is used.

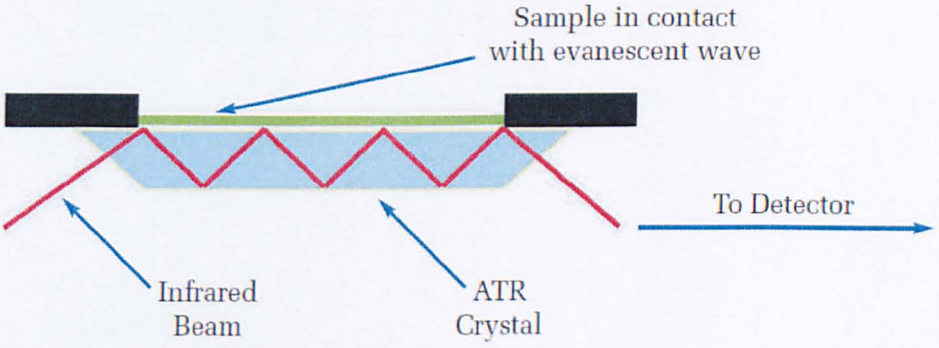

Figure 2.12: Schematic diagram of the principal ATR-FTIR spectroscopy

3. Production of individual sprayed formulations

3.1 Introduction

In this chapter, the first step towards the formulation of medicines via inkjet printing is demonstrated. APIs along with excipients have been dissolved in appropriate solvents and sprayed on to hydrophobic treated glass slides. The chosen APIs were felodipine, captopril and hydrochlorothiazide.

Felodipine dispersed in PVP is an extensively studied poorly soluble drug system [34, 120-129]. Typically the compounds are dissolved in alcohol, followed by rapid evaporation of the solvent to produce an amorphous single phase material with improved dissolution properties compared to crystalline felodipine. To prove this inkjet method, we compared the product to the published bulk methodologies for producing dispersions.

Captopril and hydrochlorothiazide have been chosen as a combination therapy used commercially (Capozide^{TM}) that the inkjet printing can reproduce in a microarray format. Hydrochlorothiazide is practically insoluble in water, whereas captopril is freely soluble in water.

The deposited products were characterized using Atomic force microscopy (AFM), scanning thermal microscopy (SThM) and nanothermal analysis, attenuated total internal reflection infra red spectroscopy (ATR-IR) and Confocal Raman microscopy (CRM) to provide complementary characterisation. In particular the release profile of the drugs was studied to assess the potential of the format for therapeutic purposes.

3.2 Active Pharmaceutical Ingredients

3.2.1 Felodipine

Felodipine is an oral calcium- channel blocker (CCB) of the dihydropyridine (DHP) class. Calcium is necessary for muscle cells to contract. Felodipine prevents calcium from being released within the muscle cells of the small arteries and thereby causes the muscles to relax and the arteries to dilate or expand. It is a well tolerated drug which is a given in an extended release tablet formulation where a single dosage can last for 24 hours [130]. Felodipine is marketed under the brand name Plendil™ by AstraZeneca and Renedil™ by Sanofi-Aventis.

3.2.1.1 Felodipine's formulation

Felodipine has been investigated extensively. As a compound practically insoluble in water, its *in-vivo* bioavailability can become limited. Dissolved felodipine can be completely adsorbed from the gastrointestinal tract so solubility can be a limiting factor to bioavailability. Hence, the concerned research mainly focuses on the improvement and modification of the release profile. The first solid dosage form was a conventional tablet which is clinically effective in a twice daily dosage. Along with the conventional release tablets, extended release has been prepared which require one dosage. Both the formulations have equal bioavailability [131].

Usually, to produce a controlled drug release profile of felodipine, it is mixed with a hydrophilic excipient, to form a uniform mixture. The most common excipients that have been used are PVP [31, 34, 121-129, 132], HPMC [31, 34, 123-125, 129], PEG [120, 132] and some polymeric surfactants [133]. In most of the cases, the drug and the excipient have been dissolved in an appropriate solvent (e.g. ethanol), followed by a rapid evaporation to produce an amorphous product.

Dissolution studies have shown that the use of a hydrophilic excipient can enhance the dissolution of felodipine, improving its bioavailability [124-125].

3.2.2 Captopril

This drug belongs to a group of medications called ACE inhibitors. It is used to treat high blood pressure (hypertension). It works by relaxing blood vessels, causing

them to widen. Lowering high blood pressure helps prevent strokes, heart attacks and kidney problems. This medication is also used to improve survival after an acute heart attack, to help protect the kidneys from damage due to diabetes, and with other drugs (e.g., "water pills"/diuretics, digoxin) to treat congestive heart failure.

Captopril is commonly marketed by Bristol-Myers Squibb under the trade name Capoten™.

3.2.2.1 Captopril's formulation

The drug is freely water soluble and has an elimination half-life after an oral dose of 1.7 h. It is stable at pH 1.2. As pH increases, the drug becomes unstable and undergoes a degradation reaction. More specifically, above pH 4 the rate of captopril degradation increases with pH, whereas below pH 4 the rate of degradation is independent of pH [134].The efficacy of Captopril after oral dosing lasts for only 6-8hours. Therefore, clinical use requires 37.5–75 mg to be taken 3 times daily. The development of oral controlled release formulations for captopril is difficult because of *in vivo* and *in vitro* instability. The drug also undergoes dose dumping and burst phenomenon (being freely water soluble) when formulated as controlled or sustained release formulation. Development of a prolonged-action dosage form of captopril should bring many benefits to patients for the following reasons: (1) a decrease in the frequency of administration should lead to an improvement in patient compliance and as a result clinical efficiency would be improved; (2) it is expected that a minimization of fluctuations in the blood concentration of the drug will decrease the risk of side-effects [135].

Various approaches have been used to develop a prolonged release oral dosage forms. These can involve the use of polymers as fillers or coatings in the preparation of tablets, pellets and matrices. Seta *et al.* have studied prolonged-action dosage forms of captopril using seven different formulations, including coated slow-release granules, enteric coated granules, an oily semisolid matrix (OSSM) and four kinds of modified release tablets [136]. A sustained release captopril formulation has also been reported by Serajuddin *et al.* which was a capsule dosage form containing captopril and a semi-solid matrix of at least one fatty acid glyceride and/orpolyethylene glycol ester [137]. Abramowitz *et al. designed a formulation*

where captopril is inside a polymeric core which is coated with an enteric polymers such as methacrylic acid copolymers, hydroxylpropyl methyl cellulose phthalate (HPMCP) and cellulose acetates or delayed release coating such as ethyl cellulose and methacrylic acid copolymers [138]. Granulated excipients of lactose or dicalcium phosphate with ethylcellulose were examined for their ability to be used as matrix materials to produce a controlled release dosage form by direct compression for captopril [139].

3.2.3 Hydrochlorothiazide

Hydrochlorothiazide (HCT) is a diuretic. It increases the amount of urine passed, which causes the body to lose salt and water. This medicine is used to treat high blood pressure. It is also reduces the swelling and water retention caused by various medical conditions, such as heart, liver, or kidney disease.

Hydrochlorothiazide is sold both as a generic drug and under a large number of brand names, Apo-Hydro™, AquazideH™, Dichlotride™, Hydrodiuril™, HydroSaluric™, Microzide™, Esidrex™, and Oretic™.

Hydrochlorothiazide is also used in combination with many common drugs used to treat hypertension such as Diovan HCT, Zestoretic, Benicar HCT, Atacand HCT, and Lotensin HCT and others.

3.2.3.1 Conventional formulations of Hydrochlorothiazide

Hydrochlorothiazide has limited solubility in water which can reduce its bioavailability. The main method to increase its bioavailability is to incorporate it within hydrophilic polymers. Verveat *et al* demonstrated that the incorporation of a liquid solubiliser into microcrystalline cellulose pellets enables the enhancement of the release of the HCT. Also, PEG 400 and PVP has been applied to increase the bioavailability [140-141]. Furthermore the dissolution enhancement by preparing solid dispersion formulation with PVP has been studied.

3.3 Aims - Objectives

The aim of this chapter is to describe the production and testing of formulations of felodipine, captopril and hydrochlorothiazide as APIs using inkjet printing. The APIs were combined with appropriate polymers to achieve the desired properties of the final formulation. The compounds were dissolved in appropriate solvents and the solutions were sprayed using a piezo driven dispenser. The dried products were subsequently analyzed using micro- and nano- analytical methods for the physic-chemical state and drug release properties.

3.4 Materials - Methods

3.4.1 Materials

Felodipine was supplied by AstraZeneca (Charnwood, Leics., UK). Captopril, Hydrochlorothiazide (HCT), Polyvinyl pyrollidone (PVP) k30, poly(lactic-co-glycolic acid) (85:15), Pluronic F-127 and DMSO 99% anhydrous were purchased from Sigma-Aldrich. Flutec fluid was purchased by F2 chemicals (Lancashire, UK).

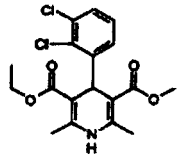

Figure 3.1: Felodipine

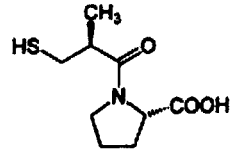

Figure 3.2: Captopril

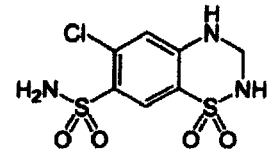

Figure 3.3: Hydrochlorothiazide

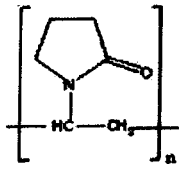

Figure 3.4: PVP K30
(n = number of monomers
MW = 30000)

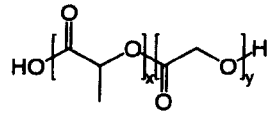

Figure 3.5: PLGA
(x: number of Lactic Acid units
y: number of Glycolyc Acid units
x/y = 85/15)

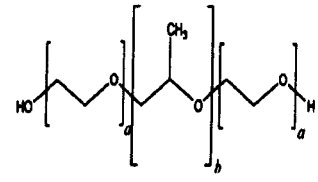

Figure 3.6: Pluronic F-127
(a/b/a/ = 130/80/100)

3.4.2 Methods

3.4.2.1 Preparation of solutions

Felodipine

Solutions of felodipine and PVP were prepared by dissolving them into a mixture of ethanol and DMSO (95/5). Felodipine is soluble in ethanol. DMSO was used to increase the boiling point of the solution to reduce chances of the dispenser clogging due to the evaporation of the solvent. The ratios of felodipine to the polymer were 1/10, 1/5, 1/2, 1/1 and 2/1 (w/w).

Capropril

Solutions of captopril and PLGA were prepared by dissolving them into a mixture of chloroform, ethanol and DMSO (75/18/7). Chloroform was also used to dissolve PLGA. Ethanol was used to dissolve captopril and to disperse DMSO, as DMSO is not miscible with chloroform. Finally, DMSO was used to increase the boiling point to the solution to avoid any possible clogging of the dispenser. The ratios of captopril to the polymer were 30/70 and 50/50 (w/w).

Hydrochlorothiazide

Solutions of hydrochlorothiazide with PVP and PLGA were prepared. When PVP was used, the compounds were dissolved into a mixture of acetone, ethanol and DMSO (55/38/7). Acetone was used to dissolve HCT, ethanol to dissolve PVP and DMSO to increase the boiling point of the solution.

In the case of PLGA, the compounds were dissolved into a mixture of acetone, and DMSO (93/7). Both HCT and PLGA are soluble in acetone. DMSO was used to increase the boiling point of the solution.

3.4.2.2 Preparation of surface

Hydrophobic surfaces suitable for retaining the sprayed micro-droplets were prepared by depositing flutec fluid on glass cover slips using a spin coating device. Flutec fluid is a fluorinated compound (4-pentafuorosulfurnitrobenzene). The hydrophobic surface was to avoid the spreading of the samples after their deposition.

3.4.2.3 Dispensing of solutions

All the solutions were ejected as pico-litre droplets using a piezo driven dispenser (GeSim A010-201 PICPIP). The solvent was evaporated under ambient conditions and the samples were kept in a desiccator until further analysis. The duration and the amount of voltage and the frequencies of cycles applied to the piezo dispenser were used to control droplet deposition. In general, the sprayed conditions were determined by the surface tension and viscosity of the solution. Solutions with higher viscosity required a higher voltage, whereas surface tension is the predominant factor which affects the droplet formation [71]. Here the optimum voltage for the samples for a single droplet was found to be in the range of 35 - 42V applied in 35 – 45 μsec pulses.

At this point, it is worth noticing that when PVP and felodipine were used as solutes in the sprayed solution, the nozzle was clogged in very few seconds (Figure 3.7), even though the solutions were stable in the vials after weeks of their preparations. This phenomenon was deteriorated increasing the concentration of solutions. Unfortunately, it was not clear whether this was happening in the higher concentration of felodipine or PVP. An explanation of this can be lying behind the chemical structure of PVP. PVP as it contains hydrophilic groups and a hydrophobic chain can act as a surfactant. Hence, it was possible that if there were bubbles in the solutions, PVP could cover them and the felodipine may precipitate there. A similar phenomenon was observed by Schubert group where when they used solvents containing amino groups the solution with polystyrene, the polymer was precipitated inside the nozzle in a couple of seconds. This group was not able to justify the reason [60].

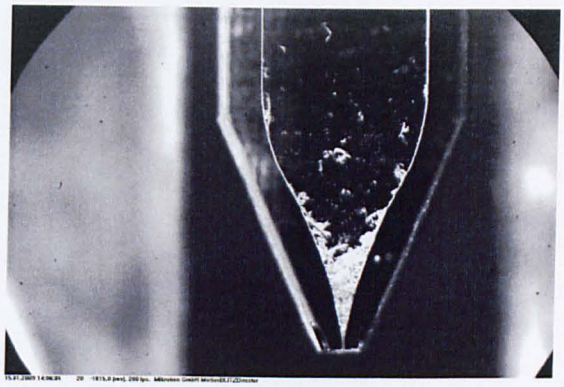

Figure 3.7: photo of the clogged piezo-dispenser.

3.4.2.4 Atomic Force Microscopy (AFM)

AFM analysis was performed in air using tapping mode with a Dimension 3000 (Nanoscope IIIa controller, Veeco, CA). Tap300 cantilevers were used (Budget Sensors, Sofia, Bulgaria). The images where analyzed using the SPIP software (Image metrology, Denmark).

3.4.2.5 Thermal Analysis

Nanothermal Analysis (NTA)

NTA was performed on single dried droplets using a Multimode AFM (Nanoscope V controller, Veeco) with a NTA modification from Anasys Instruments (Santa Barbara, CA). The probes used were AN2 (Anasys) with heating rate of 1°C/sec. The instrument was calibrated using measurements on poly(caprolactone) (PCL) (Tm = 55°C), polyethylene (PE) (Tm = 116°C) and polyethylenetelephalate PET (Tm = 238°C).

Scanning Thermal Microscopy (SThM)

SThM analysis was performed using an Explorer AFM system (Veeco) with a Wollaston wire micro-thermal tip (Veeco). To increase the signal level samples were produced with 40 droplets to increase the mass of material for analysis.

In the case of felodipine, local thermal analysis was performed with a temperature ramp rate of 10°C/sec. The same calibration samples as for NTA were employed.

Finally, the theoretical glass transition temperature of the mixture based on the Gordon-Taylor (GD) equation [142] were compared with the measured values. This

equation assumes that the two components are miscible. The GD equation is defined as

$$Tg = \frac{w_1 T_{g1} + k w_2 T_{g2}}{w_1 + k w_2} \quad (3.1)$$

The constant k is defined as $k = \frac{\rho_1 T_{g1}}{\rho_2 T_{g2}}$ (3.2)

Where w_1, w_2, T_{g1} and T_{g2} are the mass fraction and the glass transition of felodipine and PVP respectively and ρ_1 and ρ_2 the densities of felodipine and PVP. According to Konno *et al.* these are equal to 1.33mg/ml and 1.28 mg/ml respectively [123].

The value of glass transition temperatures of the PVP and felodipine that has been used to determine the constant *k* for each compound and the glass transition temperature were based on the SThM data. For PVP and felodipine these were equal to 198 °C and 46 °C respectively.

In the case of HCT/PVP system the density of HCT was from Tajber *et al.* and was equal to 1.89 mg/ml [143].

3.4.2.6 Infrared Spectroscopy (ATR – IR)

As for SThM, samples with multiple droplets were used to increase signal levels for ATR-IR. To avoid crystallization of the API, the solvent was evaporated in vacuum. The IR spectra were obtained using a Nicolet Avatar 360 FTIR using diamond as crystal.

In the case of felodipine the number of scans was 200 over the range 450 - 4000 cm^{-1} at a resolution of 4cm^{-1}. For captopril and HCT, the IR spectra the number of scans was 1000 over the range 450 - 4000 cm^{-1} at a resolution of 4 cm^{-1}.

3.4.2.7 Confocal Raman

Confocal Raman studies were performed on single droplets using a Jobin-Yvon/Horiba micro-Raman spectrometer, by means of red laser with 632nm wavelength and 600 1/nm grating. The spectrometer is equipped with an Olympus microscope BX41.

In all the cases, Raman spectra were obtained on multiple droplets with 100μm slit width, 8 sec acquisition time. Each spectrum was the mean of four measurements.

In terms of the Raman mapping, when felodipine was applied as an API, the experimental conditions were a 100μm slit width, a 100x microscope objective and 5sec exposure time. Each spectrum was the mean of two measurements. The sample profiling was performed at step increments of 1μm in x- and y- directions.

For felodipine/PVP and HCT/PVP the confocal Raman mapping was performed on a single droplet. The sample profiling was performed at step increments of 1μm in x- and y- directions.

For captopril/PLGA, HCT/PLGA and HCT/PLGA/Pluronic the Raman mapping has been performed in multiple droplets. The sample profiling at step increment in these case were performed on 5μm in x- and y- directions with 0.5 sec exposure time. Each spectrum was the mean of two measurements. The slit width was 150 μm.

All the Raman studies were carried out through 100×magnification lense. The chemical images were then constructed based on algorithms of the NGLabspec spoftware (Horiba Jobin Yvon). The eigenvalues of each principal component was calculated using Solo+MIA software (eigenvector, USA).

3.5 Results

3.5.1 Atomic Force Microscopy

3.5.1.1 Felodipine

AFM imaging of single droplet felodipine/PVP spots at the different ratios showed them to be homogenous at the nanoscale with no indication of drug crystallization and phase separation (Figure 3.8a, c, d, e, f). Although small holes can be observed in the film due to the drying phase the material deposited shows no evidence of internal structure. Intimate mixtures with PVP therefore appear to inhibit crystallization of felodipine as has been shown previously for bulk formulations. However, at the higher concentration of PVP small crystals can be formed which

must come from PVP's crystallization (Figure 3.8b). Due to the rapid evaporation of the solvent from such small drops, the felodipine deposited alone also appears to have no internal structure and therefore is likely to be amorphous (Figure 3.8a). However, when the dispenser sprays for more than a minute, crystals are formed which is caused by the slower evaporation of the solvent from such a large volume (Figure 3.8g).

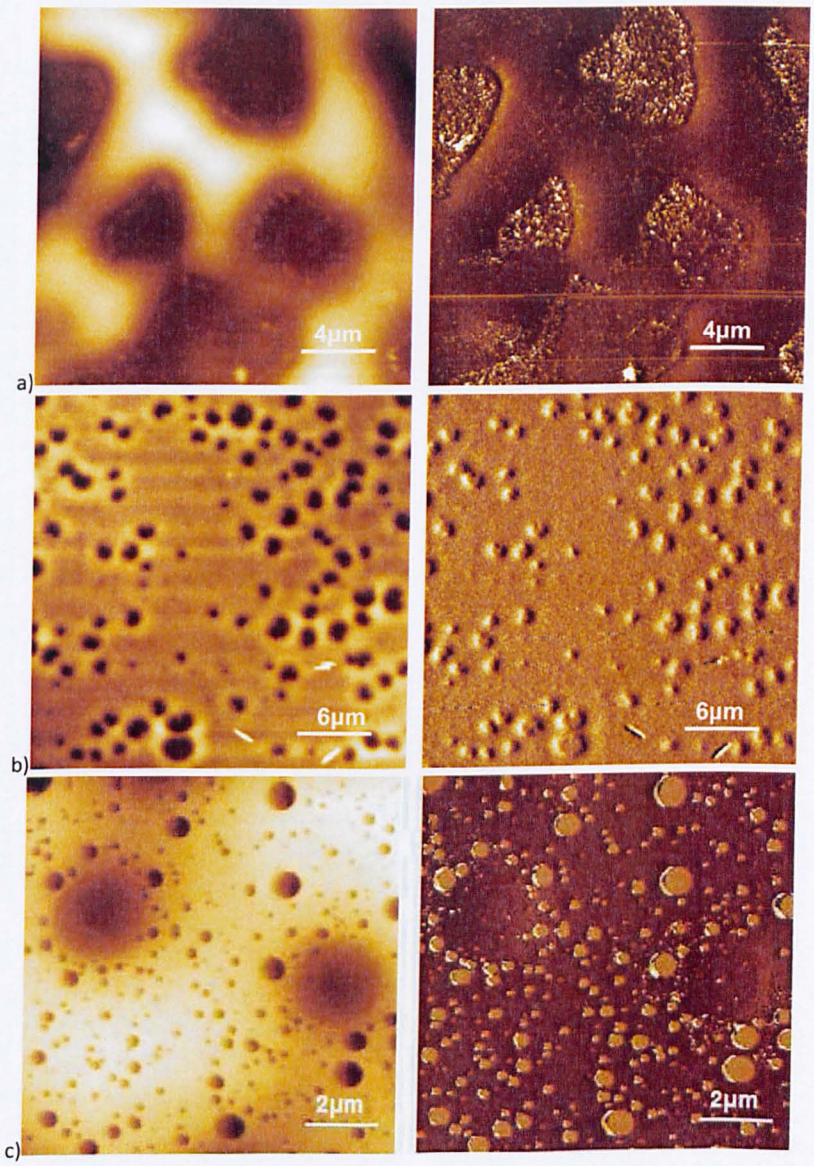

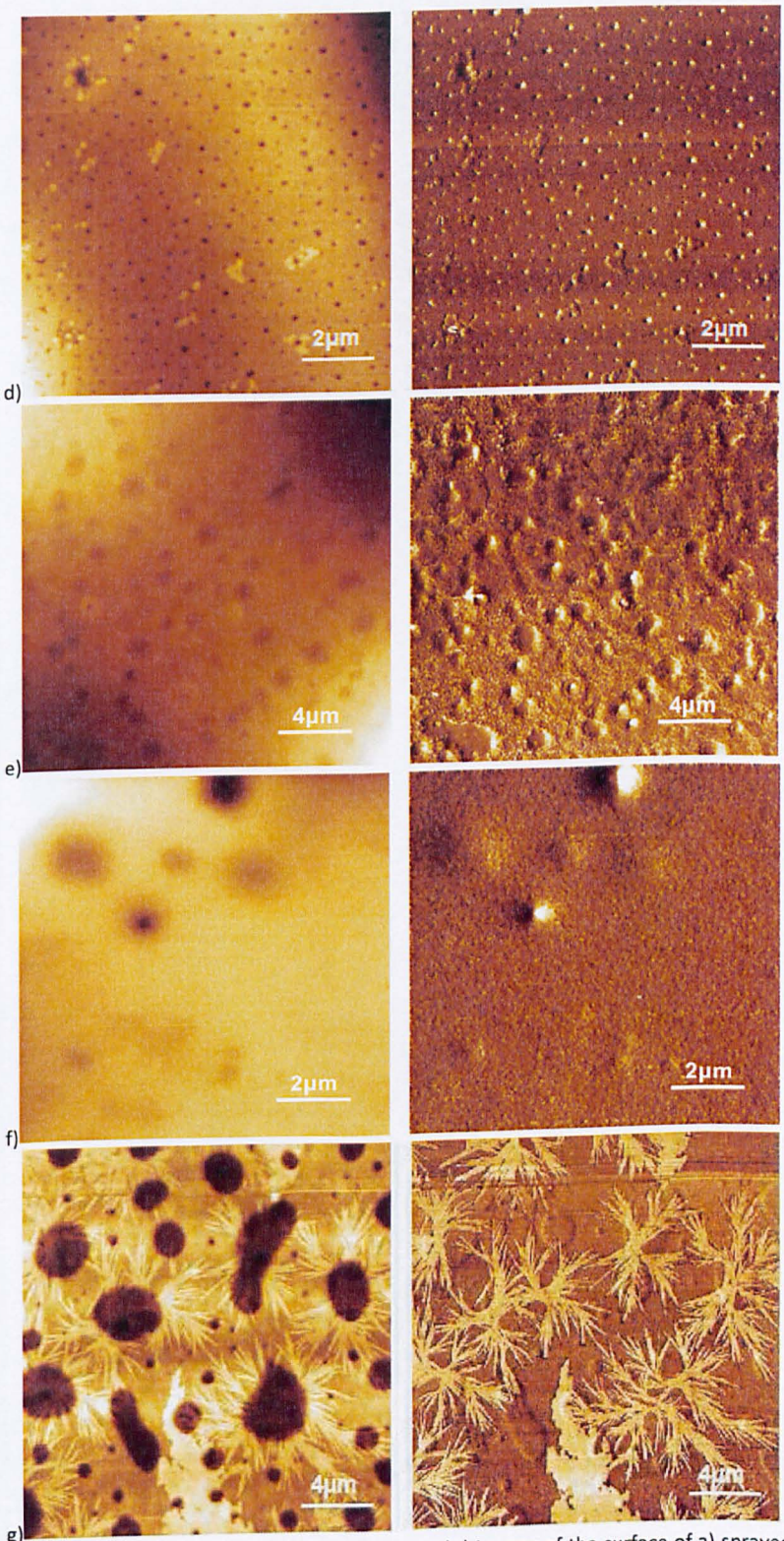

Figure 3.8: AFM topographic (left) and phase (right) images of the surface of a) sprayed felodipine and felodipine/PVP micro-deposits at ratio b) 1/10, c) 1/5, d) 1/2, e) 1/1, f) 2/1 and g) a product produced by spraying multiple droplets of felodipine/PVP = 1/10 (w/w).

3.5.1.2 Capropril

The product obtained when captopril and PLGA of different ratios were sprayed is illustrated in Figure 3.9 When PLGA was sprayed alone the deposits appeared amorphous and homogenous (Figure 3.9a). However, the addition of captopril resulted in the formation of small dots on the surface. These dots are likely to be captopril exposed on the surface (Figure 3.9 b,c).

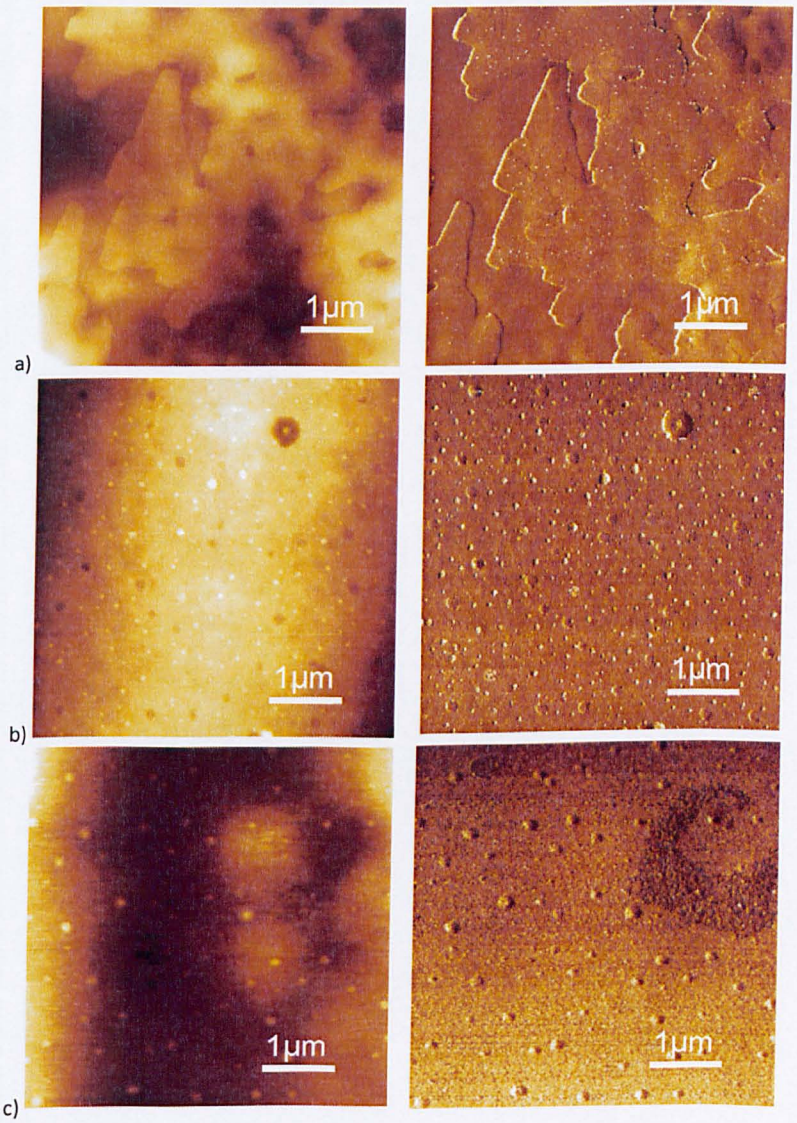

Figure 3.9: AFM topographic and phase (right) AFM images of a) sprayed PLGA and captopril/PLGA mixtures at b) 30/70, c) 50/50, w/w ratios and d) after the dissolution of captopril/PLGA mixture in water for 5 sec.

3.5.1.3 Hydrochlorothiazide

When hydrochlorothiazide was sprayed with PVP, the product was homogenous without any sign of phase separation or crystallization (Figure 3.10). As in the case of felodipine, small holes can be observed which are due to the drying phase of material deposited (Figure 3.10b and d).

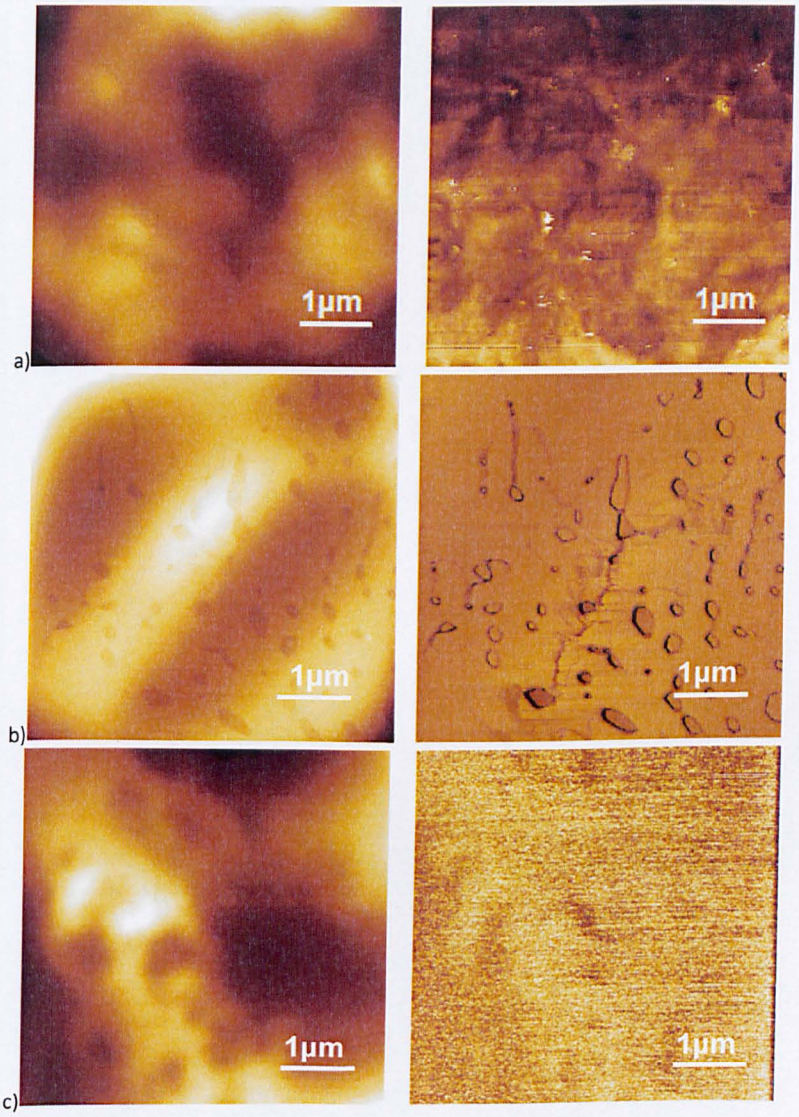

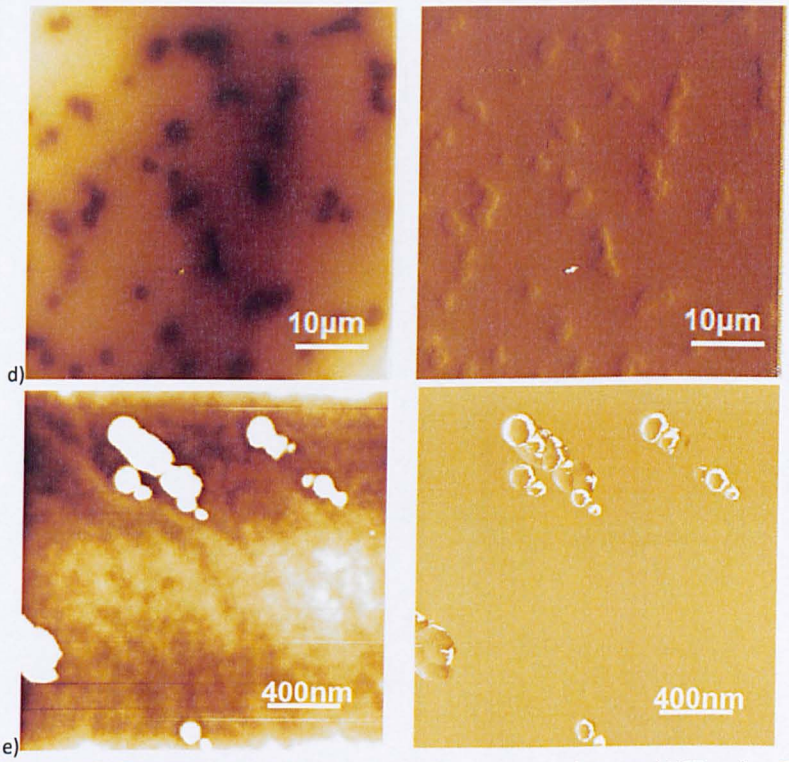

Figure 3.10: Topographic and Phase (right) AFM images of a) sprayed HCT and HCT/PVP mixture of ratio b) 1/5, c) 1/2, d)1/1, e) 2/1.

When PLGA is used although the product is amorphous there is a phase separation of the two compounds. This is identified in the phase image where certain areas appear bright in the phase contrast (Figure 3.11).

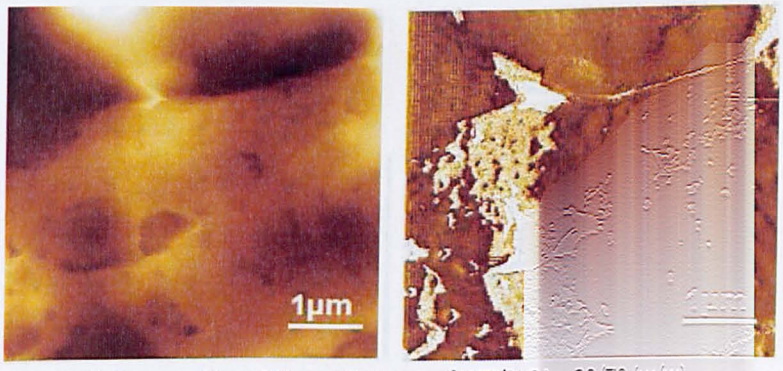

Figure 3.11: Topographic and Phase AFM image of HCT/PLGA = 30/70 (w/w).

3.5.2 Localised Thermal Analysis

3.5.2.1 Felodipine

SThM and NTA raw data are presented in Figure 3.12. Only one T_g was observed for each mixture which is consistent with a true solid dispersions being formed. It is clear that the NTA and the SThM produced comparable results. As the drug concentration increased the T_g was reduced. The values predicted from the Gordon-Taylor equation (fig. 4) are lower than the experimental values, indicating that either the sample does not ideally match the assumptions of this model (e.g. complete miscibility of the two components) or that the thermomechanical properties of the samples are a contributory factor to the experimental measurements. A more thorough analysis of how the properties of the samples and tip are represented in the discussion section in this chapter (discussion 3.6.1).

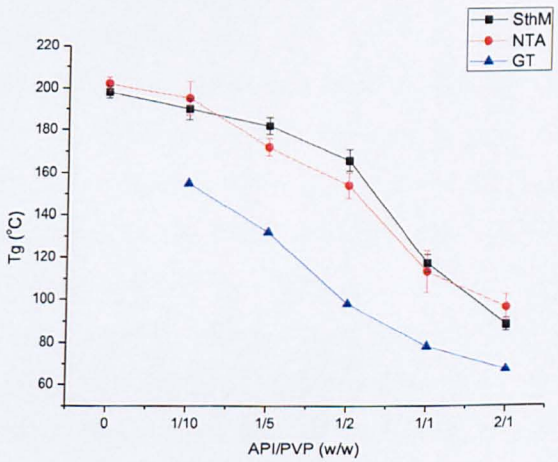

Figure 3.12: Comparisons Tg from SThM, NTA and the Gordon-Taylors equation for Felodipine-PVP mixtures.

3.5.2.2 Hydrochlorothiazide

SThM data of HCT/PVP mixture are represented in Figure 3.13. The experiment revealed a single glass transition point which is consistent with an intimate mixture of the API and the polymer. As the drug concentration increased, the observed T_g reduced. Also, the values predicted from Gordon - Taylor are lower than the experimental values as for the felodipine/PVP system.

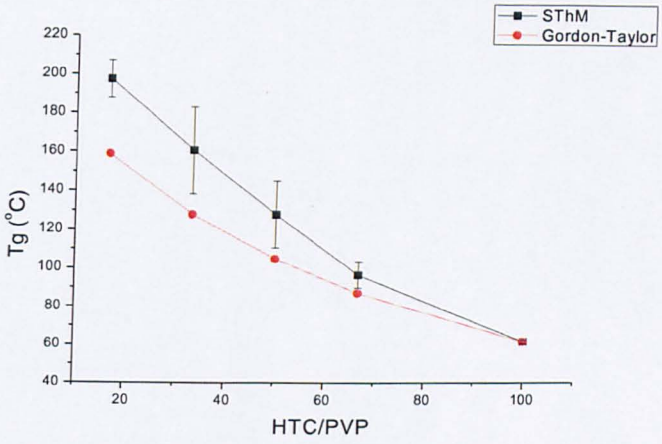

Figure 3.13: a) Comparison the data from SThM and Gordon – Taylor equation.

3.5.3 Infrared Spectroscopy (ATR-IR)

3.5.3.1 Felodipine

ATR-IR was used to examine the intermolecular interactions between felodipine and the polymer in the spot formulations. Felodipine has a secondary amine group that is capable of forming hydrogen bonds with the carbonyl groups of PVP and with the carbonyl group of other felodipine molecules. The characteristic wavelength range for the evaluation of these interactions is at the -NH stretching region between 3000 and 3700 cm^{-1}. If this -NH group interacts with the carbonyl group, its associated peak shifts to a lower wavenumber. Hence, for the crystalline drug powder one single peak is observed at 3344 cm^{-1}, but in the sprayed felodipine the peak is moved to lower wavenumber at 3324 cm^{-1} indicating that the hydrogen bonding among the felodipine's molecules are stronger in the amorphous sprayed drug as it has been previously reported (Figure 3.14c) [123, 126]. Additionally, there is simultaneous change in the carbonyl region (Figure 3.14b). Specifically, the carbonyl peak of the sprayed drug has been split in two peaks from which the former has been moved to higher wavenumbers at 1699 cm^{-1} compared to the crystalline powder, whereas the latter has been shifted to lower wavenumbers at 1688 cm^{-1}. This indicates that as there is only one peak that has been moved downwards, only one of the carbonyl groups is associated with the hydrogen bonding, whereas the other either does not compete at all or its energy is very low.

In the formulations with 2:1, 1:1 and 1:2 drug to PVP ratio the peak corresponding to the NH group is split and appears at lower wavenumbers (Figure 3.14c). This has been proposed to indicate a stronger hydrogen bonding between the felodipine and the polymer than with itself. When higher concentrations of PVP are used the -NH group is obscured by the large water peak is associated with the highly hygroscopic PVP rendering analysis difficult. Finally, it is worth noticing that the broadness of the peak is consistent with the proposed amorphous nature of the product, as the peak in question of crystalline powder is sharper.

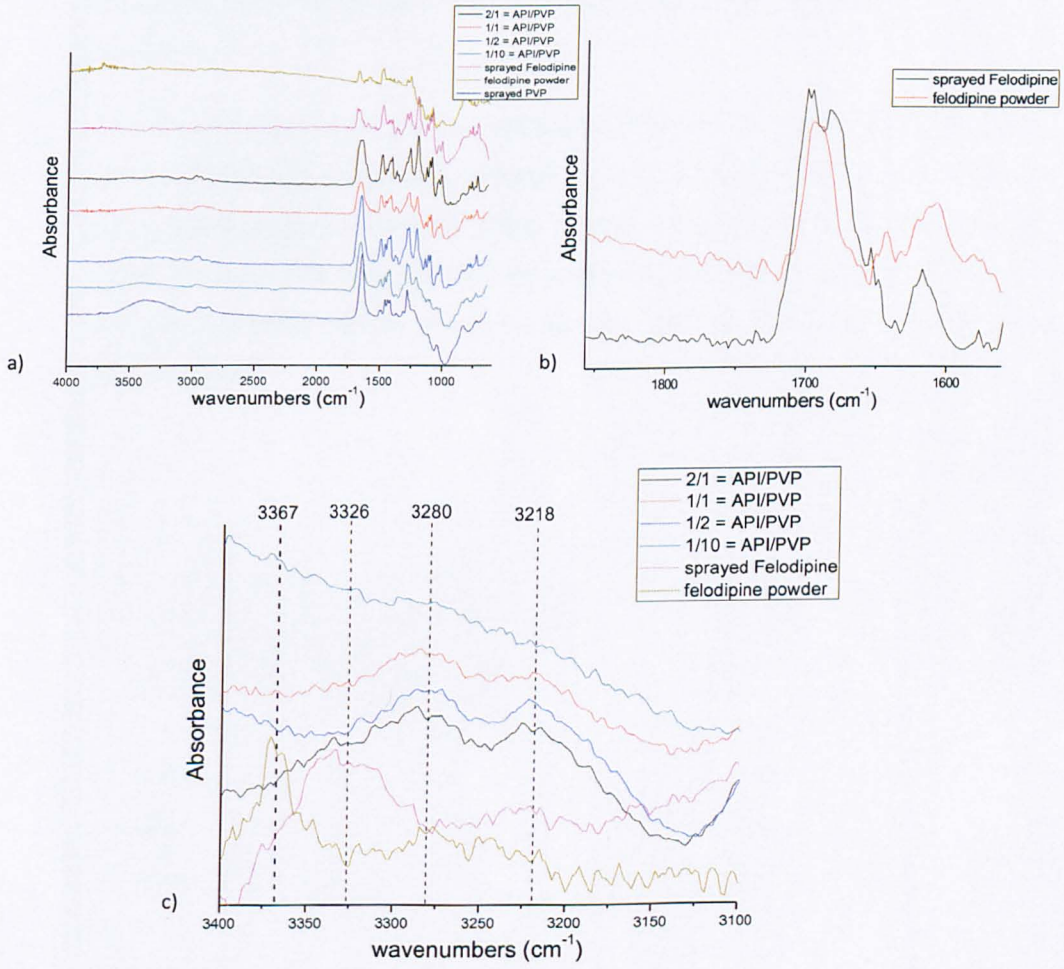

Figure 3.14: a) ATR spectra of powder felodipine, sprayed felodipine, PVP and mixtures of felodipine/PVP of various ratios, b) ATR spectra of sprayed felodipine and powder felodipine in the carbonyl region c) ATR spectra of powder felodipine, sprayed felodipine and mixtures of felodipine/PVP of various ratios in the NH region.

3.5.3.2 Captopril

ATR spectra of Captopril powder and sprayed captopril are illustrated in Figure 3.15. The peaks at 1749 and 1589 cm^{-1} corresponds to the C=O group of carboxylic acid and amide. The peaks at 1228cm^{-1} and 1220cm^{-1} corresponds to the C-O and C-N bending vibration.

By comparing the ATR spectrum of the powder captopril and the sprayed captopril in the CO region (Figure 3.15b), it is clear that the peak corresponding to the C=O group of carboxylic group has been moved towards lower wavenumbers, whereas the broadness of the amide peak in the sprayed product does not allow identifying the peak shift.

Also, by applying ATR any possible interaction between the captopril and PLGA could be investigated. Captopril could be bonded with PLGA by hydrogen bonding either of its carbonyl groups with the OH group or of the SH group with the C=O group of PLGA. However, ATR does not seem to confirm this as the carbonyl peaks of PLGA in the captopril/PLGA mixture and in the sprayed PLGA remain in the same position (Figure 3.15c)

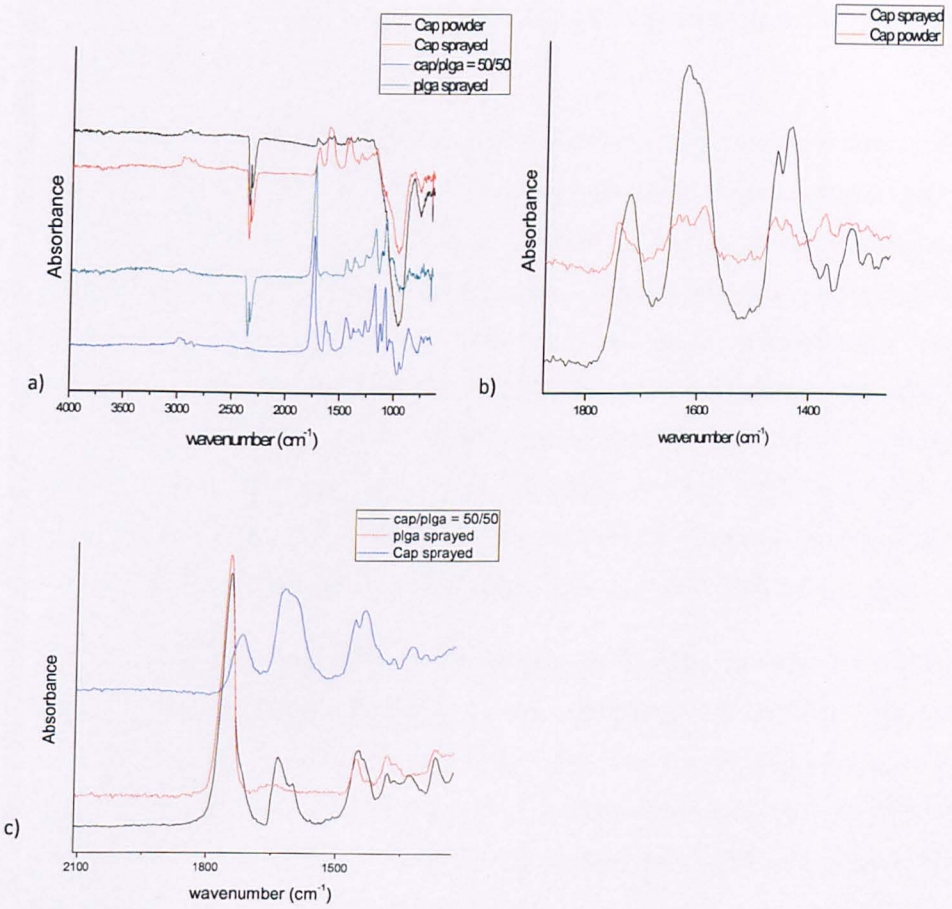

Figure 3.15: a) ATR spectra of PLGA, crystalline captopril, sprayed captopril and the mixture captopril/PLGA of various ratios, b) comparison of ATR spectra of sprayed Captopril and crystalline powder of Captopril in the CO region, c) comparison of ATR spectra of sprayed Captopril, crystalline powder and mixture of Captopril PLGA mixture.

3.5.3.3 Hydrochlorothiazide

In Figure 3.16a the ATR-FTIR spectrum of the crystalline powder, the sprayed HCT and the mixtures of HCT/PVP of various is illustrated. The most important chemical groups of HCT molecule are the four amino groups and the S=O groups since these two groups can interact either with other HCT molecules or with other potential excipients by means of hydrogen bonding. Specifically, HCT has four amino groups from which two are coming from the primary sulphonamide, one from the secondary sulphonamide and there is one secondary amino group. In the crystalline powder the peaks which correspond to the NH groups are at 3359 cm^{-1}, 3262 cm^{-1} and at 3166 cm^{-1}. The symmetric stretching vibration of SO groups appeared at 1149 and 1163 cm^{-1} whereas the antisymmetric stretching vibration of SO group is detected at 1317

cm^{-1} and 1333 cm^{-1}. The strong peak at 1600 cm^{-1} corresponds to the C=C group of the aromatic ring.

In the sprayed HCT the peaks of the spectrum were broadened, an indication of the amorphous nature of the product. The NH peak at 3166 cm^{-1} has been overlapped by the peak at 3262 cm^{-1} (Figure 3.16b). In terms of the SO peaks the two peaks assigned to the asymmetric stretching vibration has overlapped each other to a broad intense peak detected at 1320 cm^{-1}. The peaks corresponding to the symmetric SO vibration at 1149 and 1163 cm^{-1} has been shift to 1154 and 1167 cm^{-1} respectively (Figure 3.16c). Finally, the peaks correspond to the NH scissoring vibration have been shift from 1521 and 1555 cm^{-1} to 1515 and 1553 cm^{-1} respectively (Figure 3.16c). All the peak movements described above, it is an indication of a rearrangement of the hydrogen bonding in the sprayed material.

ATR-FTIR has been implemented to investigate the bonding between PVP and HCT. Figure 3.16d shows the comparison of the amorphous HCT with the 2/1 (w/w) HCT/PVP mixture. HCT has four NH groups which can be associated with the C=O group of PVP. It is illustrated that when PVP is added, then the two peaks of amino group are moved to lower wavenumbers due to hydrogen bonding between the NH groups of HCT with the carbonyl group of PVP.

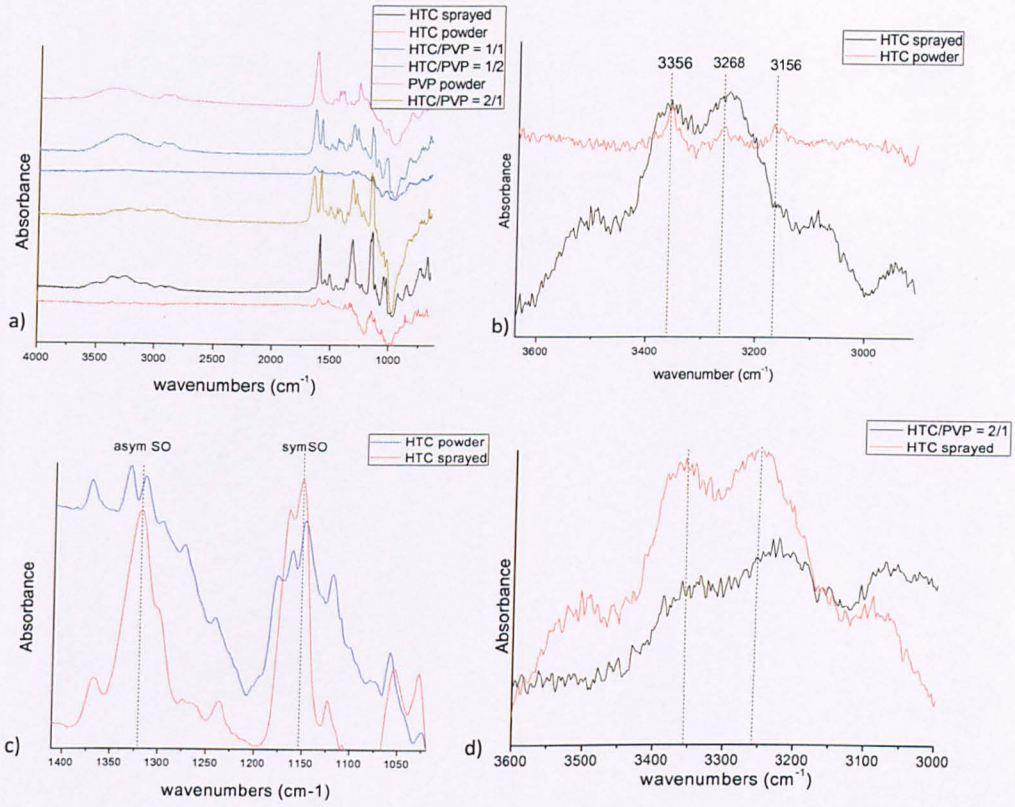

Figure 3.16: a) ATR spectra of powder HCT, sprayed HCT, PVP and mixture of HCT/PVP of different ratios, b) comparison of powder HCT and sprayed HCT in the region of NH group c) comparison of powder HCT and sprayed HCT in the carbonyl region between 1100 cm^{-1} – 1700 cm^{-1} d) comparison of sprayed HCT and HCT/PVP in the region of NH group.

The ATR-FTIR spectrum of PLGA has also implemented to investigate any possible interactions between HCT and PLGA. HCT can be associated by means of hydrogen bonding not only between the C=O groups of PLGA and the NH groups of HCT but also between the S=O groups of HCT with the OH group of PLGA. The former bond could be detected by a peak shift of the carbonyl peak of PLGA and the NH peak of HCT. Figure 3.17b shows that the NH peak at 3258 cm^{-1} of the sprayed HCT has been slightly shifted to lower wavenumbers in the mixture with PLGA. This is more obvious in the HCT/PLGA = 70/30 where the HCT signal is stronger due to its higher concentration. However, the peak of the carbonyl group of PLGA remained in the same position with the pure compound. Also the peak which corresponds to the asymmetric vibration of SO has slightly moved to higher wavenumbers at 1328 cm^{-1} from 1322 cm^{-1} of the sprayed HCT (Figure 3.17c).

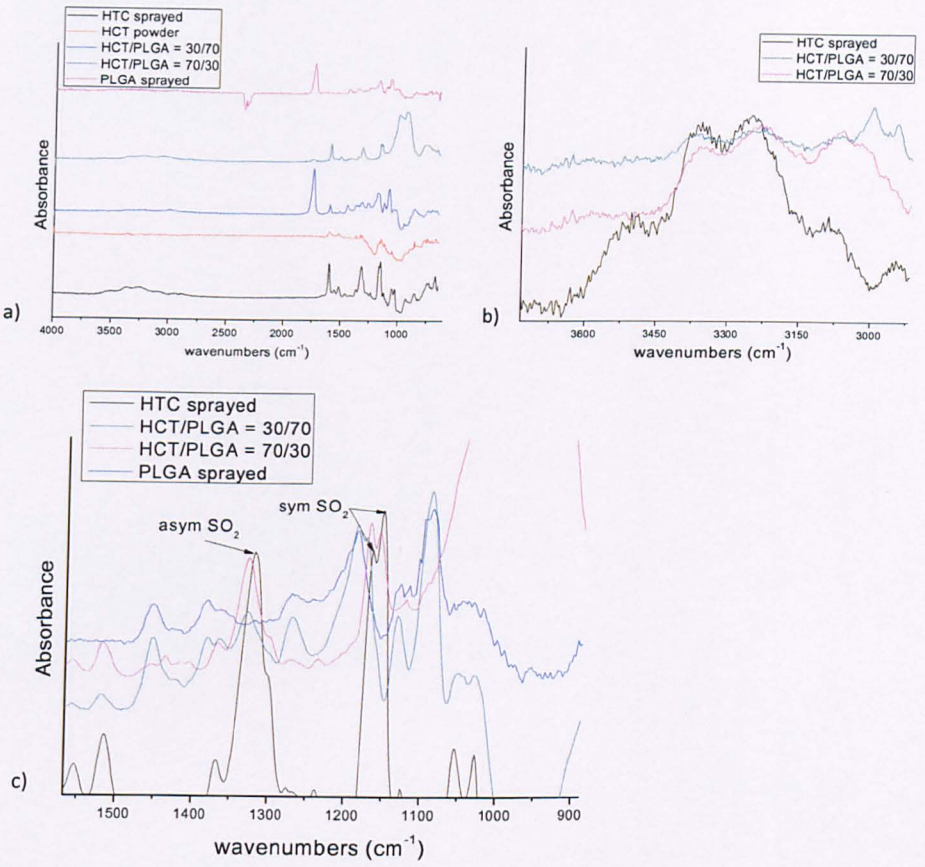

Figure 3.17: a) ATR spectra of powder HCT, sprayed HCT, PLGA and mixture of HCT/PLGA of different ratios, b) comparison of sprayed HCT and mixtures of HCT/PLGA of different ratios in the region of NH group c) comparison of sprayed HCT and HCT/PLGA mixtures in the sulphonic region from 900 cm^{-1} to 1600 cm^{-1}.

3.5.4 Raman

3.5.4.1 Felodipine

From the Raman spectrum of felodipine crystalline powder, it has been observed that there is a characteristic peak at 3335 cm^{-1} which corresponds to the NH stretching vibration and a characteristic peak at 1639 cm^{-1} corresponding to the free carbonyl stretching mode. In the sprayed felodipine the characteristic peak of NH group in addition to become broader losing lots of its intensity and moves towards lower wavenumbers indicating that the hydrogen bonding among felodipine's molecules are stronger than in crystalline powder (Figure 3.18). Also, in the samples where PVP is added the peak of amino group is disappeared, possibly due to the low

concentration of the felodipine. Also, the carbonyl group of the PVP is covered by the carbonyl group of felodipine. As the concentration of PVP increases, its characteristic peaks are increasing (Figure 3.19).

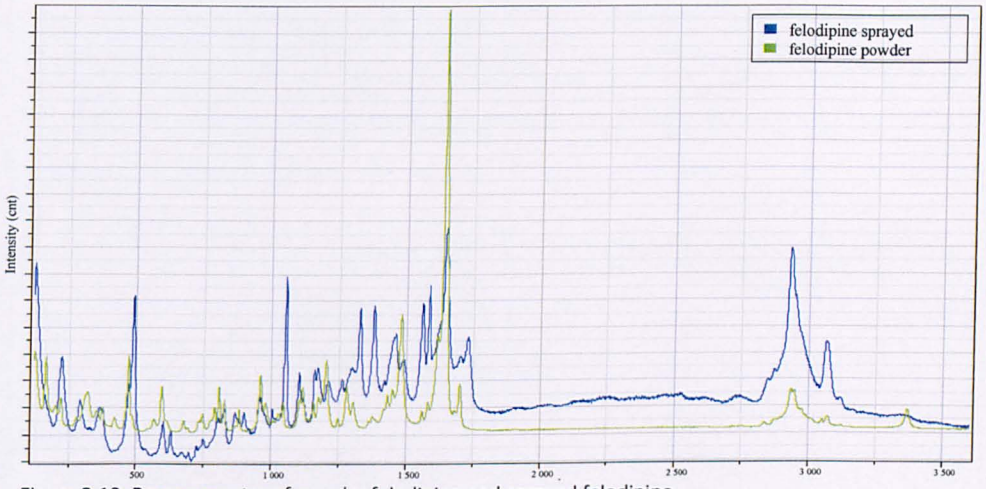

Figure 3.18: Raman spectra of powder felodipine and sprayed felodipine.

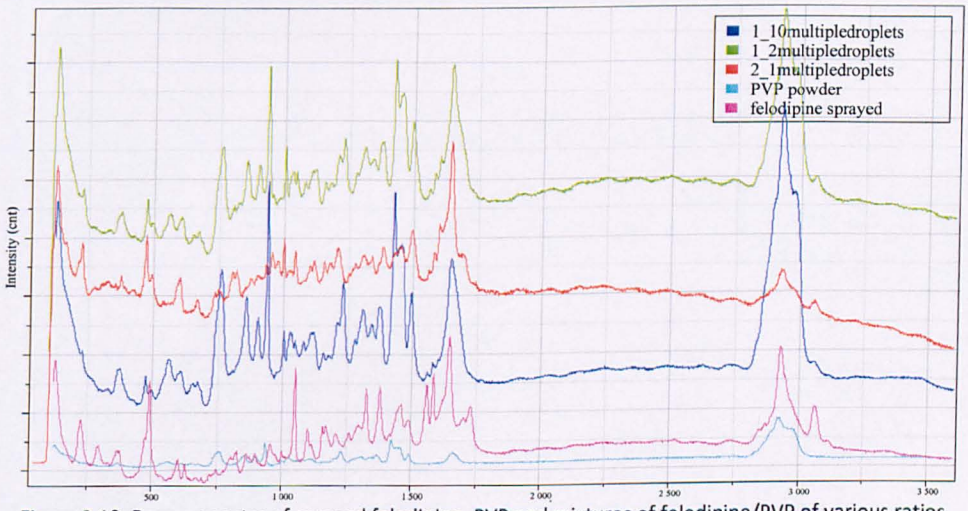

Figure 3.19: Raman spectra of sprayed felodipine, PVP and mixtures of felodipine/PVP of various ratios.

3.5.4.2 Captopril

The Raman microscope spectra of the crystalline powder of captopril and the sprayed captopril are shown in Figure 3.20. In the captopril powder the C=O stretching vibration of the carboxylic group of captopril is assigned at 1745 cm^{-1} and the C=O stretching vibration of the amide group at 1603 cm^{-1} and at 1583cm^{-1}. In the sprayed drug the former peak has been shifted to 1727 cm^{-1} whereas the latter has

been shifted to 1616 cm^{-1}. Moreover, due to the broadness of the peak, it is not clear if both the peaks of the amide of the crystalline have been shifted.

Confocal Raman microscopy has been also implemented to investigate any possible interactions between the captopril and PLGA. The position of the characteristic peaks of captopril and PLGA is in the same position with their pure product indicating that the nature of the compounds remains the same and no interaction between them takes part (Figure 3.21).

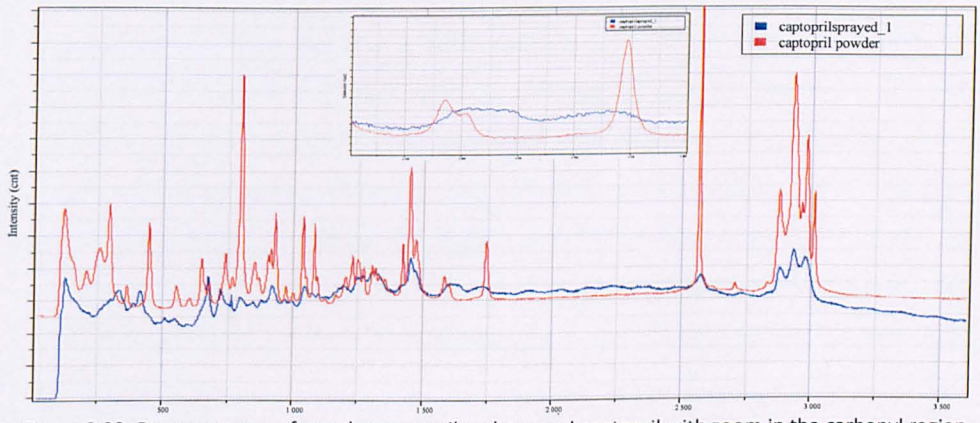

Figure 3.20: Raman spectra of powder captopril and sprayed captopril with zoom in the carbonyl region at 1550 – 1800cm^{-1} .

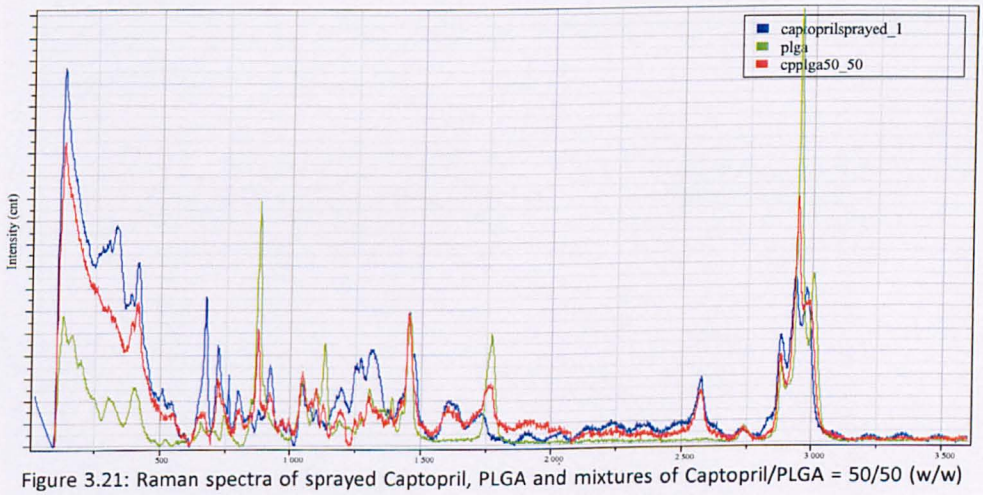

Figure 3.21: Raman spectra of sprayed Captopril, PLGA and mixtures of Captopril/PLGA = 50/50 (w/w) mixture.

3.5.4.3 Hydrochlorothiazide

In Figure 3.22 the Raman spectra of HCT on various forms is illustrated. The NH groups of HCT occur at the area between 3100 and 3370 cm^{-1} which correspond to the symmetric vibration of secondary N-H group, the NH_2 symmetric vibration and

the symmetric vibration of the NH group of the primary and secondary sulphonamide. The strong peaks at 1150 and 1165 cm^{-1} corresponds to the symmetric vibration of SO_2 whereas the peaks at 1295 and 1313 cm^{-1} correspond to the asymmetric vibration of SO_2. The strong peak at 1596 cm^{-1} assigned to the NH_2 bending vibration. Also, the strong peaks at 680 cm^{-1} and 710 cm^{-1} correspond to the CS stretching vibration.

In the sprayed HCT the peaks corresponding to the NH group which are in the range 3160 – 3500 cm^{-1} wavenumbers became broader indicating the amorphous nature of the product. Furthermore, the second peak moved to lower wavenumbers than in crystalline material indicating that the hydrogen bonding between the HCT molecules are stronger than in the crystalline form whereas the peak of the amino group at 3360 cm^{-1}, even though it is broader than in crystalline form it has been remained in the same position indicating that the certain amino group does not compete to the hydrogen bonding. Also, it is worth noticing that the peak at 3167 cm^{-1} looks to have shift to higher wavenumbers and unified with the peak at 3263 cm^{-1} (Figure 3.22).

Furthermore, the peak which corresponds to the symmetric vibration of SO_2 group looks to be in the same position with the crystalline, even though it is difficult to elucidate it due to their broadness.

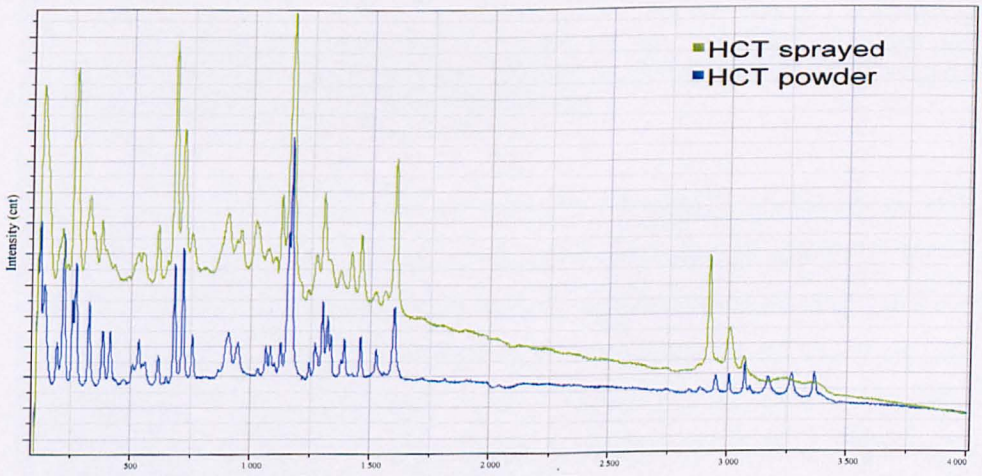

Figure 3.22: Raman spectra of powder HCT and sprayed HCT.

When PVP is added to the formulation its characteristic peak appears, whose intensity increases as its concentration increases (Figure 3.23). The most characteristic peaks of PVP are the peak corresponding to the carbonyl group at 1662 cm^{-1} and the carbonyl ring at 938 cm^{-1}. The carbonyl group of PVP can interact via hydrogen bonding with the NH group of HCT. Focusing on the NH region of sprayed HCT and 2/1 = HCT/PVP mixture, it is observed that both the peaks corresponding to amino groups have been slightly shifted indicating hydrogen bonding between the PVP and HCT. However, the carbonyl group of PVP remains in the same position with the pure material. Finally, the peaks of symmetric and asymmetric SO stretching have been shift slightly to higher wavenumbers.

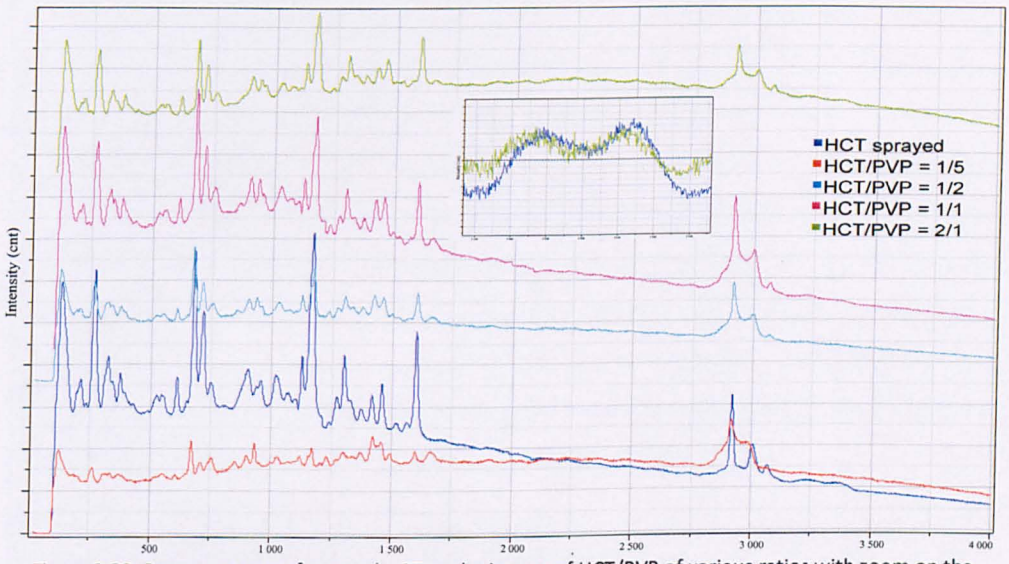

Figure 3.23: Raman spectra of sprayed HCT, and mixtures of HCT/PVP of various ratios with zoom on the NH area of sprayed HCT and 2/1 = HCT/PVP sprayed mixture.

The spectra of HCT/PLGA in different ratios are illustrated in Figure 3.24. As in the case of PVP, when PLGA is added, its characteristic groups are appeared. The C=O group of PLGA can interact with NH group via hydrogen bonding, however there is no peak shift of neither the NH groups of HCT, nor the C=O group of PLGA which does not confirm any hydrogen bonding between the API and the polymer. Also, PLGA could interact with HCT via hydrogen bonding of its OH group with the SO groups of HCT. Nevertheless, the peaks corresponding to the SO group at

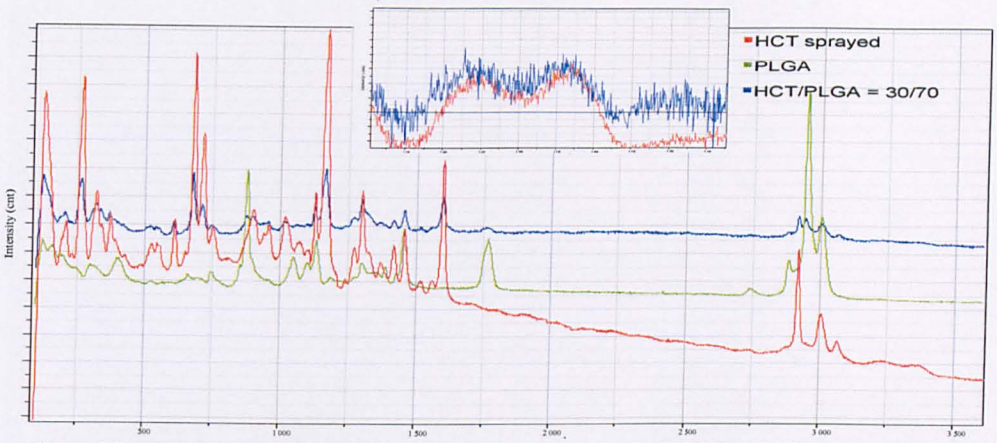

Figure 3.24: Raman spectra of sprayed HCT, PLGA and mixture of HCT/PLGA = 30/70 with zoom in the area of NH group.

In Figure 3.25 the Raman spectrum of the mixture of HCT with PLGA and Pluronic is shown. Due to its low concentration the pluronic's peak can not be detected in the spectra of the mixture. Pluronic can interact with the PLGA and HCT with hydrogen bonding of its hydroxyl group. However, this could not be confirmed as the carbonyl peak of PLGA remained at the same position in the mixtures. Also, the second peak of NH group of HCT looks to be slightly shifted indicating hydrogen bonding between the NH group of HCT and the CO group of PLGA (Figure 3.26a). Finally the peaks that correspond to the SO_2 group of HCT which can be associated with pluronic via hydrogen bonding remains in the same position with the sprayed HCT indicating that no interaction between HCT and pluronic took place (Figure 3.26b).

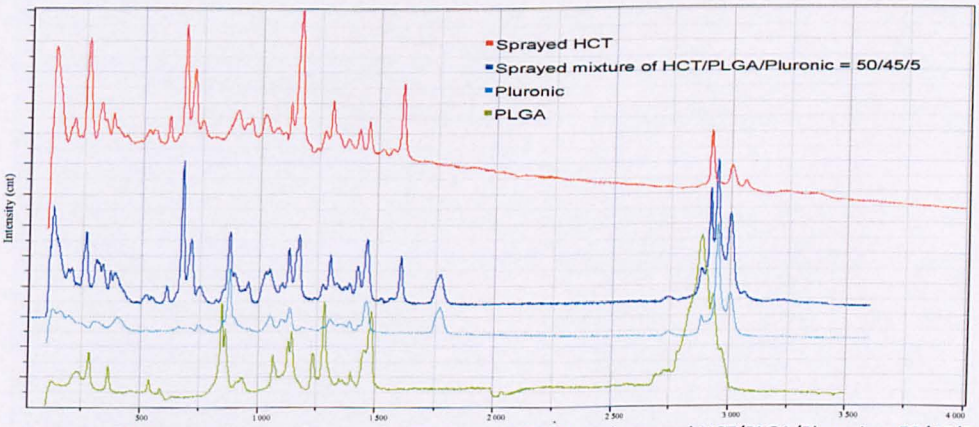

Figure 3.25: Raman spectra of sprayed HCT, pluronic, PLGA and sprayed HCT/PLGA/Pluronic = 50/45/5 mixture.

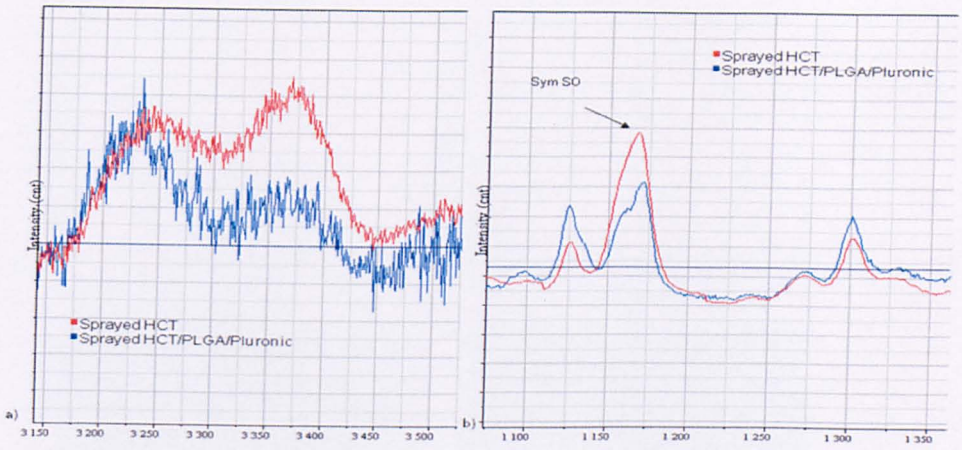

Figure 3.26: Raman spectra of sprayed HCT and sprayed mixture of HCT/PLGA/Pluronic = 50/45/5 mixture in the a) NH region and b) SO region.

3.5.5 Raman Mapping

3.5.5.1 Felodipine

Confocal Raman Microscopy has been applied to study the drug distribution and state within the micro-spots. The spectral peaks chosen to plot the map were the characteristic carbonyl group of felodipine at 1667cm^{-1} and the characteristic carbon ring breathing of PVP at 937cm^{-1}. Figure 3.27a,Figure 3.28a, Figure 3.30a, Figure 3.31a show the Eigenvalues for each principal component. It is observed that the Eigenvalues are reduced dramatically after the first factor and it is almost zero after the third factor which indicates that the contribution of more than three factors is limited. Hence, the chemical map of the product has been created by using three principal components (PCs) for the mixtures of felodipine/PVP 2/1, 1/2 and 1/10 and two principal components for the mixtures 1/2 and 1/5.

As it can be seen from the model spectra and the chemical maps (Figure 3.27,Figure 3.28,Figure 3.29,Figure 3.30 and , b and c), the API and the polymer is evenly distributed as the characteristic peaks of felodipine and PVP coexist in the model spectra. The model spectra used to create the chemical maps were separated based on the intensity of the peaks. Therefore, the model spectra with the less intensity correspond to areas with a less concentration of material and are located at the edge due to the curvy shape of the droplet.

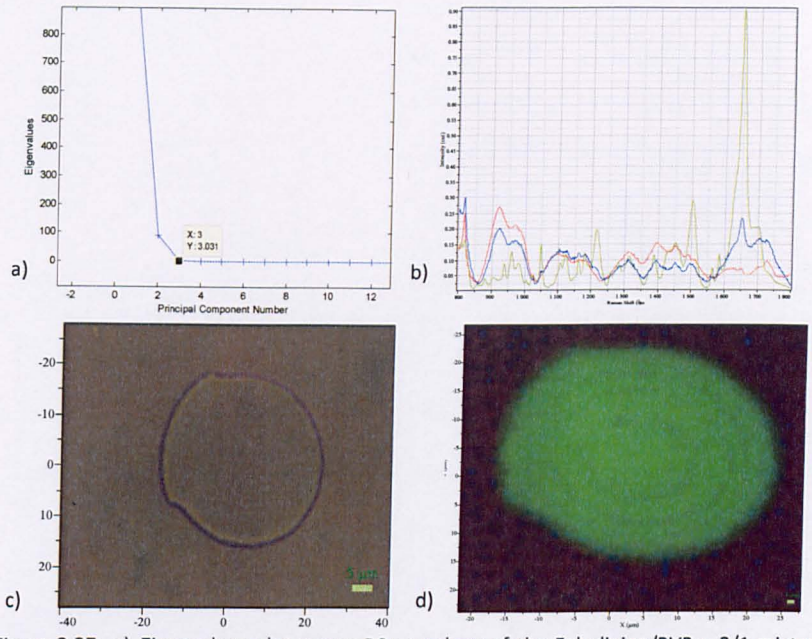

Figure 3.27: a) Eigenvalues plot versus PCs numbers of the Felodipine/PVP = 2/1 mixture b) 3 model spectra used to create the chemical map where the red, blue and green correspond to background, both background and sample respectively)optical microscope image of deposited product d) Chemical image of the mixture.

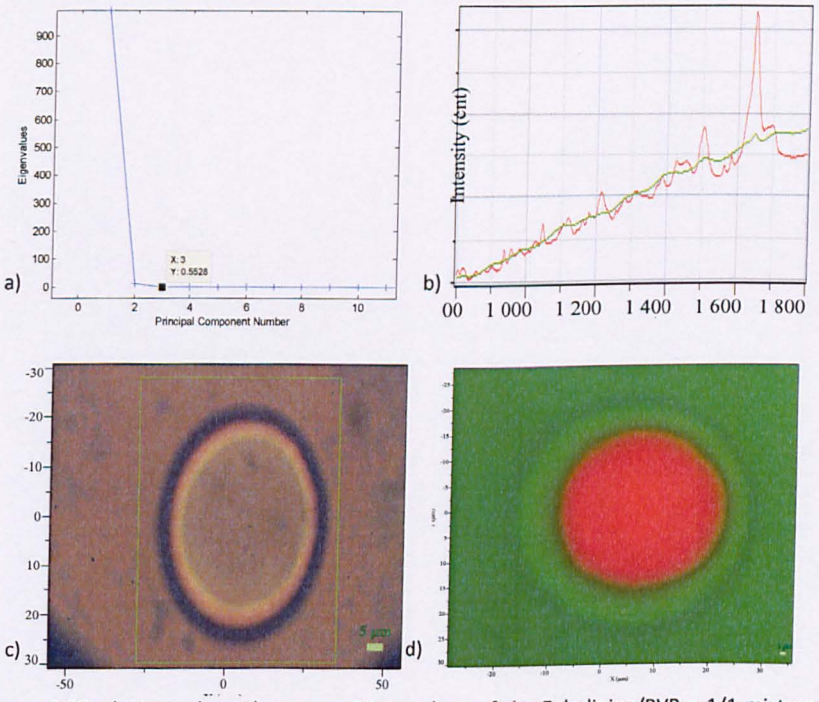

Figure 3.28: a) Eigenvalues plot versus PCs numbers of the Felodipine/PVP = 1/1 mixture b) 2 model spectra used to create the chemical map, where the red and the green correspond to the sample and background respectively c)optical microscope image of deposited product d) Chemical image of the mixture.

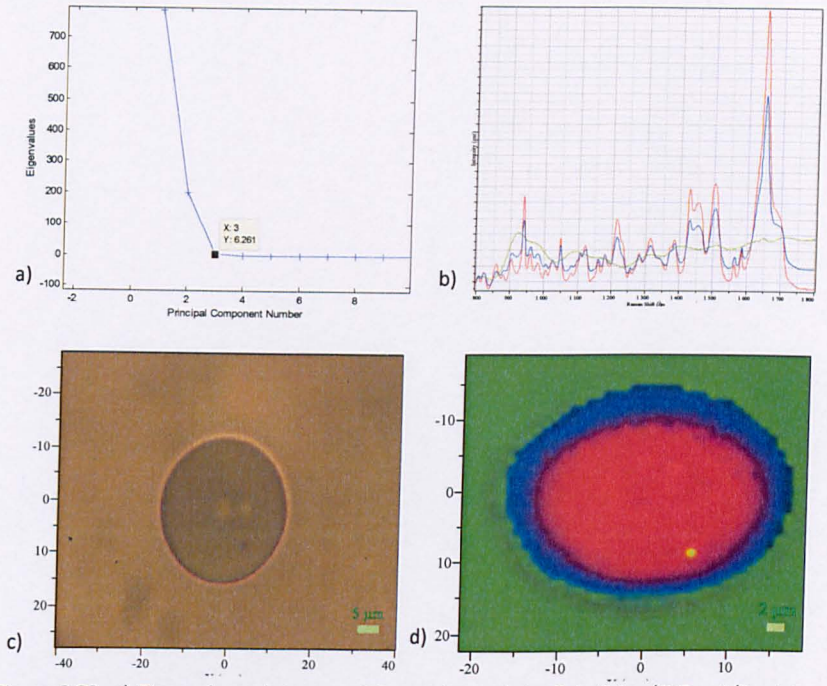

Figure 3.29: a) Eigenvalues plot versus PCs numbers of the Felodipine/PVP = 1/2 mixture b) 3 model spectra used to create the chemical map, where the red, blue and green correspond to background, both background and sample respectively c)optical microscope image of deposited product d) Chemical image of the mixture.

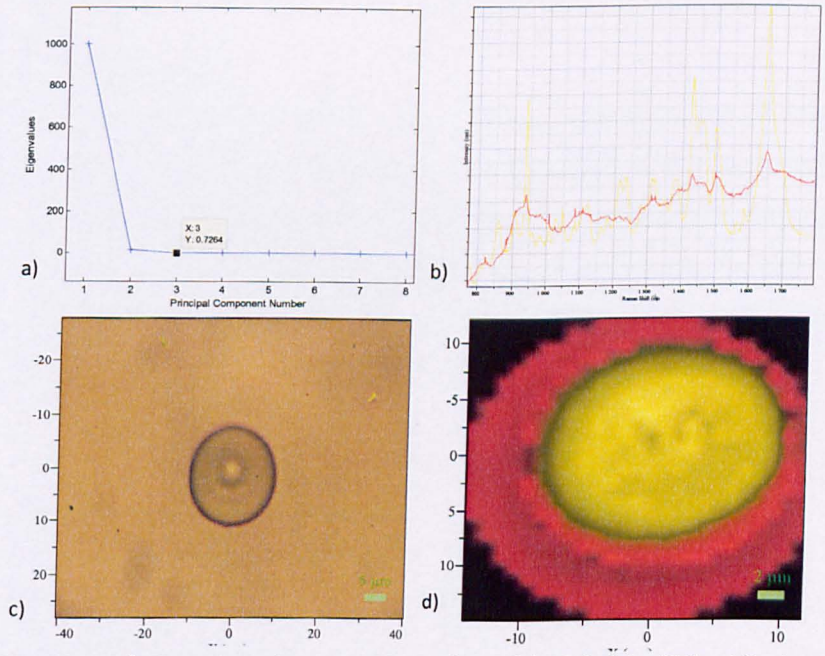

Figure 3.30: a) Eigenvalues plot versus PCs numbers of the Felodipine/PVP = 1/5 mixture b)2 model spectra used to create the chemical map, where the red, and the yellow correspond to background, and the sample respectively c)optical microscope image of deposited product d) Chemical image of the mixture.

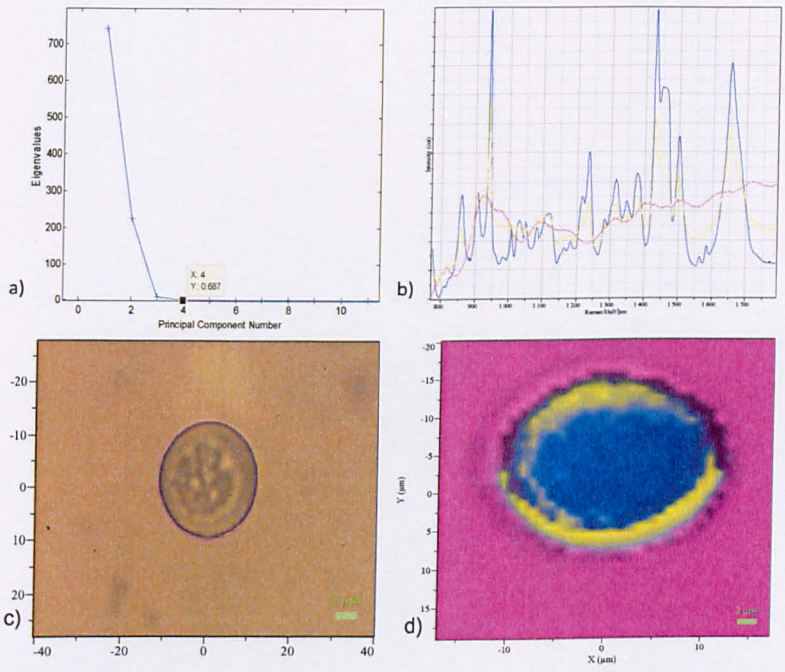

Figure 3.31: a) Eigenvalues plot versus PCs numbers of the Felodipine/PVP = 1/10 mixture b) 3 model spectra used to create the chemical map, where the purple, yellow and blue correspond to background, both background and sample respectively c)optical microscope image of deposited product d) Chemical image of the mixture.

3.5.5.2 Captopril

Figure 3.32 shows the chemical image for the captopril PLGA formulation. The image has been separated into three components. The differences of the model spectra are negligible as all of them contain peaks of both the captopril and PLGA leading to the conclusion that the product is homogenous. The red and the blue spectra are separated based on their intensity whereas the green spectra correspond to areas with very little material or to out of focus areas.

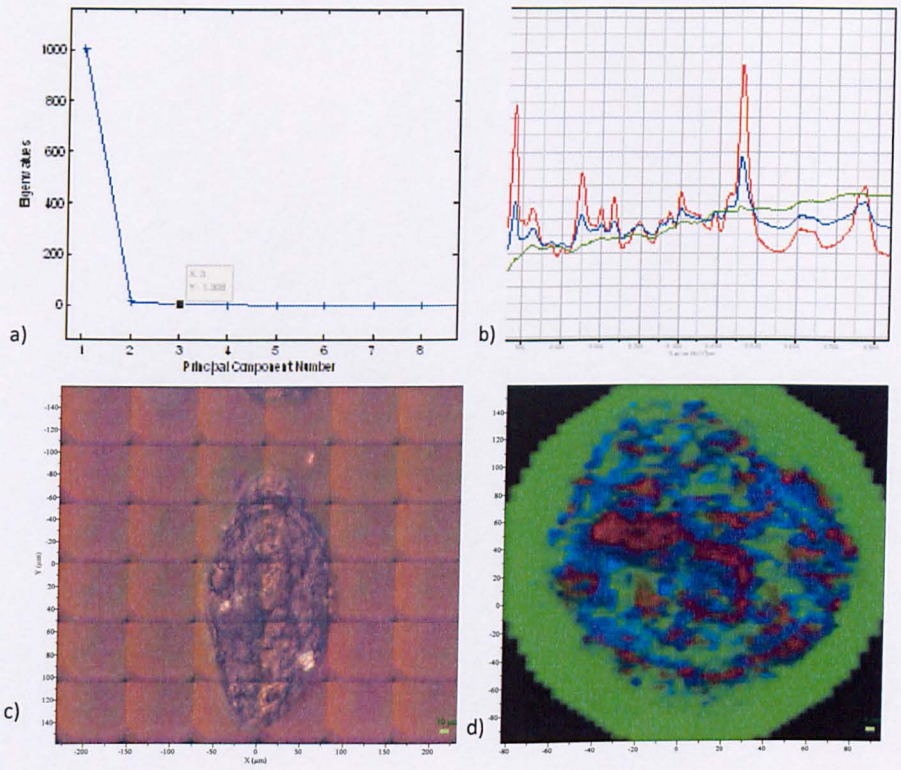

Figure 3.32: Eigenvalues plot versus PCs numbers of the Cap/PLGA = 50/50 mixture b) 3 model spectra used to create the chemical map, where the green corresponds to background areas and the red and blue to captopril/PLGA mixture c)optical microscope image of deposited product d) Chemical image of the

3.5.5.3 Hydrochlorothiazide

As shown from the eigenvalue plot versus the PC numbers (Figure 3.33,Figure 3.34a,Figure 3.35a and Figure 3.36a), PCA analysis suggests using 2 factors to create the chemical image of the sample except the 1/1 HCT/PVP sample. Like in the case of felodipine/PVP system, the model spectra, indicates that the product of all the ratios HCT/PVP is homogenous as all model spectra contain peaks of both HCT and PVP. Moreover the green spectra in all the cases correspond to areas with less quantity material. Moving to the centre of the droplets the deposited material increases and the model spectra became stronger. The yellow areas correspond to areas where both the green and the red spectrum contribute to the spectrum in this areas.

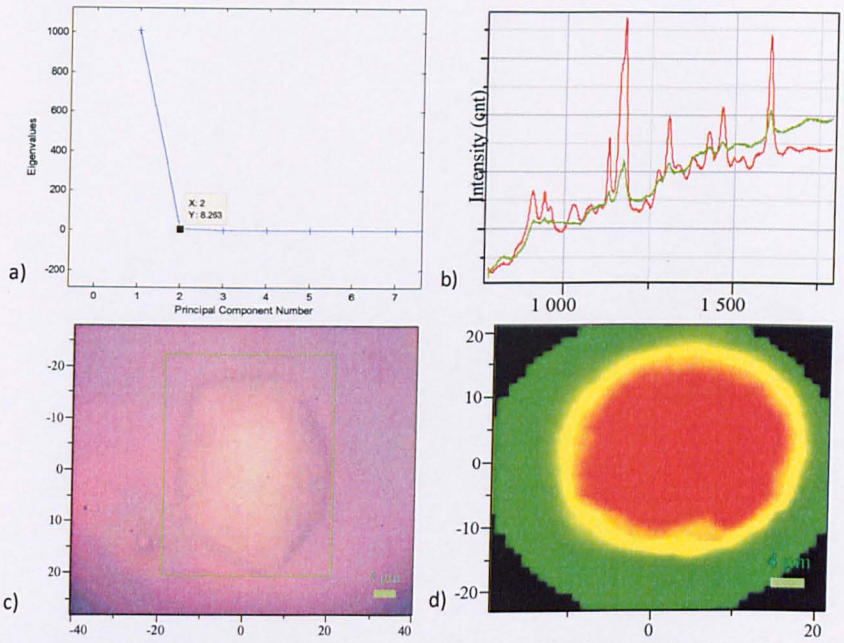

Figure 3.33: a) Eigenvalues plot versus PCs numbers of the HCT/PVP = 2/1 mixture b) 2 model spectra used to create the chemical map, where the green and red correspond to both background and sample respectively c)optical microscope image of deposited product d) Chemical image of the mixture.

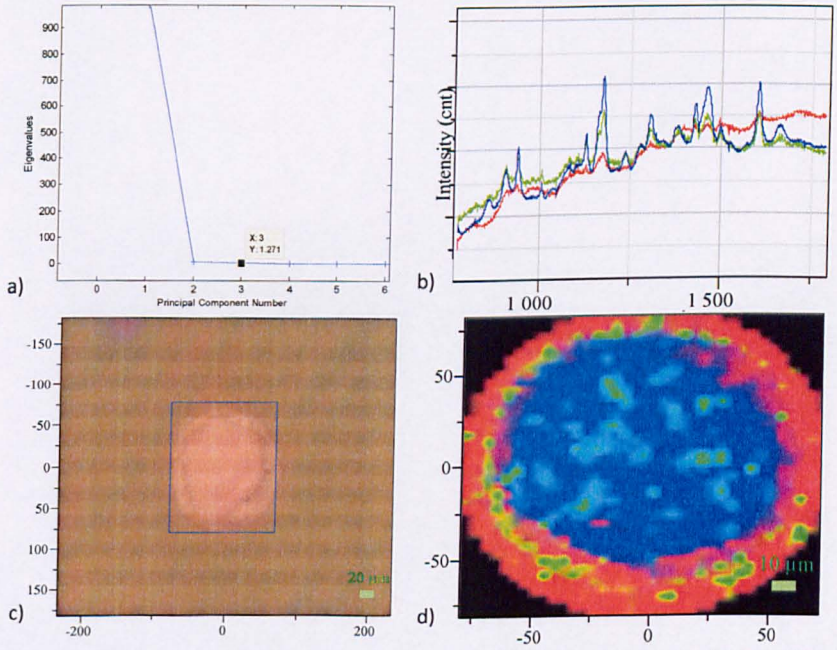

Figure 3.34: Eigenvalues plot versus PCs numbers of the HCT/PVP = 1/1 mixture b) 2 model spectra used to create the chemical map, where the red corresponds to background areas and the blue and the green to the captopril/PLGA mixture c)optical microscope image of deposited product d) Chemical image of the mixture.

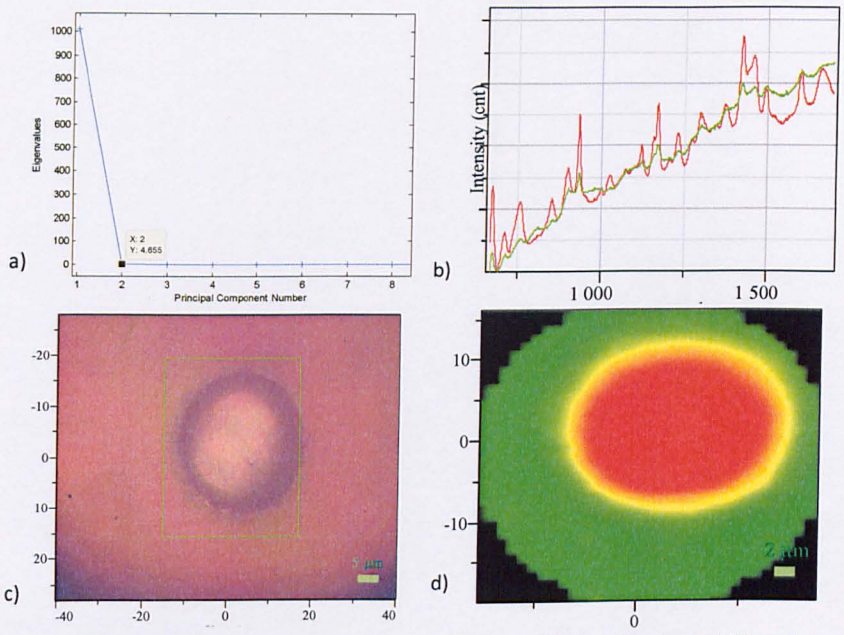

Figure 3.35: Eigenvalues plot versus PCs numbers of the HCT/PVP = 1/2 mixture b) 2 model spectra used to create the chemical map, c)optical microscope image of deposited product . The green corresponds to background and the red to HCT/PVP mixture d) Chemical image of the mixture.

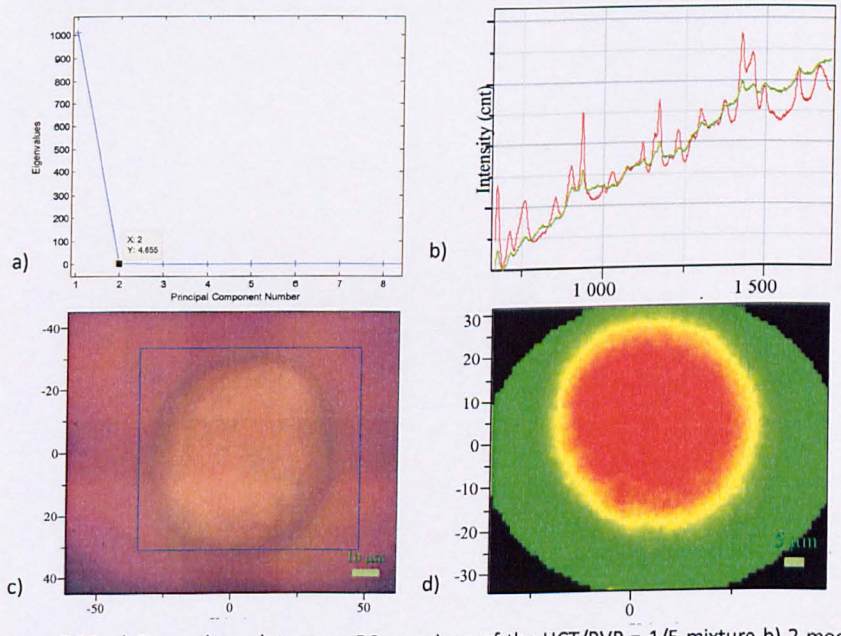

Figure 3.36: a) Eigenvalues plot versus PCs numbers of the HCT/PVP = 1/5 mixture b) 2 model spectra used to create the chemical map, c)optical microscope image of deposited product d) Chemical image of the mixture.

In Figure 3.37a the Eigenvalues plot with the principal components for the HCT/PLGA 30/70 is illustrated. From this plot, it is clear that the factors that can contribute to the obtained spectra are the first five. The chemical map Figure 3.37d has been

created by separating the spectra in to five principal components. Hence, the areas corresponding to yellow model spectrum are areas containing only HCT since the characteristics peaks of PLGA such as the carbonyl group at 1760cm^{-1} are missing in model spectra. The red, purple and blue area contain both HCT and PLGA as the model spectra corresponding to these contain the characteristic peaks of HCT and the characteristic peak of PLGA at 1760cm^{-1}. However, they are not equally distributed as the ratio of these characteristic peaks of HCT and PLGA is not the same to all the model spectra. Hence, the blue areas where the ratio of the C=C of HCT to the carbonyl group of PLGA is the biggest, contains the higher concentration of HCT where the red and purple areas the lower concentration as the ratio is the smallest. Also, the optical microscope image combined with the chemical image shows that the polymers have been accumulated at the top of the sample, in contrast with the drug which is distributed in all the place.

The chemical images of the mixtures of HCT and PLGA at ratios of 30/70 and 20/80 are illustrated in Figure 3.37 andFigure 3.38. In the case of 30/70 HCT/PLGA the green spectrum corresponds to the background whereas the others correspond to the sprayed product. As these spectra, contains peaks of both the compounds such as the strong C=C peak of HCT at 1604 cm^{-1} and the carbonyl peak of PLGA at 1750 cm^{-1}, both the compounds are distributed to all the sample.

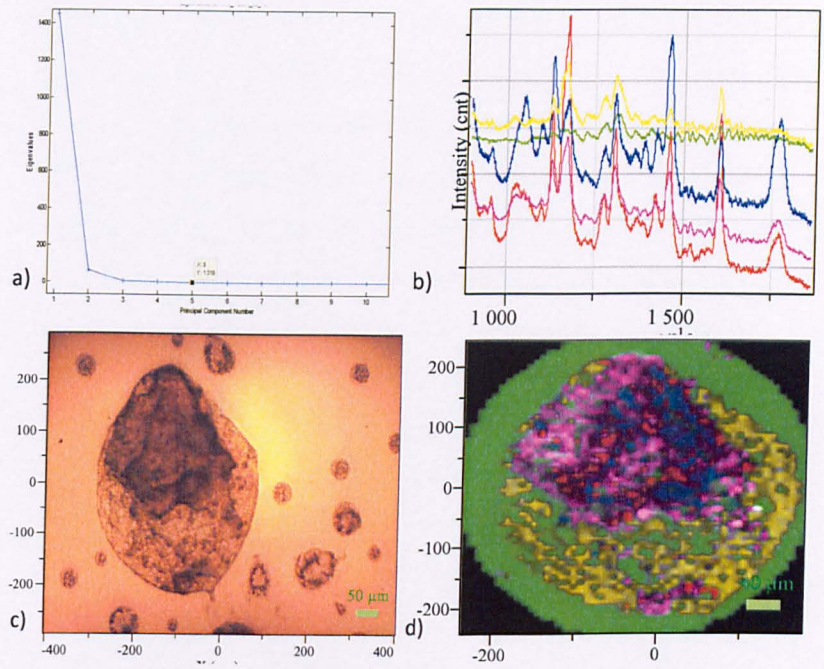

Figure 3.37: : a) Eigenvalues plot versus PCs numbers of the HCT/PLGA = 30/70 mixture b) 5 model spectra used to create the chemical map, where the green, yellow correspond to background and to HCT respectively whereas the red, blue and purple correspond to areas with mixture of HCT and PLGA in different concentrations c) optical microscope image of deposited product d) Chemical image of the mixture.

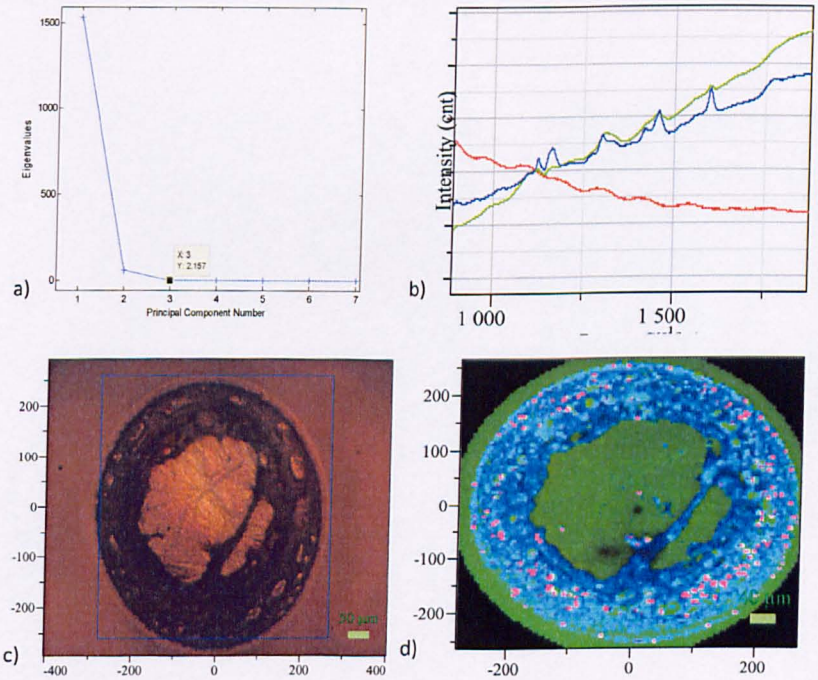

Figure 3.38: : a) Eigenvalues plot versus PCs numbers of the HCT/PLGA = 20/80 mixture b) 2 model spectra used to create the chemical map, c)optical microscope image of deposited product d) Chemical image of the mixture.

In the case of the mixture of HCT/PLGA/Pluronic mixture the PCA analysis showed that four factors contribute to the spectra obtained (Figure 3.39a). Hence, the chemical map of the spot has been separated in to four PCs. The purple and blue spectra contain peaks of both HCT and PLGA indicating the coexistence of the two compounds. The red spectrum corresponds to areas with HCT as only the peaks of API appeared. The green model spectra express areas which contain the less material. Unfortunately, Raman was not able to distinguish the pluronic's characteristic peak due to its low concentration and because most of the pluronic peaks are overlapped from those from PLGA and HCT. Finally, the optical microscope image combined with the chemical image shows that the API is evenly disturbed combared with the polymers.

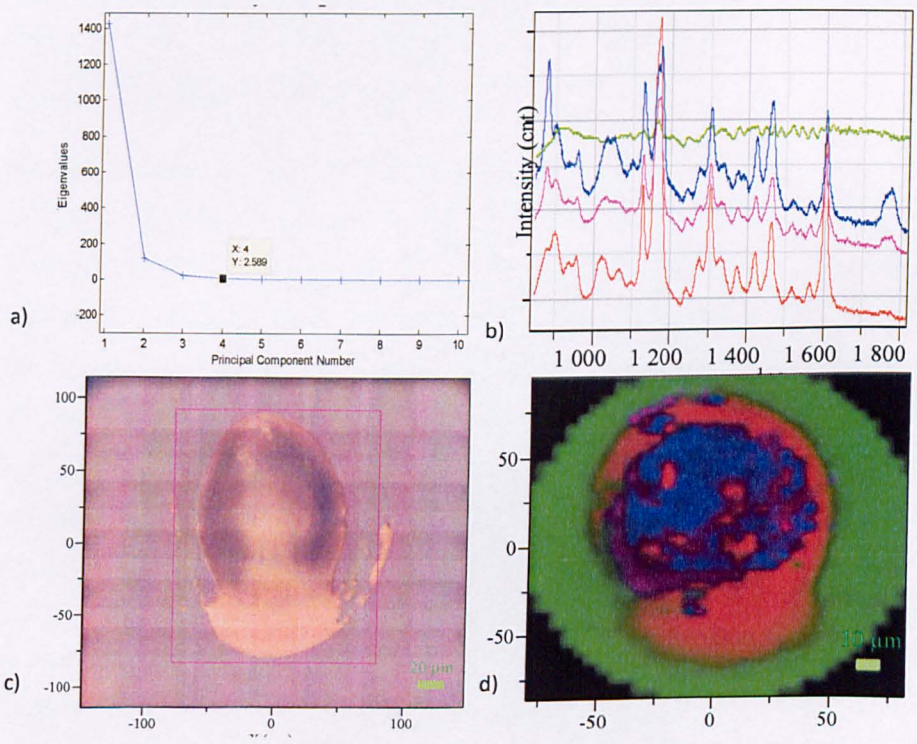

Figure 3.39: a) Eigenvalues plot versus PCs numbers of the HCT/PLGA/Pluronic = 50/45/5 mixture b) 4 model spectra used to create the chemical map. The green spectrum corresponds to background, the red spectrum corresponds to pure HCT and the pink and the blue spectra correspond to the mixture of HCT/PLGA c)optical microscope image of deposited product d) Chemical image of the mixture.

3.6 Discussion

In this chapter, drug formulations of felodipine, captopril and hydrochlorothiazide with polymers have been prepared by using the inkjet printing method. A combination of micro and nano analytical methods has been implemented to study the physicochemical properties of these formulations.

3.6.1 Felodipine

In terms of the felodipine/PVP system AFM confirms that the product is homogenous, amorphous without phase separation at the drug-polymer ratios used. Also, the importance of the evaporation rate has been confirmed as it can affect the physical form of the final product. A slow evaporation rate can lead to crystallization, which can lead in turn to a dramatic change in therapeutic properties of the medicine through a reduced solubility.

The homogeneity of the product was confirmed by LTA, where only one glass transition point was detected for the mixtures at the micrometre (SThM) and nanometre scale (NTA). However, it is worth noticing the differences between the measured T_g and the theoretical values derived from the Gordon-Taylor equation. The reason for this is probably related to the fundamental principle of LTA. In general, at both the micro and nano-scale the thermomechanical contribution of the physical contact area of the tip is an important factor in the thermal response of the samples. Tsukruk *et al.* investigated this mechanical contribution by measuring the probe heat dissipation which is dependent on the probe/surface contact area for a certain material. The results showed that at an increasing indentation depth, there is an increase in the observed temperature for a glass transition above its actual value [144]. This phenomenon has a smaller effect on the measurements of the SThM due to the larger size of the initial contact region [145]. It is important to note that these phenomena do not affect the observation of a single T_g.

ATR spectroscopy reveals the association of felodipine with PVP to be via hydrogen bonding consistent with previous publications. In comparison to the literature the current study reveals the association of the drug and the polymer with two kinds of bonds even at a 2/1 Felodipine/PVP. Previous studies of solid dispersion of felodipine

with the PVP showed that at the higher concentration of felodipine only one peak at the higher wavenumbers of the amino group appears indicating only weak hydrogen bonds are formed [132]. This may be due to the inkjet printing method, where the amount of product is much less than in bulk solid dispersion methods. Consequently, the solvent is evaporated more rapidly possibly leading to a more intimate interaction of the PVP and felodipine. Also, ATR revealed that the hydrogen bonding among the felodipine's molecules in the amorphous sprayed material are stronger than in crystalline powder as the peaks corresponding to the amino group move to lower wavenumbers. This has also been confirmed by previous work [121].

Confocal Raman microscopy has been applied as an additional analytical method to confirm the homogeneity of the product. The chemical map of the samples were processed using direct classical least square (DCLS) based on the algorithms of the NGLabspec. In order to choose the number of factors that contribute to the plot of chemical mapping, the Eigenvalues of each principal component was analysed. The PC Eigenvalues decrease with the number of components and level off when the complete signal is taken into account. For the experiments in this thesis, they sharply decrease after the first PC. Based on this behavior, it can be concluded that it is quite likely that two components exists. Indeed, the results indicate that in most of the cases two PCs, one coming from the samples and the other from the background, are enough to characterize the samples which show that both the compounds are evenly distributed along the mixture. Karavas *et al* by applying confocal Raman mapping to solid dispersions mixture of felodipine with PVP and using the ratio of carbonyl peak to carbon ring band suggested that at elevated concentrations of felodipine aggregations of API's molecules can be observed [128]. However, in our case by using NTA, a technique which can offer a much higher spatial resolution than confocal Raman microscopy did not reveal such agglomerations as all the measurements taken along the sample were far away from the glass transition temperature of felodipine.

3.6.2 Hydrochlorothiazide

AFM of HCT/PVP confirms that the product is homogenous, amorphous without phase separation at the drug-polymer ratios used. In the formulations where PLGA

has been applied the product is amorphous and there is a phase separation between the API and the polymer.

SThM also confirmed the homogeneity of the product, since only one glass transition point has been detected. As in the case of felodipine/PVP system the values from LTA are increased compared to the theoretical values from the Gordon – Taylor equation. The explanation from this phenomenon must be sought again in thermomechanical issues that govern the method. At this point, it is worth to noticing that both the lines plotted from the experimental and theoretical data are approximately parallel. This is an indication of a constant offset factor. Also, the homogeneity of the product is confirmed by the histogram of the SThM values, where in all the samples except the HCT/PVP = 1/1 sample the values are effectively constant. In the case of HCT/PVP, the high distribution of T_g values can come from the uneven distribution of the HCT in the sample, where the lower T_g values correspond to areas with highly HCT concentration.

ATR has been implemented to identify possible interactions between the HCT and the polymers. HCT can interact with PVP via hydrogen bonding of its amino groups with the carbonyl group of PVP. The potential hydrogen donors of HCT are the two amino groups of the primary sulfonamides, one from the secondary sulfonamide and one from a secondary amino group. The assignment of the NH peaks has been done previously by Tajber *et al.* [143]. In general, the best hydrogen bond donor will bond to the best hydrogen bond acceptor. Moreover, hydrogen bond donating abilities correlate with the acidities, as the more highly acidic group is a better donor among the similar functional groups. In the case of HCT, according to Adsmond et al. [146] the amido proton is more acidic than the proton in the amino group, due to the strong electronegative character of the SO group which is able to polarise the nitrogen atom positively which in turn facilitates the release of the proton. Consequently, the API will interact with PVP via the amido group and therefore the peaks corresponding to NH of the sulphonamides will be shifted. Consequently, from the Figure 3.16d the first and second peak in the crystalline HCT powder can be assigned to the to the primary and secondary sulphonamide N-H peak, as these two peaks were shifted to lower wavenumbers when PVP was added. Unfortunately, the ATR spectrum was not able to distinguish the other two amino groups.

Raman spectra are consistent with the ATR spectra as the amino peaks became broader in the sprayed material and are moved to lower wavenumbers. From Figure 3.23 the peak of the amino group at 3360 cm^{-1} of the powder has shifted slightly when PVP is added and hence it will correspond to the asymmetric bonded stretch of the amino group of the primary sulphonamide. The amino groups at 3267 cm^{-1} moved to even lower wavenumbers and therefore corresponds to symmetric stretch of either the amino group of either the primary sulphonamide or to the secondary sulphonamide. Unfortunately, due to the broadness of the peaks, it is not clear whether the amino peak at 3168 cm^{-1} has moved to a lower wavenumber (Figure 3.22). However, Tajber *et al.* by using FTIR suggested that this peak must correspond to the stretching vibration of the primary sulphonamide [143]. The stretching of the secondary amino group is covered at by the peak of the asymmetric NH_2 stretch.

Also, vibrational spectroscopy was applied to investigate any possible interaction between the HCT and the PLGA. HCT and PLGA both can act as donor and acceptor in a hydrogen bond, as the hydroxyl group of PLGA can bond with the SO group of HCT and also the carbonyl group can interact with the amino groups of HCT. However, considering the large polymeric chain of PLGA, where only the carbonyl group exists, whereas only one hydroxyl moiety is present for each polymeric chain, PLGA can be expected to act as an acceptor rather than a donor. Nevertheless, neither ATR nor Raman confirmed any peak shift of the carbonyl peak of PLGA remains in the same position with the pure PLGA. However, ATR showed a peak shifting of SO of HCT to higher wavenumbers for both the ratios of HCT/PLGA which is in a lower position from the crystalline powder (Figure 3.17c). This can be justified by a possible disruption of the SO···HN hydrogen bond among the molecules of HCT and direct formation of CO···HN hydrogen bond between the HCT and PLGA. This event can increase the energy of SO groups moving the peak to higher wavenumbers. The reason why this chemical and energetic transformation is not reflected by a peak shift of NH groups of HCT could be due to the peak broadness and the loss of their intensity which makes the analysis difficult. Also, it is likely that a limited number of HCT's molecules took part to the hydrogen bonding with the polymer, which also can explain the phase separation between the two compounds which was observed from the AFM.

To plot the chemical map of HCT with the others polymers the Direct Classic Least Square (DCLS) method has been used based on algorithms from the NGLabspec software. All the results confirmed the AFM results. Like in the case of felodipine/PVP the Hence, the HCT/PVP mixture results in a homogenous product at all the ratios applied, where both the compounds were distributed evenly in the samples. HCT/PLGA results to a product where the API is homogenously distributed in the samples whereas the polymer is accumulated in a certain area of the sample. Eigenvalues, as they sharply decrease after the first PC, suggest it is quite likely that two components exist. Even though, that in the phase separated samples they can be at least 3 components, the drug, the polymer and mix of drug and polymer, there are no pure polymer areas. The main reason for the phase separation is the Marangoni effect. According to this affect the liquid and hence any solute dispersed on it is moved towards the edge of the droplet due to unbalanced surface tension forces. This surface tension gradient is caused by the solvent evaporation which cools the droplet non uniformly. The temperature at the liquid-air surface at the top centre of the droplet is the lowest due to a longer thermal conduction path to the substrate, and the surface tension is highest at this point. This produces an inward flow near the droplet surface, whose shear stress balances the Marangoni stress, i.e, the surface-tension gradient [147-148]. Another theory which has been developed by Witten's group takes into consideration the generic properties of the substrate-solvent interaction, the presence of surface roughness or chemical heterogeneities that produce contact line pinning which causes the gathering of the solute to the edge [149]. A description of the phenomenon is illustrated in Figure 3.40. If the contact line is not pinned during the evaporation, the hashed region would be removed from the drop, the interface would evolve from the solid line to the dashed line and the contact line would be moved from A to B. In the case where the contact line is pinned then there must be a flow that replenishes the liquid that is removed from the edge. At this point, it is worth noticing that these two theories complement each other; the Maragoni effect exists always but its effect can be minimized by reducing the evaporation rate of the solvent, whereas the phenomena described by the latter theory can be minimized by using a highly hydrophobic substrate (as used here) as the contact line will not be pinned. Consequently, the Maragoni effect is likely to play a dominant role in the form of the deposited material in this work. One

of the reasons for this phenomenon may be the fact that hydrochlorothiazide is soluble in acetone but not soluble in DMSO, whereas PLGA is freely soluble in both the solvents. Specifically, it has been shown by the Schubert's group that the usage of a mixture of two solvents where one of them has a low vapour pressure can improve the quality of the droplet and make it more homogenous [150-151]. As the DMSO evaporates more slowly than acetone, the concentration of DMSO at the edge will gradually increase. This will cause a decrease in the local vapour pressure, and therefore a decrease in the rate of evaporation at the edge and the amount of liquid that is transported from the centre to the edge. The 'coffee ring' effect can also be avoided by the usage of a mixture of two solvents, one with low solubility and a high boiling point and one with a low boiling point and high solubility for the compounds. In this case the dissolving potential of the solvent gradually decreases during evaporation and the compounds precipitate before a ring is formed [150]. Hence, HCT as it is insoluble in the DMSO it precipitated before the ring formation whereas PLGA as it is soluble in both, it precipitated after the evaporation of DMSO where due to the capillary forces by the evaporation will move the polymer. At this point it is worth noticing that in the case of felodipine/PVP mixture, any coffee ring formation was avoided as both compounds are soluble in ethanol and DMSO and also because of the hydrophobic which made the droplet not to e pinned on the substrate.

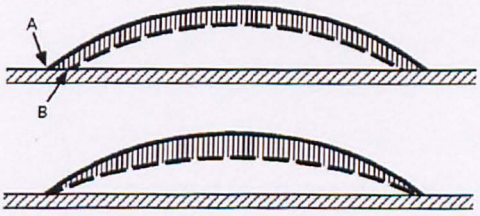

Figure 3.40: Schematic diagram of the droplet evaporation. When the contact line is not pinned, (top picture) uniform evaporation removes the hashed layer, the interface moves from the solid line to the dashed line, and the contact line will move from A to B. However, if the contact line is pinned (bottom image) then the motion from A to B must be prevented by an outflow to replenish the liquid removed from the edge.

3.6.3 Captopril

AFM reveals phase separation between the captopril and PLGA. Captopril appears as small dots which disappear after the sample is exposed to water.

ATR has been applied to investigate whether there is any conformational changes during the spraying of captopril and also if there is any possible interaction between the API and the polymer. To begin with, as shown in Figure 3.41 captopril like other proline containing peptides normally has an equilibrium conformation between cis and trans isomers.

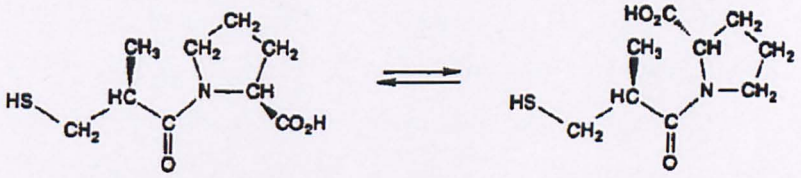

Figure 3.41: trans and cis (right) isomerization of captopril [152].

Furthermore, the trans:cis ratio at room temperature is 6:1 in aqueous solution, but the active form of captopril is the trans isomer when bound to the enzyme. However, this conformation is pH dependent. Around neutrality there is a significant amount of cis- isomer and so binding of cis isomer to the enzyme cannot be excluded a priori [153]. Therefore, the cis-trans interconversion of captopril is very important in pharmaceuticals and a number of studies have focused on its conformational analysis [154-156]. Rabenstein *et al.* found that the trans isomers of captopril in the solution were constructed by intramolecular hydrogen bonding of the amide group and the carboxylic acid hydrogen [155]. Consequently, in the trans isomer the intermolecular hydrogen bonding should be reduced due to the formation of the aforementioned intramolecular hydrogen bonding. As a result, the C=O stretching mode of carboxylic acid group and of amide group will shift to higher and lower frequencies respectively. The ATR results indicate that the sprayed drug is in cis form as the peak of carbonyl group of the carboxylic acid was moved to lower wavenumbers. Unfortunately, the peak corresponding to the C=O group of the amide is not clear enough in the crystalline material to have a clear conclusion of the chemistry of the sprayed captopril. However the double peak of the carbonyl group of the amide group indicates a coexistence of the cis and trans form.

Raman analysis confirmed the ATR results as it is clear that the C=O group of carboxylic moved to lower wavenumbers, whereas the C=O group of amide moved to higher wavenumbers, indicating the formation of the cis-isomer. Nevertheless, Raman did not show any co-existence of the two isomeric form of captopril which is

probably due to the broadness of the peak caused by the amorphous nature of the product.

When PLGA was added to the solution the C=O peak of the carboxylic group of captopril was masked by the C=O group of PLGA both in ATR and Raman spectrum. From the amide peak of captopril, ATR showed the coexistence of the two isomeric forms of captopril. Moreover, the Raman spectrum of the sprayed captopril and the captopril in the mixture Cap/PLGA are matching each other regarding the peaks of captopril, which confirms that captopril maintains the same chemical state.

Another interesting point is the absence of the SH vibration peak in the ATR. This peak should be detected at 2500 – 2600 cm^{-1} wavenumbers. Its absence could lead to the erroneous conclusion of the formation of disulfide, since captopril in aqueous solution can form disulfide (Figure 3.42).

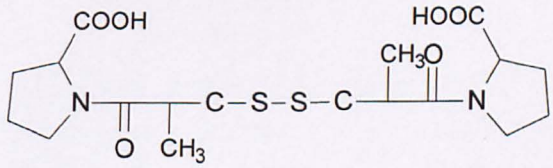

Figure 3.42: Structure of captopril disulphide.

However, the fact that the peak in question was not detected even in the powder, and that the Raman shows the SH vibration leads to the conclusion that the only forms of captopril in the solution are the cis and trans isomers.

An additional under investigation issue of the captopril/PLGA system is any possible interaction of the compounds by means of hydrogen bonding. Captopril can act either as a donor via the SH and carboxylate groups or as an acceptor via its two carbonyl groups. PLGA, as was mentioned earlier, can act as an acceptor through its carbonyl groups and as a donor through the OH group. ATR did not confirm any hydrogen bonding between the C=O group of PLGA and the SH group of captopril since the C=O peak remain at the same position with the sprayed material. Moreover, the SH peak in the Raman spectrum remains in the same position as well. For the same reason hydrogen bonding via the C=O groups of captopril and the OH group of PLGA was not confirmed as the amide peak remains in the same position

whereas the carboxylic peak was not able to be investigated as it is covered by the stronger peak of PLGA.

Raman microscopy also showed that, the compounds are evenly distributed. This does not agree with the findings from the AFM where it showed that captopril is phase separated from PLGA. The reason why the phase separation is not detected by the Raman microscopy is because of its resolution limitation which is around 1μm equal to the size of the beam. In terms of the distribution of the API and the polymer in the product, confocal Raman microscopy showed that the API tends to move to the centre, leaving the polymer at the edge. This can be justified by the fact that the polymer is deposited first and as the droplet was shrinking during the evaporation due to the hydrophobic surface the remaining compounds are deposited in the centre.

3.7 Conclusions

In this chapter three different APIs along with certain excipients were successfully printed using a piezoelectric driven dispenser. Felodipine and PVP produced a homogenous product as AFM and LTA confirmed. The interactions of felodipine with the polymer by means of hydrogen bond were also established by ATR – FTIR. Finally, Confocal Raman microscopy showed that both felodipine and PVP are distributed along the surface.

The micro-printing of captopril/PLGA solution results in a phase separated product. Also, it appears that the deposited captopril was converted from trans to cis form as shown by Raman and ATR. Finally, vibrational spectroscopy did not prove any interaction between captopril and PLGA.

Hydrochlorothiazide/PVP results are similar with the felodipine/PVP system. More specifically, it produced a homogenous product according to the AFM, LTA and Confocal Raman mapping analysis. Interaction between the two compounds has been also confirmed by ATR.

In contrast, in the HCT/PLGA system the two compounds are phase separated according to AFM. Finally, ATR showed that there can be hydrogen bonding between the NH group of HCT and the CO group of PLGA.

4. Investigation of the release of felodipine from individual printed felodipine/PVP spots

4.1 Introduction

In this chapter, the investigation of inkjet printing as a method to prepare medicines is extended. In every drug formulation, one of the most important aspects is to investigate how the drug is released. Typically, an *in vitro* drug release profile from the formulation is determined using standard dissolution apparatus type I or II following the USP standards, with the drug concentration in solution being determined by UV spectroscopy or HPLC. Specifically, the medicine is exposed to an appropriate solvent at 36°C and samples are taken at regular time points. The UV absorbance of the characteristic wavelength of the API of interest is measured and subsequently, the release profile of the API is plotted, as the concentration of the compound is proportional to the UV absorbance according to the Beer – Lambert law [157-159].

However, here, the low quantity of the deposited material does not allow the use of UV spectroscopy for the dissolution experiments. Therefore, confocal Raman microscopy was applied to investigate the dissolution properties of felodipine/PVP mixture, since the intensity of the bands of Raman spectrum are proportional to the concentration of the chemical group corresponding to the chemical group.

4.1.1 Potential incorporation of conventional control released techniques to inkjet printing

A common approach to increase the solubility of a drug substance is to reduce its particle size and thus increase the surface area in contact with a solvent for a given mass of material. Inkjet printing can provide this opportunity by spraying different quantities of material, producing a microarray, where each sprayed product will have different dissolution properties depending on the drug loading [160]. Also, the spraying of a relatively insoluble API with a soluble excipient can provide a solid dispersion product with improved dissolution properties. Application of this concept is demonstrated in this chapter where the poorly soluble API, felodipine is incorporated with soluble PVP to produce a solid dispersion mixture.

Moreover, there are various concepts which can help to prepare solid drug dosage forms by modifying the release profile of the API. For example, API could be incorporated with a slowly biodegradable polymer which can serve as a slow-release polymer matrix. This concept has been applied by Xie *et al.* where they prepared biodegradable films with controllable thickness for control sustained release applications of paclitaxel encapsulated in poly(lactic-co-glycolic acid) PLGA [161]. This concept is also discussed in chapter 6 where the release profile of hydrochlorothiazide and captopril was modified by co-spraying with PLGA.

Another potential way to modify the release profile of the drug is to spray a suitable coating onto the API. Coatings have been used to delay drug release and to protect the drug from undesirable physiochemical conditions in parts of body such as gastric environment, releasing the API at a desired location [162]. For instance ethyl cellulose in combination with hydrophilic polymers such as the co-polymer PVA-PEG [163] or HPM [164] can modify the release and protect the API from being dissolved until it reaches the desired therapeutic area.

4.1.2 Quantitative Raman Analysis

Raman spectroscopy has been proved to be an excellent tool not only as a qualitative method of analysis but also for quantitative determination of compounds in a mixture [165-166]. Several quantitative Raman studies have been applied to mixtures of liquids [167-169]. However, the use of Raman to quantify compounds in

solids mixtures is a complicated issue because the Raman bands depend on external factors such as sample alignment and homogeneity. Therefore, to gain quantitative information the ratio of two bands is used, unless an internal standard can be found [165] such as a solvent which does not interfere with the sample. In more complex systems, quantitative data are processed using chemometrics techniques based on multiple linear regression or principal component regression which depend on band intensity comparison [165-166].

In theory, the intensity of a Raman peak is dependent on the polarizability of the electrons in the molecules which leads to a complex expression of the intensity [170]. A simple formula for the intensity which is analogous to the Beer – Lambert law and it is suitable for analytical purposes can be expressed as;

$$I = KVC_0 \qquad (4.1)$$

Where I_0 is the intensity of the exciting radiation, V is the volume of sample illuminated by the source and viewed by the spectrometer, C is the concentration of the sample and K is the constant for each band.

In this chapter, the proportional association of the intensity of characteristic bands of felodipine and PVP has been used to quantify the amount of the compounds in the mixture.

4.2 Aims - Objectives

This chapter aims to study the dissolution properties of a single material spot consisting of various ratios of felodipine and PVP. Due to the low quantity of the deposited materials, the release of the API has been investigated by using the intensity of the characteristics peaks of PVP and felodipine in Raman spectra of the felodipine/PVP mixtures.

4.3 Materials - Methods

4.3.1 Materials

Felodipine was supplied by AstraZeneca (Charnwood, Leics, UK), PVP k30 and DMSO 99% anhydrous were purchased from Sigma-Aldrich. Flutec fluid was purchased by F2 chemicals (Lancashire, UK).

4.3.2 Methods

4.3.3 Preparation of solutions

Solutions of felodipine and PVP were prepared by dissolving them into a mixture of ethanol and DMSO (95/5). Felodipine is soluble in ethanol. DMSO was used to increase the boiling point of the solution to reduce chances of the dispenser clogging due to evaporation of the solvent. The ratios of felodipine to polymer were 1/10, 1/5, 1/2 (w/w). 200 droplets of each solution were sprayed onto flutec coated glass coverslips. The samples were dissolved in 2ml of deionised water and dried in the vacuum. AFM and confocal Raman studies were executed before and after dissolution.

4.3.4 Atomic Force Microscopy

AFM analysis was performed in air by tapping mode using a Dimension 3000 (Nanoscope IIIa controller, Veeco, CA). Tap300 cantilevers were used (Budget Sensors, Sofia, Bulgaria). The images were subsequent analysed using SPIP software

4.3.5 Confocal Raman

Confocal Raman studies were performed on the dried deposits from the 200 droplets using a Jobin-Yvon/Horiba micro-Raman spectrometer, by means of a red laser with a 632nm wavelength and a 600 1/nm grating. The spectrometer is equipped with an Olympus microscope BX41.

The chemical images were obtained using a 100μm slit width, a 100x microscope objective and 1 sec exposure time. Each spectrum was the mean of two

measurements. The sample profiling was performed at step increments of 5μm in x- and y- directions.

To investigate the dissolution profile of felodipine from the spot formulations, these were exposed to 2 ml deionised water media for a range of time periods, dried and the Raman spectra acquired from several points of the sample (Figure 4.1). The mean spectrum of these was applied for the analysis. The mean spectrum was created by merging individual spectra shifting the data to make the same average intensity levels on the overlapping sections. The intensity of each peak is proportional to the concentration of the chemical group that corresponds to that peak. In Figure 4.2 the change of the intensity of the carbonyl and carbon ring of PVP as a function of felodipine and PVP's concentration is represented. These figures show that as the concentration of felodipine and PVP increases, the intensity of the carbonyl peak and the carbon peak increases in proportion. Consequently, any alteration of the peaks of the carbonyl group of felodipine and of the C-ring's peak of PVP can be used to quantify the proportional change of the corresponded compound. To achieve this, a calibration curve of the concentration of the felodipine as a function of the ratio of the carbonyl peak to carbon ring peak was produced (Figure 4.3a). Based on this calibration, the change of the drug concentration in the formulation during the dissolution of the samples was determined.

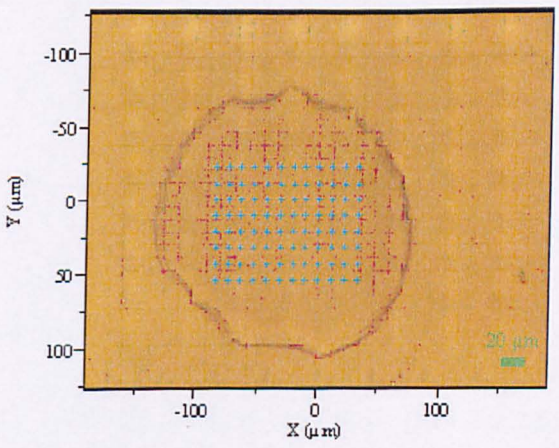

Figure 4.1: A representative optical microscope image magnified x100 of 1/5 felodipine with the points highlighted where the spectrum obtained. For the dissolution studies the mean spectrum of these were used.

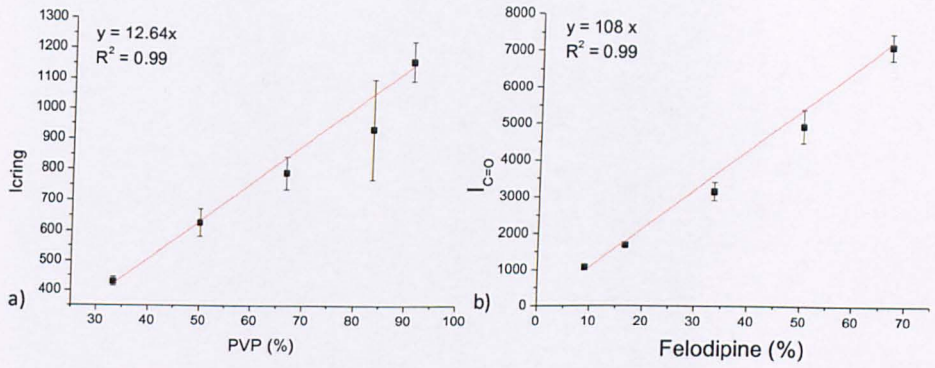

Figure 4.2: a) Change in the intensity of the carbon ring as a function of the concentration PVP in the felodipine/PVP mixture, b) Change in the intensity of the carbonyl ring as a function of the concentration felodipine in the felodipine/PVP mixture.

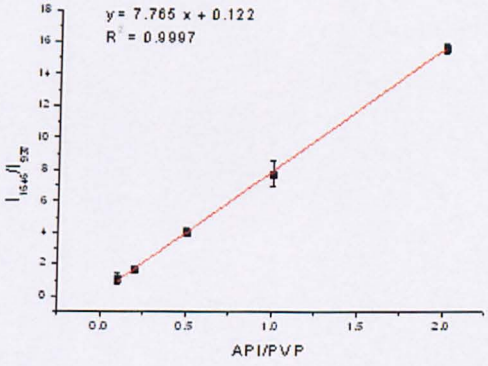

Figure 4.3: Change in the ratio of carbonyl peak to the carbonyl ring as a function of the API/PVP ratio.

4.4 Results

4.4.1 Atomic Force Microscopy

4.4.1.1 Felodipine/PVP = 1/10

Figure 4.4 shows a topographic and phase AFM image of the 1/10 felodipine/PVP mixture. Before the dissolution of the mixture small holes were typically observed due to the drying of the mixture onto the substrate. After dissolution for 3sec, larger holes could be observed whereas after 5 sec these holes had become interconnected due to the loss of more material. After 10 sec dissolution time the product was topographically homogenous as more material was lost extinguishing all the features leaving small of little holes on the sample.

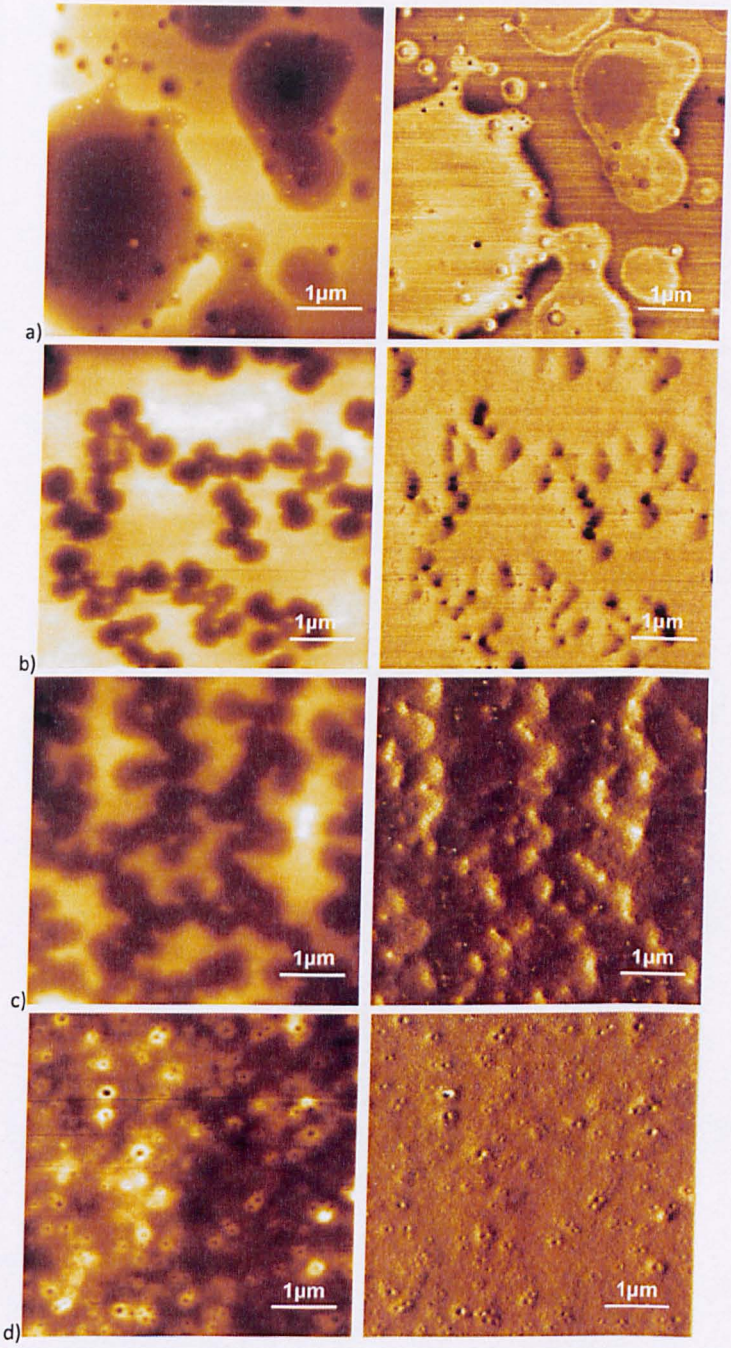

Figure 4.4: Topographic [152] and phase (right) AFM images of 1/10 felodipine/PVP mixture a) before the dissolution in water and after the dissolution for b) 3sec, c) 5sec and d) 10sec.

4.4.1.2 Felodipine/PVP = 1/5

From topographic AFM images 1/5 felodipine/PVP mixture (Figure 4.5), it is clear that as the dissolution time increases, more material was removed as expected due to the

dissolution of PVP. Also, AFM phase data did not illustrate any phase separation of the compounds or crystallization.

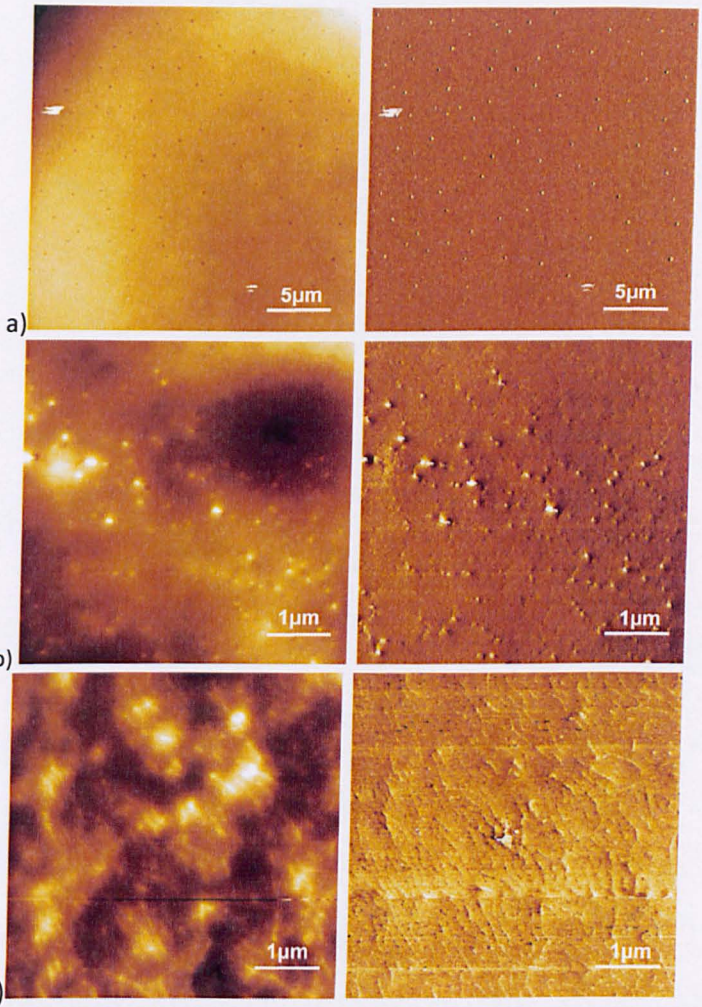

Figure 4.5: Topographic [152] and phase (right) AFM images of 1/5 felodipine/PVP mixture a) before the dissolution in water and after the dissolution for b) 3sec, c) 10sec.

4.4.1.3 Felodipine/PVP = 1/2

Figure 4.6 illustrates topographic and phase AFM images of a 1/2 felodipine/PVP mixture. The results are similar to the previous two mixtures. Hence, the dissolution results in a loss of material, however the product remains homogenous without any sign of phase separation or crystallization.

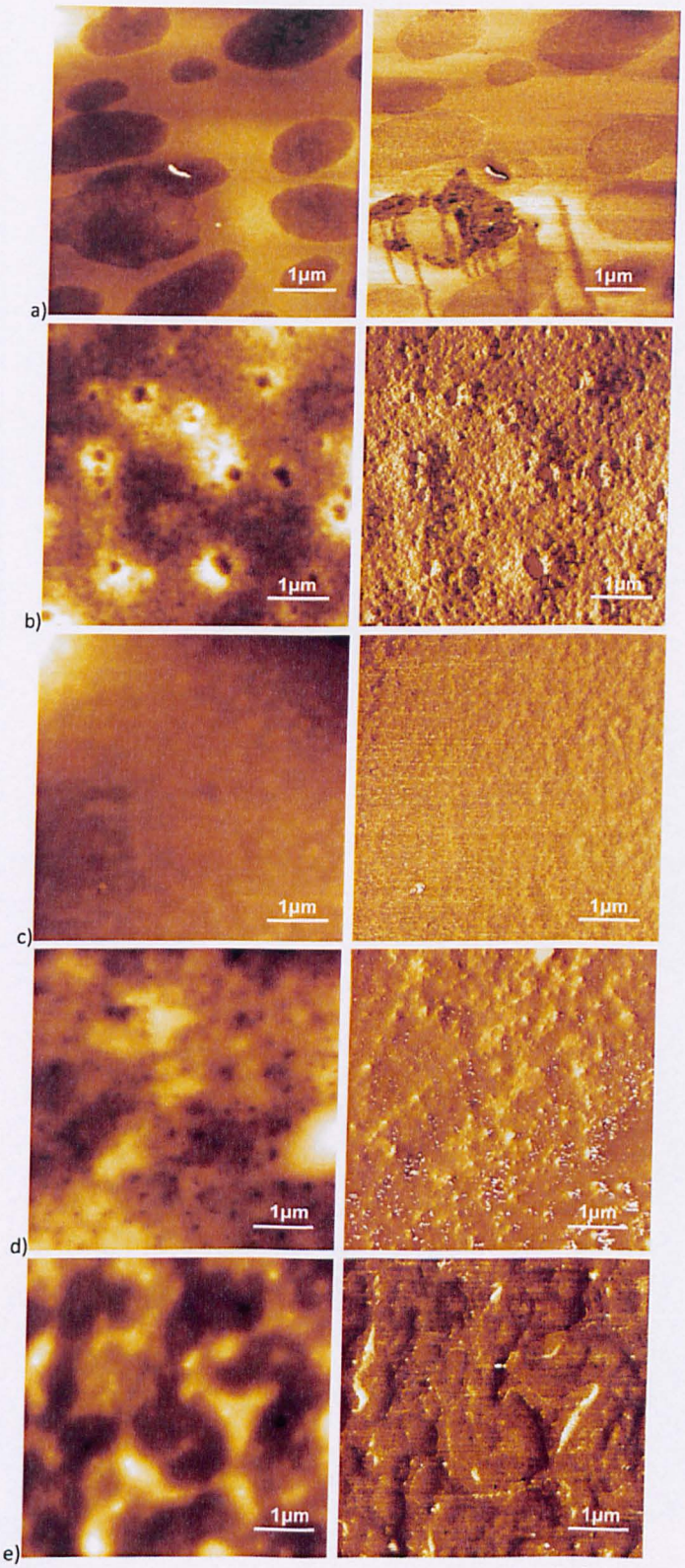

Figure 4.6: Topographic [152] and phase (right) AFM images of 1/5 felodipine/PVP mixture a) before the dissolution in water and after the dissolution for b) 3sec, c) 10sec and d) 15sec, e) 20sec.

4.4.2 Confocal Raman mapping

The most appropriate peaks of the spectra to investigate the sample during the dissolution were the carbonyl peak of felodipine at 1660cm^{-1} and the peak corresponding to the carbonyl ring at 937 cm^{-1}.

4.4.2.1 Felodipine/PVP = 1/10

Raman mapping images of the felodipine/PVP mixtures have been separated into four components. In the case of 1/10 felodipine/PVP mixture the model spectra for all the dissolution times contains the peaks of felodipine and PVP indicating that there is no phase separation between the components at the scale of observation of the Raman (approx. 0.5 μm). The model spectra have been created based on the intensity of the spectra's peaks.

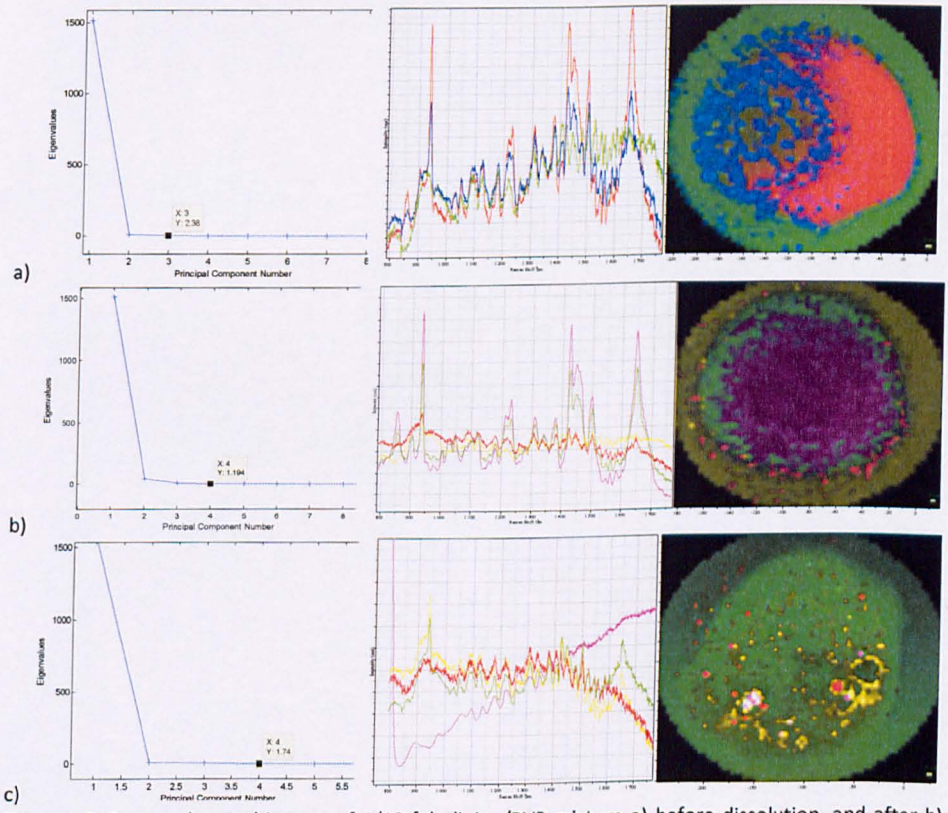

Figure 4.7: Raman chemical images of 1/10 felodipine/PVP mixture a) before dissolution, and after b) 3sec, c) 5sec, exposure to dissolution media.

4.4.2.2 *Felodipine/PVP = 1/5*

Similar data are observed for the 1/5 felodipine/PVP mixtures as for the 1/10 felodipine/PVP mixture (Figure 4.8). The product remains homogenous at all time points. Also, it is worth noticing that in the sample which is dissolved for 5sec, there are areas assigned in red colour which indicates a higher concentration of felodipine as the ratio of the carbonyl peak to the carbon ring peak of PVP is larger in the spectrum corresponding to these areas (Figure 4.8c).

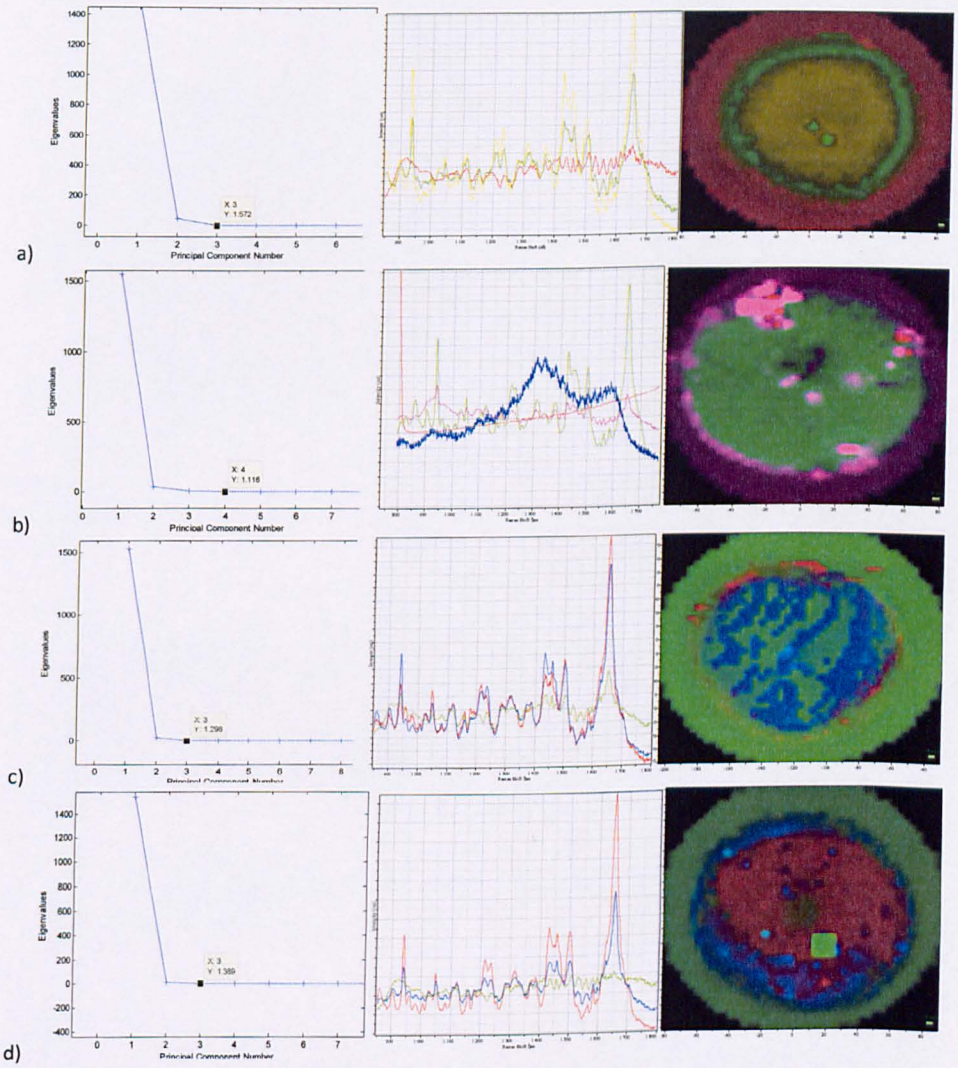

Figure 4.8: : Raman chemical images of 1/5 felodipine/PVP mixture a) before the dissolution, and after b) 3sec, c) 5sec, d) 10sec

4.4.2.3 Felodipine/PVP = 1/2

In the case of the 1/2 felodipine/PVP mixture the product continues to remain homogenous. The spectra at all the dissolution time points are qualitatively similar indicating that the sample remains homogenous during dissolution.

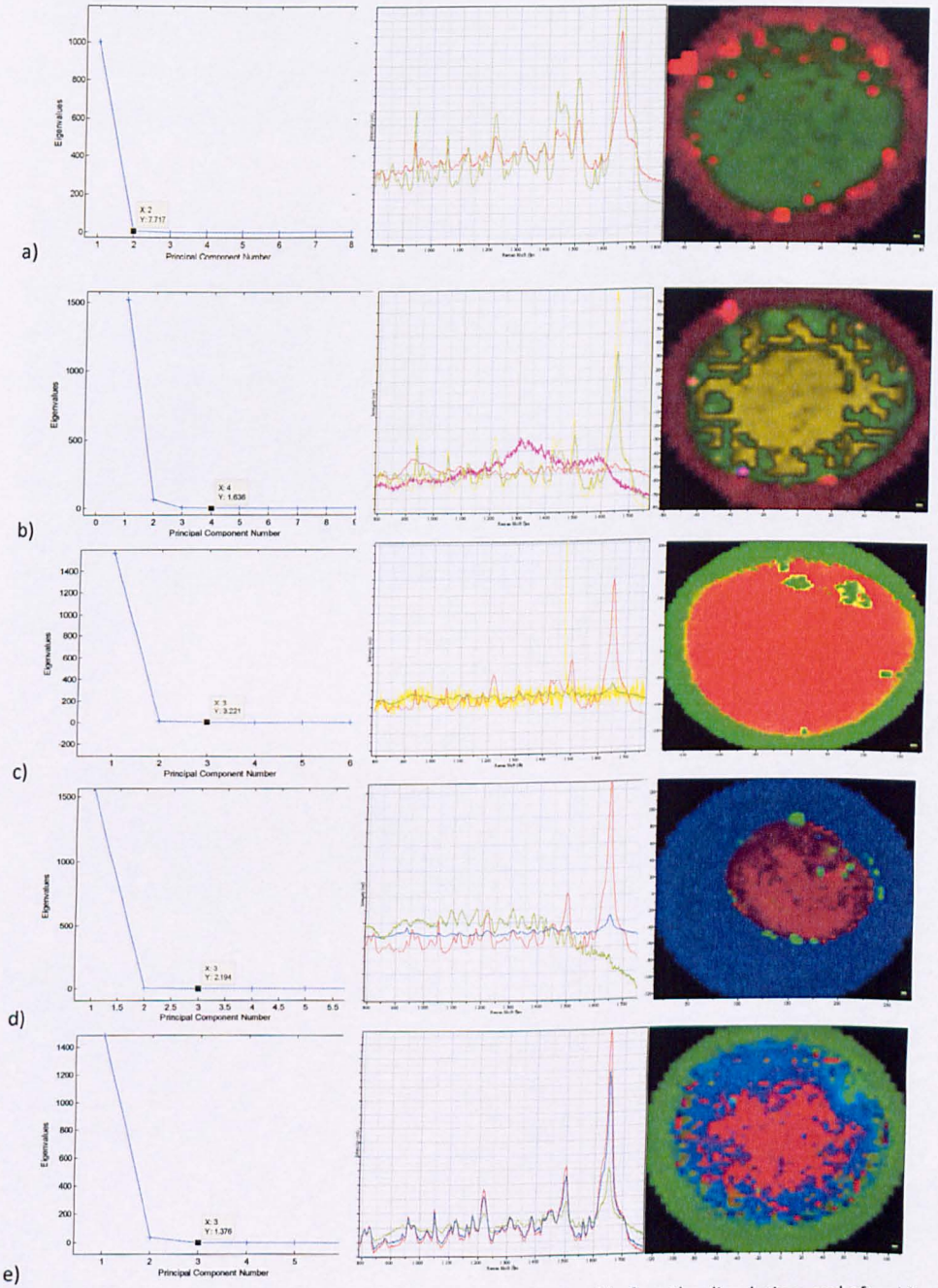

Figure 4.9: Raman chemical images of 1/2 felodipine/PVP mixture a) before the dissolution, and after b) 3sec, c) 10sec, d) 30sec, e) 45 sec..

4.4.3 Dissolution profiles

Figure 4.10 shows the mean Raman spectra at the different dissolution time points for each of the felodipine-PVP ratios. It is clear that in the case of 1/10 felodipine/PVP mixture the intensity of all the peaks are reduced, indicating that both the felodipine and the PVP are being released into solution (Figure 4.10a). In the case of 1/5 and 1/2 felodipine/PVP mixtures the peaks of PVP are reduced, whereas the peaks corresponding to felodipine increase their intensity (Figure 4.10b, c).

The dissolution profiles of felodipine from the deposited spots, i.e. the mole fraction of API versus dissolution time are illustrated in Figure 4.11 for different drug/PVP ratios. It is appears from this that the PVP is preferentially removed from the spot as the dissolution experiment progresses resulting in a relative increase of API. For ease of comparison, these data are recast as the change in the amount of felodipine during the dissolution relative to the initial amount in Figure 4.12b. Here it is clear that the loading of the drug in the deposited spots plays an important role in the dissolution properties of the formulation with the dissolution rate reduced at higher loadings.

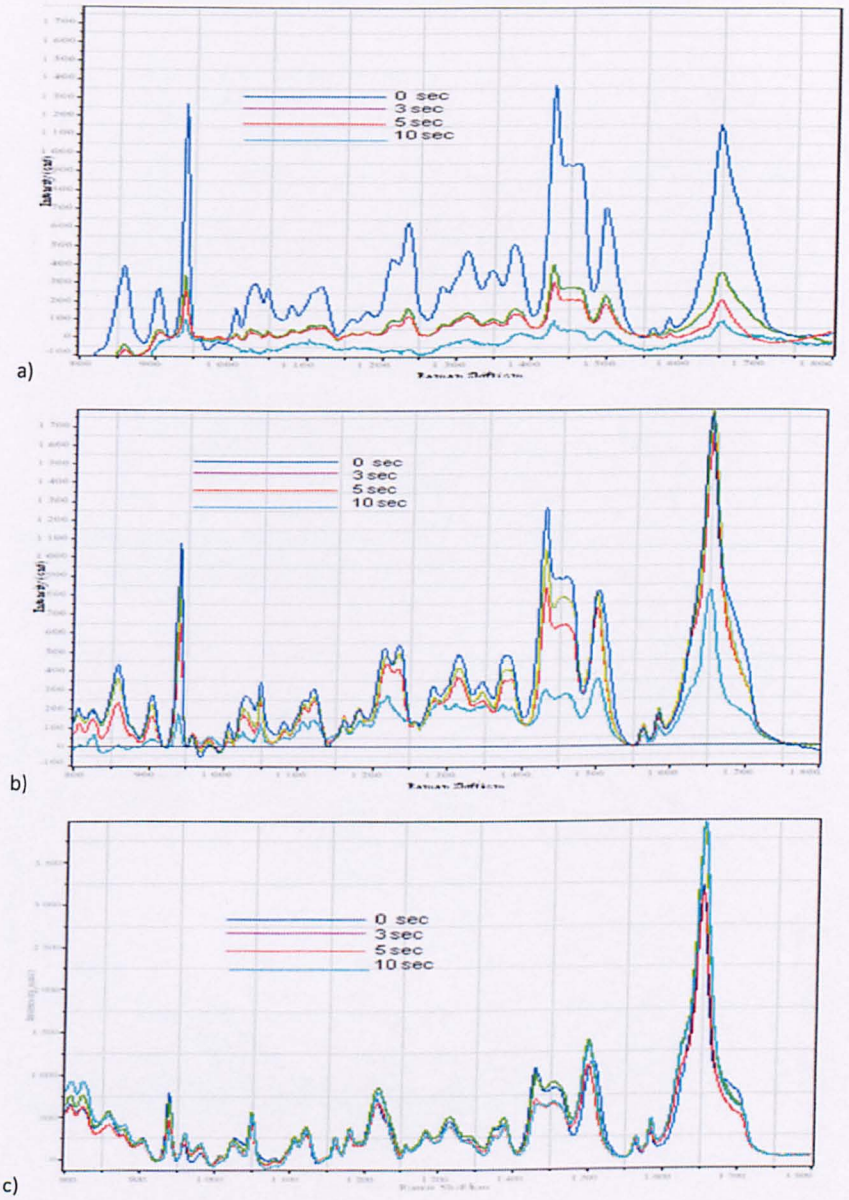

Figure 4.10: Mean Raman spectra of a) 1/10 felodipine/PVP mixture, b) 1/5 felodipine/PVP mixture and c) 1/2 felodipine/PVP mixtures

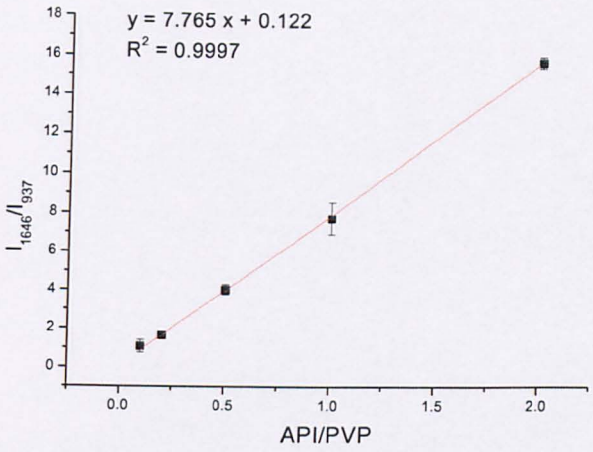

Figure 4.11: Change the ratio of the intensities of the carbonyl group at 1647cm^{-1} to the carbon ring at 937cm^{-1} as a function of the API/PVP (w/w) ratio

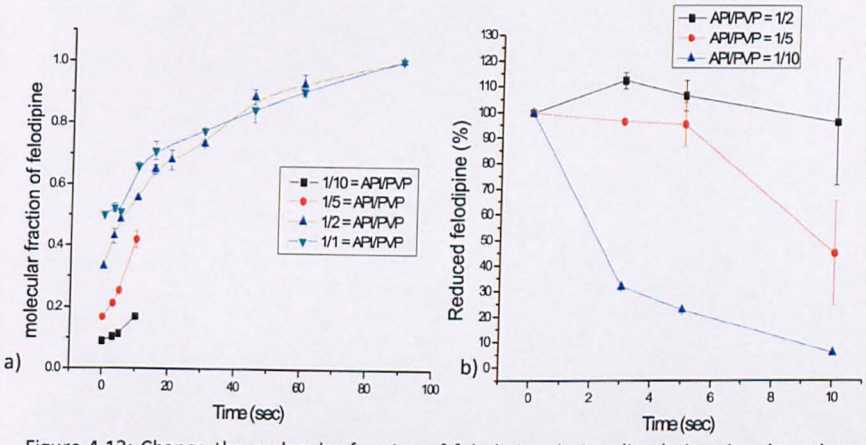

Figure 4.12: Change the molecular fraction of felodipine during dissolution time in various mixtures of felodipine/PVP, c) dissolution profiles of felodipine/PVP mixture.

4.5 Discussion

From the phase images of AFM and from Confocal Raman mapping showed that all the mixtures are homogenous without phase separation and remain so during the dissolution conditions employed. At this point, it is worth noticing that the mixture remains homogenous during the dissolution probably due to the strong interactions between the drug and the polymer, which inhibits mobility of the drug and hence its potential to phase separate and crystallize. Phase separation between felodipine and PVP is a common phenomenon in bulk formulations, for example due to the

influence of humidity. Marcac *et al.* showed that storing films of felodipine/PVP mixture in elevated moisture, leads to crystallization and subsequently phase separation [171]. However, this process was relatively slow, beginning after the first hour with a phase separation of the compounds and crystallization of felodipine after four hours. In these cases water is believed to plasticize the polymer within the dispersion leading to an increased mobility of the drug. In our case after the dissolution of the samples for some seconds, they were dried in vacuum and stored in a desiccator to avoid such humidity effects.

The dissolution studies showed that the drug dissolution profile is highly dependent on the initial drug loading. At higher loadings no detectable amount of drug was released within the timescales studied. Also, confocal Raman microscopy revealed that in simulated dissolution studies, PVP is dissolved much more rapidly than felodipine for all the drug loadings. In literature, PVP has been extensively used to increase the dissolution rate of various insoluble compounds [172-174]. Specifically, it has been shown that as the proportion of PVP increased, felodipine dissolution rates increased and reached a plateau at a ratio of 1:10 [125, 128-129]. Moreover, Kin *et al.* showed that during the dissolution process of PVP solid dispersions, the concentration of felodipine in the medium reached around eight times the solubility of crystalline felodipine and then slightly decreased with time [125] which is due to suppression of felodipine's recrystallization by the PVP[124], which is known as an inhibitor of drug recrystallization in general due to the hydrogen bonding between the drug and the polymer [175].

Moreover, it has been proved that the main factor which affects the release profile of felodipine is the intensity of this hydrogen bonding with the polymer matrix [126]. These interactions can promote the dispersion of the drug that is surrounded, in molecular level, by polymer chains, and restrict its ability to form crystal lattices with its neighbouring drug molecules [124, 126]. Also, Karavas *et al.* showed that a maximum interaction is achieved when the polymer's concentration is more than 75% (w/w), whereas below 60% (w/w) there is a dramatic decrease. Furthermore, it has been confirmed that the required molar ratio between felodipine and PVP in order for the interaction to be fully developed is 1:40 [176]. In our case both compounds are dissolved in ethanol and DMSO. As the solvents are evaporated, the

less soluble compound, felodipine in this case [177-178], will be precipitated first. Consequently, the higher concentration of felodipine is used the more material which is not associated with the PVP can exist.

Here, preliminary studies showed that when the concentration of the sprayed solution decreased from 20mg/ml to 10mg/ml in the 1/2 felodipine/PVP mixture, almost all the API was dissolved in 10secs. Figure 4.13 shows an optical microscope image of the remaining product after being dissolved in deionised water for 10sec and the model spectra used to create the mapping. As can be seen, the model spectra are the spectra of pure PVP indicating that all the API has dissolved in contrast with the 20mg/ml solution where API was remained on the surface. This phenomenon can be justified if we note that the deposited material is on a hydrophobic coated surface. This makes the product more compact on the substrate. During drying and loss of solvent the API molecules will become more crowded promoting molecular interactions.

There are also other possible technical reasons why in the present study that the drug is not to dissolved when a higher concentration of API is used. First and foremost, the intensity of the Raman peak can be affected by sample topography after the dissolution and also by any conformational change of any chemical group. It is well documented that the intensity of the Raman peak depends on the orientation of chemical groups [179-181]. For instance, when the polar orientation of a specific chemical group is parallel to the incident beam the intensity of the Raman band is at a maximum. Consequently, it is difficult to predict what effect the dissolution of the sample in water would have. Even though, AFM showed that the samples are relatively flat, on the microscale the shape of the under investigation product was topographically completely different for the dried droplets before and after dissolution.

Due to the aforementioned technical issues related to the intensity of the band, the concentration of the API was measured by both the intensity of the carbonyl peak and by the ratio of the carbonyl peak to the ratio of carbon ring of PVP. From the Figure 4.14, it is clear that there is a linear relationship between these two approaches, indicating that they are consistent.

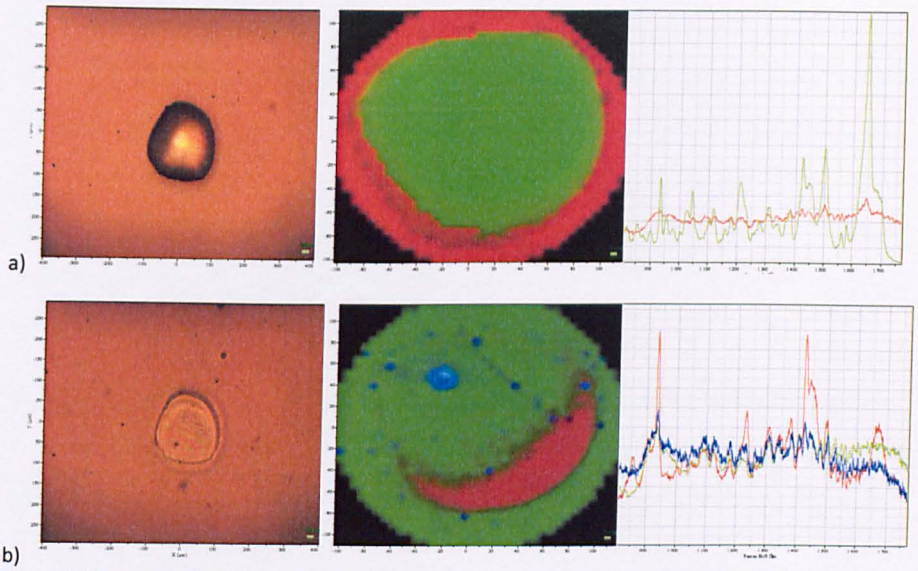

Figure 4.13: optical microscope, chemical image and the model spectra used to plot the chemical map.

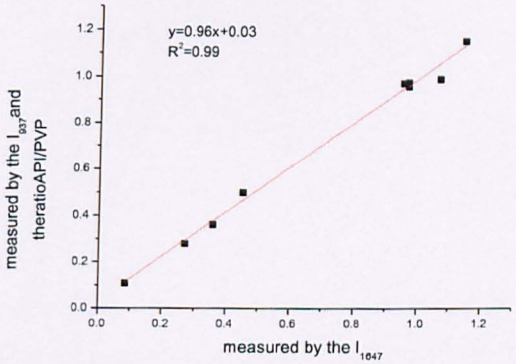

Figure 4.14: Correlation of the API's release, measured by the intensity of carbon ring and the ratio of API/PVP with the API's release measure by the intensity of carbon ring.

4.6 Conclusions

In this chapter, the release of the API from a single spot was investigated using confocal Raman microscopy. This method was used as a substitute for the conventional UV techniques. The results showed that the dissolution of felodipine is highly dependent on the concentration of API to the formulation since in the formulation where the API was less concentrated, the drug was almost all released, whereas in the other formulations with higher drug loading the drug remained on the substrate. Even though, the reason for this is unclear, it can be speculated that the increased concentration of API in the sprayed solution with the hydrophobic

substrate can bring felodipines' molecules closer inducing hydrogen bonding among them which can not break apart during the dissolution. Moreover, preliminary studies showed that the dissolution of the drug is also dependent on the concentration of the sprayed solution since by reducing the concentration to half, even the drug at 1/2 felodipine/PVP mixture was dissolved It was interesting to notice also that during the dissolution, the remaining PVP still was in homogenous mixture.

The dissolution results presented in this chapter are proof that inkjet printing can be a viable method to produce solid dispersion formulation with tailored release and for instant consumption.

5. Production of an array of a single API

5.1 Introduction

Previous chapters proved the feasibility of producing drug formulations of various APIs and excipients in dried deposits of spayed micro-droplets. The next step was to scale-up the production process and prepare a dosage form with therapeutic capabilities through the production of arrays of dried droplets. Microarray printing technology has emerged as a key tool for high throughput screening of chemical compounds.

One of the basic challenges and obstacle that had to be overcome for the preparation of the drug dosage forms based on inkjet printing was the low quantity of sprayed material in each droplet that had to be produced and analysed. To reach a therapeutic dose the sprayed solutions should be highly concentrated but this increases the viscosity of the solution. In particular, solutions of high concentration of a polymer can be highly viscous. The piezodispenser used in these experiments can spray solutions up to a viscosity of 5cp at the most and any increase in concentration of the solution should be used with caution.

To avoid an undesirable increase in the concentration of the sprayed solutions, multiple droplets can be deposited on each spot. However, as we have seen in chapter 3, the deposition of multiple droplets can cause crystallization of product due to the slower solvent evaporation.

In addition consideration should be given to possible blockage of the dispenser due to compound precipitation as described in chapter 3. To avoid this, the dispenser

was coated externally and internally with a hydrophobic material. Even though that it is not clear yet the effect that it had, there was no blockage of the dispenser.

5.2 Time of flight ion mass spectroscopy (Tof-Sims)

To show the reproducibility of the product produced by the microarray printer regarding the distribution of the API, Tof-Simns was applied.

In Tof-Sims a beam of primary ions which is accelerated to a surface causes a series of collisions that eventually lead to the emission of a variety of species from the surface, including electrons, photons, neutral species and positively and negatively charged secondary ions. This is called the sputtering effect. Secondary ion mass spectrometry (SIMS) uses this effect to obtain information about the composition of the surface by analysing the fragments sputtered from the surface with a mass spectrometer. In static SIMS, the ion dose of the primary beam is kept low (< 1013 ions cm^{-2}) in order to minimize the damage to the surface, whereas the higher dose of the ion beam used in dynamic SIMS causes erosion of the surface.

In (ToF-SIMS), sputtered ions of one polarity are accelerated to a given potential. Before reaching the detector the fragments drift through a field-free path. Since all ions have the same kinetic energy at the beginning of the path, the time it takes them to travel a ¯xed distance only depends on their mass. Lighter ions reach the detector earlier than heavier fragments and can therefore be separated from each other. The main advantage of this method is that all ions of a given charge can be analysed at the same time [182].

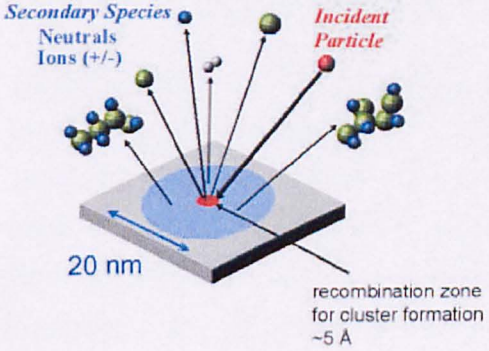

Figure 5.1: Particle beam interaction using ToF-SIMS. Incident particles bombard the surface liberating single ions (+/-) and molecular compounds.

5.3 Aims - Objective

The aim in this chapter was to produce a viable dosage form (in terms of dosage) of felodipine mixed with PVP. Microarrays of felodipine/PVP were produced and characterised using AFM, SThM, confocal Raman microscopy and Tof-SIMS Dissolution studies of the formulation were utilised HPLC.

5.4 Materials - Methods

5.4.1 Materials

Felodipine was supplied by AstraZeneca (Charnwood, Leics., UK). Polyvinyl pyrollidone (PVP) k30, poly(lactic-co-glycolic acid) (85:15) and DMSO 99% anhydrous were purchased from Sigma-Aldrich. Flutec fluid was purchased by F2 chemicals (Lancashire, UK). FASSIF powder was purchased by Phares (Basel, Switzerland).

5.4.2 Methods

5.4.2.1 Preparation of FASSIFsolution

FASSIFphosphate buffer was prepared by dissolving 0.42 gr of NaOH, 3.954gr $NaH_2PO_4 \cdot H_2O$ and 6.186gr NaCl in deionised water. The pH of the buffer was adjusted to 6.5 using NaOH. Subsequently, 2.24gr of Phares SIF Powder were dissolved in the buffer.

5.4.2.2 Preparation of substrates

Glass slides were coated by flutec fluid using dip-coating method.

5.4.2.3 Preparation and spray of solutions

Felodipine and PVP were dissolved to acetone ethanol and DMSO (80/15/5). Ethanol was used to dissolve the PVP. Acetone was used because it was found that it sprayed easier than ethanol. Also, acetone increases the evaporation rate of the solution which can inhibit the formation of crystals. DMSO has been used to decrease the evaporation rate avoiding clogging of the piezo dispenser.

Polymer microarrays were formed using an ink-jet printer (*i*) (SciflexarrayerS5, Scienion). 10 mls of wash solution (Acetone) was flushed through the system at 60 µl/s. Nozzle was then connected to the system and flushed with a further 2 mls of acetone at 10 µl/s. The nozzle used was a 90 µm hydrophobic nozzle. Printing conditions were 15ºC base temperature, 22ºC air temperature, 34% humidity, 509 Hz frequency, 164 V pulse and 64 µs pulse width. The number of spots 16×49 where 300 droplets deposited on each.

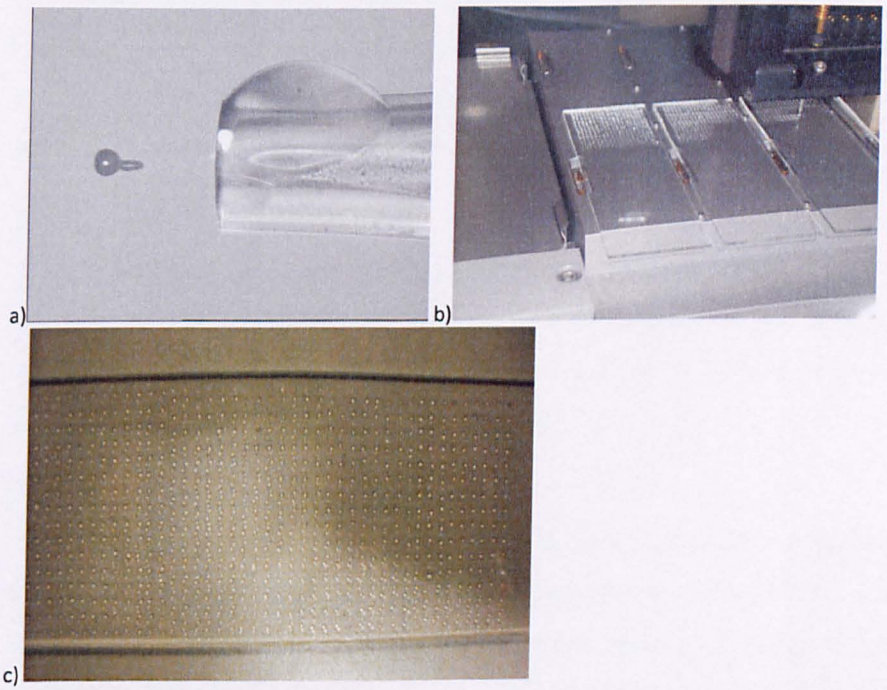

Figure 5.2: photrographic images of a) the spray of solution from the dispenser, b) the production of microarray and c) representative microarray of the sprayed felodipine/PVP mixture.

5.4.2.4 Atomic Force Microscopy

AFM analysis was performed in tapping mode using a Dimension 3000 (Nanoscope IIIa controller, Veeco, CA). Tap300 cantilevers were used (Budget sensors tapping in the air). SPIP software (Image metrology) was used to analyse the images.

5.4.2.5 Scanning Thermal Microscopy

SThM analysis was performed using an Explorer AFM system (Veeco, Santa Barbara, CA) with a Wollaston wire micro-thermal tip (Veeco). Local thermal analysis was performed with a temperature rate of 5°C/sec. The instrument was calibrated using

measurements on poly(?-caprolactone) (PCL) (Tm = 55°C), polyethylene (PE) (Tm = 116°C) and polyethylenetelephalate PET (Tm = 238°C) .

5.4.2.6 Confocal Raman

Confocal Raman studies were performed on single spots using a Jobin-Yvon/Horiba micro-Raman spectrometer, by means of red laser with 632nm wavelength and 600 1/nm grating. The spectrometer is equipped with an Olympus microscope BX41.

Confocal Raman mapping has been applied to Felodipine/PVP mixture. The sample profiling at step increment were performed on 5μm in x- and y- directions with 0.7 sec exposure time. The data analysis was carried out in the NGLabSpec software. After acquisition PCA was carried out using routines from the software.

5.4.2.7 Tof-Sims

ToF-SIMS analysis was performed using an ION-TOF IV (GmbH, Münster, Germany) instrument. To obtain spectra from eachpolymer spot secondary ions were sampled from a 100 x 100 μm area on each spot. Images and spectra were obtained using a Ga+ primary ion beam, operated at 25 kV energy.

5.4.2.8 Dissolution study of the microarray

The dissolution rate of felodipine/PVP microarray printing has been measured using a beaker shaken with a shaking stage. Each sample was placed in FASSIFsolution in a concentration of 0.056 mg/ml. At predetermined time intervals, samples of 1ml were withdrawn from the dissolution medium, filtered through 0.2μm PTFE filter and assayed using the HPLC method for the drug. The calibration curve was constructed by dissolving felodipine in methanol in known concentrations.

Figure 5.3: photographic image of the dissolution experiment.

5.4.2.9 *HPLC analysis*

The chromatographic system was an HP agilet 1050. It consisted of a C_8 gemini analytical column (100mm x 4.6mm). The mobile phase consisted of methanol and 0.05M phosphate buffer (pH 3.5) (75/25 v/v). The autosampler was set up to make 20µl injections, every 7mins. The flow rate of the mobile phase was 1ml/min and the detection was at 228nm at 40°C. The calibration curve was constructed by dissolving felodipine in methanol in known concentrations.

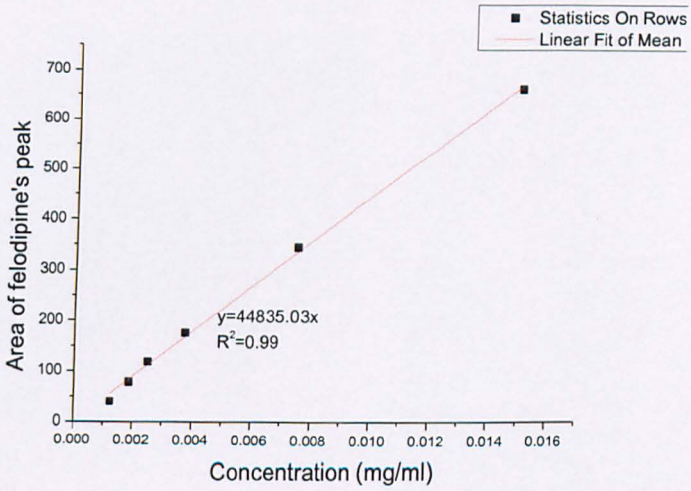

Figure 5.4: calibration curve of felodipine.

5.5 Results

5.5.1 Atomic Force Microscopy

Figure 5.5 shows AFM images of the sprayed product produced by the microarray printing device. From these images, the products in all the cases appear homogenous and there is no sign of crystallisation. The holes that appear on the surface in all the cases are proposed to be due to the dehydration of the sample during the evaporation of the solvent

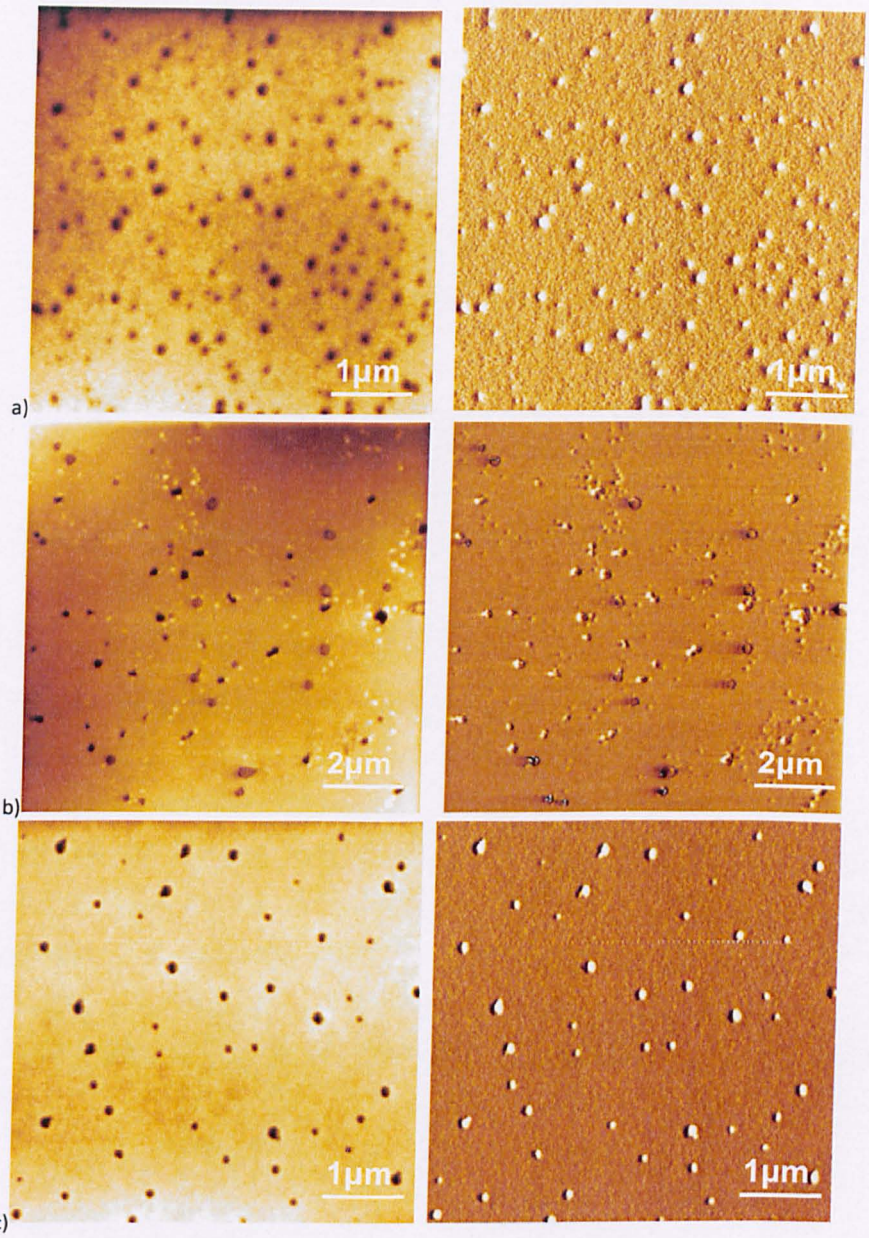

Figure 5.5: topographic (right) and phase [152] AFM images of a) 1/2, b) 1/5, c) 1/10 felodipine/PVP mixture produced by the microarray printing device.

5.5.2 Scanning Thermal Microscopy

Figure 5.6 shows the SThM results of a spot produced by the microarray printer and the DSA 100. In both graphs, there is single transition point, which increases as the concentration of polymers indicating intimate mixture of the drug and the polymer.

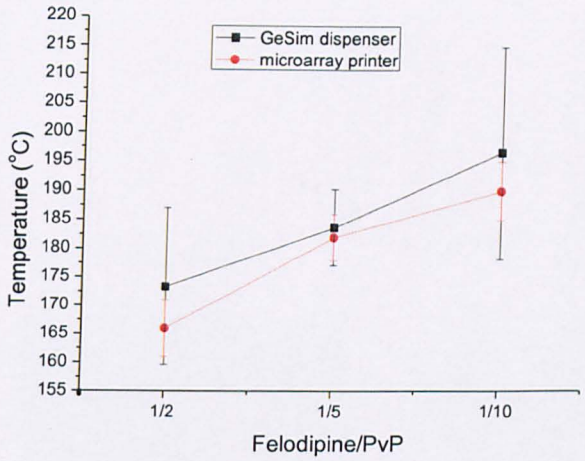

Figure 5.6: comparison the SThM results produced by the microarray printer and by the GeSim dispenser.

5.5.3 Confocal Raman Mapping

The chemical images of felodipine/PVP mixtures are illustrated in Figure 5.7,Figure 5.8 andFigure 5.9. The differences among the spectra which allow the plot of the chemical images of the samples are based on the intensity of the spectra. In all the cases, the green spectra correspond to an area with the lowest quantity of material, whereas the red spectra is the highest quantity of material as the peaks are more intense. As all the model spectra have peaks from the felodipine and PVP, the samples is homogenous without phase separation or any other chemical modification at least at the sale of observation (approx 500nm).

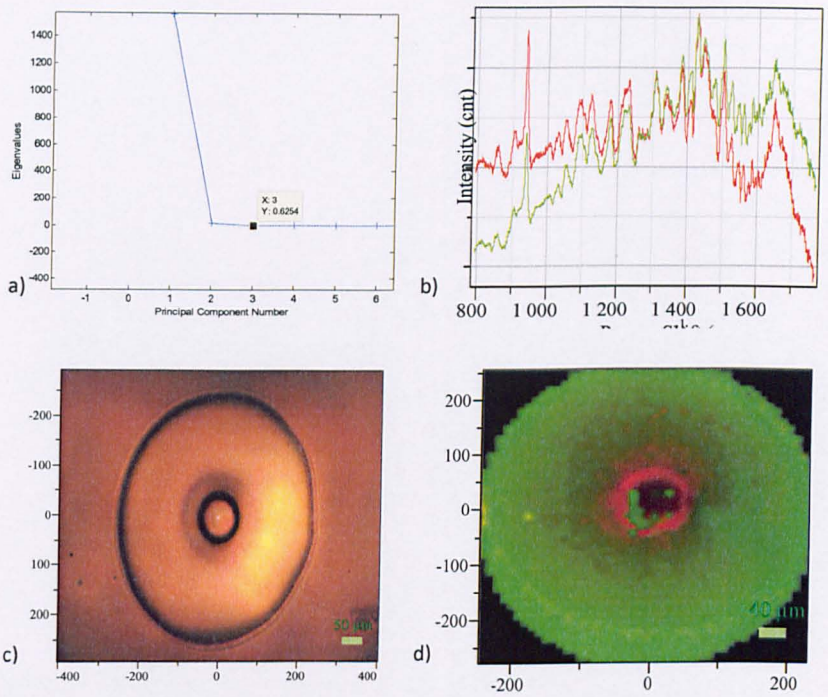

Figure 5.7: a) Eigenvalues versus principal components number, b) the model spectra used to plot the chemical map, c) optical microscope image, d) chemical map of the felodipine/PVP mixture 1/10 ratio.

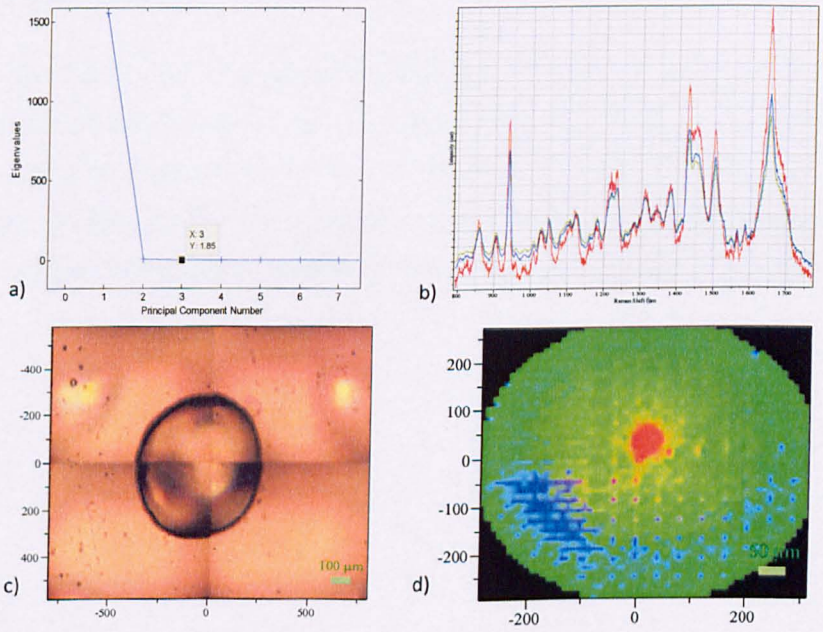

Figure 5.8: a) Eigenvalues versus principal components number, b) the model spectra used to plot the chemical map, c) optical microscope image, d) chemical map of the felodipine/PVP mixture 1/5 ratio.

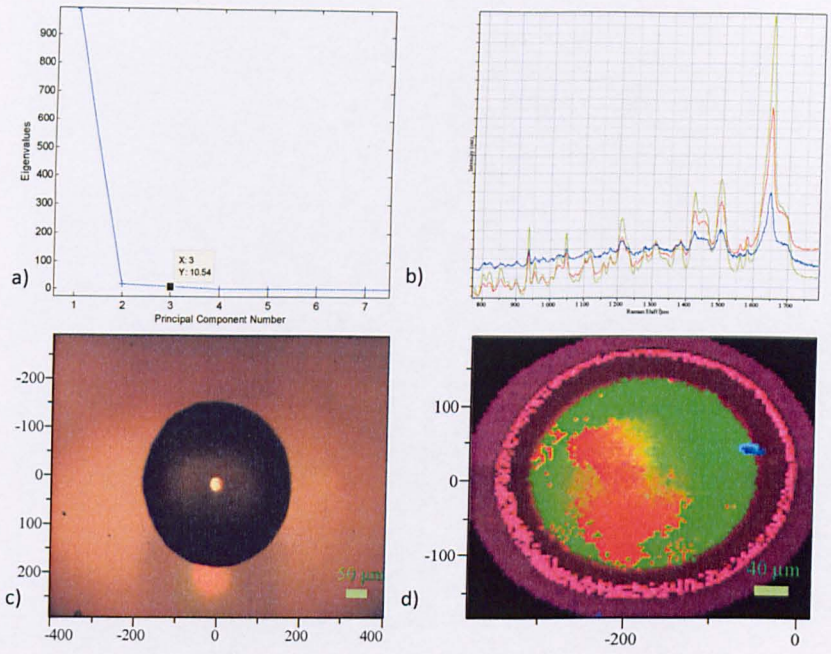

Figure 5.9: a) Eigenvalues versus principal components number, b) the model spectra used to plot the chemical map, c) optical microscope image, d) chemical map of the felodipine/PVP mixture 1/5 ratio.

5.5.4 Tof-Sims

Figure 5.10 shows the chemical image for of a pair of droplets of all the various concentration produced. As it is shown from the chlorine chemical distribution, felodipine is distributed evenly on the surface with perfectly reproducibility among the samples. Finally, it was shown that the fluorinated compound remained on the substrate without being mixedwith the solute during the solvent evaporation.

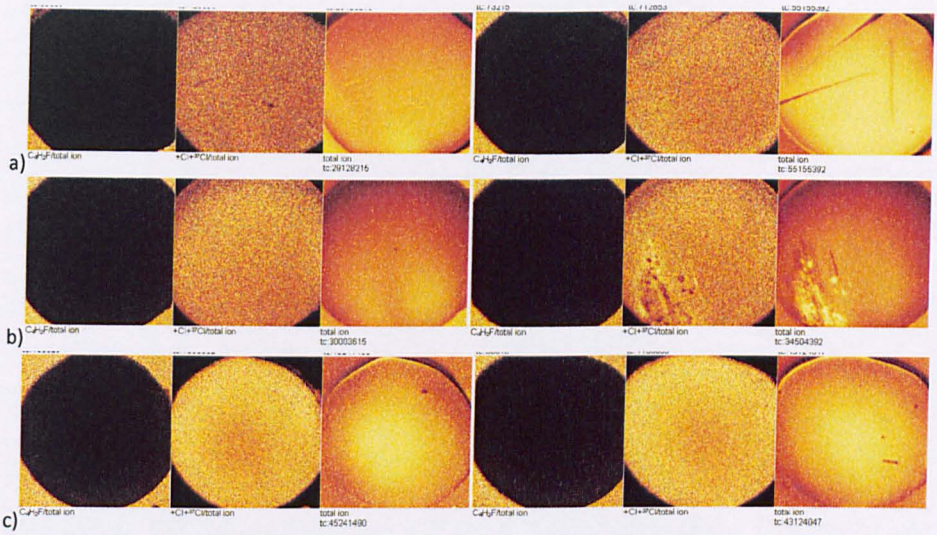

Figure 5.10: Tof-Sims images of two droplets of felodipine/PVP mixtures of ratio a) 1/10, b) 1/5, c) 1/2 produced from microarray printing machine. The left image of each pair show the substrate using C5H8F as a marker. The middle image corresponds to the position of the API using Cl as a marker and the third image corresponds to the total ion.

5.5.5 Dissolution studies

Figure 5.11 shows the dissolution profiles of felodipine from a microarray of felodipine/PVP mixtures and the pure API. In the present study, the dissolution rates of felodipine in the FASSIF solution were significantly faster than that of the pure API. The drug in the mixture with the PVP is released completely and very rapidly after its immersion in the medium.

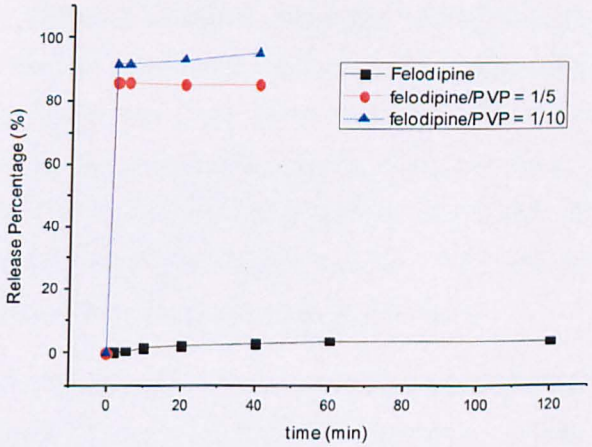

Figure 5.11: dissolution profiles of pure felodipine, and the sprayed felodipine/PVP mixture 1/5 and 1/10 mixtures.

5.6 Discussion

Atomic force microscopy shows that the sample is homogenous without any phase separation at the nanoscale or indication of crystallization. It is worth mentioning, the difference in the colour in the phase images comes from the topographical variations of the sample. The holes in the sample appear brighter in the phase image. This is because, as the tip goes inside the hole, the interactions between the tip and the sample increase due to the increase in tip-sample contact area. This is encouraging data, as it indicates that the sample is similar to the those produced in a smaller scale.

Moreover, the SThM results are remarkably comparable for drops produced by both the devices. They both gave the same pattern with the sample produced by the microarray printer providing lower values for the thermal transitions. A possible reason is that the sample produced by the microarray printing, due to the hygroscopic nature of PVP absorbed more water than the ones produced by the GeSim dispenser as they are contain more material, reducing the glass transition temperature of the sample. Besides, it was shown from previous publication that the increasing the water uptake of the samples results to a decrease in glass transition temperature of the polymers [183] which was also confirmed for felodipine/PVP mixture [123].

In terms of the confocal Raman mapping, the chemical images were plotted, separated in three principal components, as the samples consist of three different compounds felodipine, pvp and glass. Before concluding to this number of PCs, the chemical images were separated in more factors where it was confirmed that the use of more than three factors does not offer any more increase in the detection resolution. This indicates that there are no different forms of the three components in the sample and that an intimate amorphous mixture of PVP and felodipine has been created. The separation of the components occurred based on the intensity of the peaks and not on the quality differences.

There are limited numbers of papers which investigate the dissolution of felodipine in FASSiF solution. Felodipine is neutral and exhibits a water solubility of 1μg/ml at 37°C. However, FASSIF increases the solubility of felodipine by a factor of ca. 50

[184]. These experiments showed that the pure felodipine dissolves extremely slowly. Even in two hours only 3% of the drug was dissolved. In contrast, when felodipine is associated with the PVP, it releases completely and rapidly. The rapid dissolution of the mixtures may be a result of the dispersed state that the API in the polymer matrix and the low quantity of material deposited in a single spot which increases the surface area which is in contact with the dissolution medium. The reduction of particle size is a common technique used to improve the dissolution of an ingredient [185-186]. It is interesting also the fact that the felodipine dissolves very rapidly, contrary to previous work where the API when associated to PVP dissolves in a gradual manner. This is because each spot act as an independent formulation which due to the quantity will be dissolved rapidly.

However, when blank FASSIF was used as a medium, felodipine did not dissolve. In Figure 5.12 the optical microscope image and the Raman spectrum of the remaining material are illustrated. From the Raman spectrum, it is shown that the remaining felodipine is amorphous due to broadness of the amino peaks. Also, the peaks of the polymer have disappeared indicating that only the API remained on the surface. The optical microscope image, shows that some of the material was released as only approximately half of the dots remains, again most probably because of the PVP dissolution. The most probable reason why felodipine is not released from the formulation is the high concentration solution which was used in the sprayed droplet and the hydrophobic substrate. These two parameters may result the felodipine becoming associated with the substrate, inhibiting dissolution. This belief is supported by the fact that reducing the concentration of the API in the solution of the 1/2 felodipine/PVP allows the drug to be released as shown in the previous chapter.

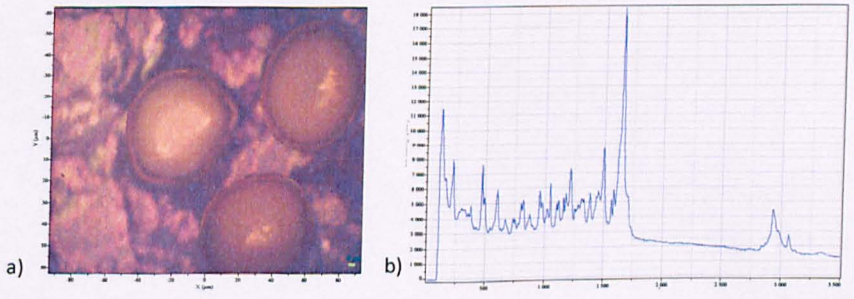

Figure 5.12: a) optical microscope image of the remaining after the dissolution product, b) Raman spectrum of the the remaining product.

5.7 Conclusions

In this chapter the production of a proper solid drug dosage form based on the current technology of inkjet printing was described. This technique can be the predecessor of a real tailored therapy. Its flexibility to spray samples with different concentration in API, which individually will follow a different dissolution profile, could allow tuning of the release drug profile according to the patient's needs.

This chapter showed that the production of a proper dosage form with the current technology is feasible. However the restriction to increase the concentration of the sprayed solution can limit the application of the technique.

In this chapter, microarrays of felodipine and PVP mixtures were prepared. AFM and confocal Raman data confirmed that the product is similar to what is produced by the GeSim dispenser as described in chapter 3, namely homogenous and amorphous. The release of the API in the FASSIF solution is rapid whereas in contrast it is almost insoluble in blank FASSIF.

6. Production of arrays of multiple APIs

6.1 Introduction

In this chapter, it is attempted to produce a proof of principal combination therapy by inkjet printing. The therapy contains two active pharmaceutical ingredients captopril and hydrochlorothiazide. These two drugs are combined in a dosage form and are marketed by the brand name Capozide™.

A challenge that needs to be faced in order to prepare a proper product is to control the release of these APIs as both are freely soluble in the medium used. For this purpose PLGA was used to create a polymer matrix which would control the release of the APIs. However, PLGA produces more viscous solutions than PVP, which was used in the case of felodipine. Hence in the previous chapter the main technical issue, we needed to overcome was the ejection of highly concentrated solutions. Also, due to the fact that PLGA produces a more viscous solution than PVP only 10mg/ml of PLGA was able to be sprayed.

6.2 Capozide formulation

Capozide™ for oral administration combines two antihypertensive drugs, captopril and hydrochlorothiazide. Capozide™ is available in four formulations of captopril with hydrochlorothiazide 25 mg with 15 mg, 25 mg with 25 mg, 50 mg with 15 mg, and 50 mg with 25 mg.

The rationale for using fixed-dose combination therapy, as in the case Capozide™, is to obtain increased blood pressure control by employing two antihypertensive agents with different modes of action and to enhance compliance by using a single tablet that is taken once or twice daily. Monotherapy is effective in achieving the target goal in only about 50 percent of patients, treatment with two or more agents from different pharmacologic classes is often necessary to achieve adequate blood pressure control. Specifically, by using a single therapeutic, the efficacy increases by the dose of a particular agent. However, as you increase the dose of that same agent, there is a simultaneous increase in dose-dependent side effects. Using low doses of two different agents can also minimize the clinical and metabolic effects that occur with maximal dosages of the individual components of the combined tablet [187-188].

The rationale behind the utilization of combination of captopril and hydrochlorothiazide is to increase the output urinary levels of potassium. More specifically, thiazides cause a reduction in intracellular sodium (Na_i) and in intra- and extracellular potassium (K_i, K_e). Since in many patients K_e losses are greater than K_i losses, the K_i/K_e ratio (which is directly related to membrane potential and thus to vascular tone) increases. Captopril also reduces Na_i but its effects on K_e and K_i are quite different from those of thiazides. Captopril in fact causes an increase in K_i inducing a net increase in K_i/K_e. This increase can also be observed when captopril is given in combination with thiazide. Therefore the combination of captopril and hydrochlorothiazide has an additive effect on Na_i, and increases K_i/K_e in the vast majority of patients [189]. Also, captopril can prevent hypokalaemia and hyperuricaemia observed with hydrochlorothiazide alone in addition to its antihypertensive synergy [190].

6.3 PLGA and Pluronics in drug delivery

PLGA is a well-known biodegradable and biocompatible polymer with a history of safe use in orthopaedics [191], bone plates [192], and extended release pharmaceuticals [95, 193-196]. Macromolecular drugs such as proteins [197-198], peptides [198-199], genes [200], vaccines and antigens can be successfully

incorporated into PLGA or PLGA-based nano/microparticles [201]. PLGA degrades chemically by hydrolytic cleavage of the ester bonds in the polymer backbone. The degradation products lactic acid and glycolic acid are water soluble non-toxic products. Polymer degradation influenced by amorphous/crystallinity, hydrophilicity, molecular weight, and the presence of excipients play an important role [202]. Consequently, the drug release kinetics from the PLGA are mainly determined by both diffusion of drug through the preformed aqueous pores and interconnected channels, as well as an erosion of the polymer matrix. Thus, the drug release rate can be affected by the inherent drug properties such as molecular size and water solubility and initial microsphere morphologies such as porosity and tortuosity.

Triblock copolymers of poly(ethylene oxide) (PEO) and poly(propylene oxide) (PPO) (PEO-b-PPO-b-PEO), available under trade name "poloxamer" or "Pluronic," are recognized as pharmaceutical multipurpose excipients capable of increasing aqueous solubility and stability of drugs. These amphiphilic copolymers are nontoxic and commercially available in a wide range of molecular weights and architectures, which determine their hydrophilic/lipophilic properties and hence show the ability to form nanoscopic core-shell structures in water. The incorporation of drugs into the core of the micelles formed by Pluronic® results in increased solubility, metabolic stability and circulation time for the drug [203].

Nowadays there is a plethora of research papers that investigate the incorporation of PLGA with pluronic. These papers mainly focus on the preparation of micro- and nanoparticles which encapsulate the biologic compound protecting it not only from the environment but also from its inactivation that may be caused by its incorporation with PLGA only [204-206].

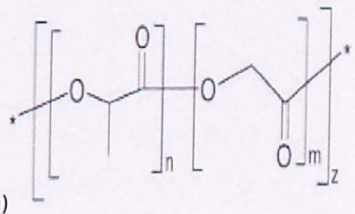

a)

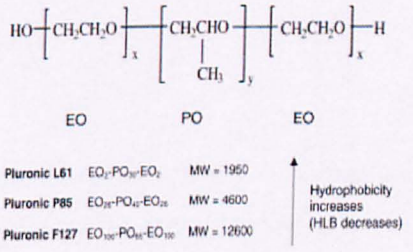

b)

6.1: chemical structure of a) PLGA b) pluronic

6.4 Mathematical models in drug release from polymer matrix

There are number of mathematical models used to describe the release of the API from a polymer matrix [43-44, 48, 207]. The main drug release mechanisms are drug diffusion from the non degraded polymer (diffusion controlled system), enhanced drug diffusion due to polymer swelling (swelling-controlled system) and drug release due to polymer degradation and erosion (erosion-controlled system). Mathematical modelling concerns unifications of all the individual parameters involved in the drug release, which involves not only mass transport and chemical processes but also design parameters such as the device geometry and drug loading.

The zero-order model expresses the dissolution from pharmaceutical dosage forms which do not disaggregate and release the drug slowly. Zero order describes a system where the release is independent from the concentration (eq. 6.1). First order release rate is concentration dependent (eq. 6.2). The Higuchi model has developed in 1963 and it was the first to specifically describe the release of drugs from a polymer matrix. It is expressed as a square root of time dependent process based on Fickian diffusion (eq. 6.3) [208]. The Hixson-Crowell cube root law (eq. 6.4) describes the release from systems where there is a change in surface area and diameter of particles or tablets (Hixson and Crowell, 1931).

$$Q_t = Q_0 + k_0 t \qquad (6.1)$$

This relationship can be used to describe the drug dissolution of several types of modified release pharmaceutical dosage forms, as in the case of some transdermal systems, as well as matrix tablets with low soluble drugs in coated forms, osmotic systems [133, 209-210].

$$\log Q_0 = \log Q_t - {}^{kt}/_{2.303} \qquad (6.2)$$

This relationship can be used to describe the drug dissolution in pharmaceutical dosage forms such as those containing water-soluble drugs in porous matrices [211].

$$Q = k_H t^{1/2} \qquad (6.3)$$

This relationship can be used to describe the drug dissolution from several types of modified release pharmaceutical dosage forms, as in the case of some transdermal systems [212] and matrix tablets with water soluble drugs [213].

$$\sqrt[3]{Q_0} - \sqrt[3]{Q_t} = k_{HC}t \qquad (6.4)$$

This model can be applied to a pharmaceutical dosage form whose drug release rate is proportional to the surface area of dosage form, such as in erosion-dependent release systems [44, 214] .

In the above equations Q_0 is equal to the initial amount of drug, Q_t is the cumulative drug release at time t, k_0 the zero order release constant, k the first order release constant, k_H the Higuchi constant and k_{HC} the Higgson-Crowler release constant

Finally, a simple empirical equation from Korsmeyer et al was introduced to describe the release behaviour from controlled release polymeric matrices.

$$\frac{M_t}{M_o} = kt^n \qquad (6.5)$$

The value of n gives an indication of the release mechanism. Hence it was stated that n is 0.5 for Fickian diffusion, $0.5 < n > 1.0$ for non- Fickian transport and 1.0 for case II transport. When $n > 1.0$ super case II transport is apparent. Case II transport involves polymer dissolution and chain disentanglement. In the case of a cylinder n = 0.45 instead of 0.5 and 0.89 instead of 1 must be used [215].

6.5 Aims - Objectives

The aim of this chapter is to produce a combination therapy based on inkjet printing. Captopril and HCT mixtures with PLGA were prepared by means of inkjet printing and also by deposition solution with pipette. The deposited products were characterised by AFM and Raman. Finally the release of the drugs was investigated using HPLC.

6.6 Materials - Methods

6.6.1 Materials

Captopril, hydrochlorothiazide, poly(lactic-co-glycolic acid) (85:15), Pluronic F-127 and DMSO 99% anhydrous were purchased from Sigma-Aldrich. Flutec fluid was purchased from F2 chemicals (Lancashire, UK).

6.6.2 Methods

6.6.2.1 Preparation of solutions

Captopril

To deposit mixtures of captopril and PLGA onto substrate, solutions of captopril and PLGA were prepared by dissolving them into a mixture of chloroform, ethanol and DMSO (75/18/7). Chloroform was used to dissolve PLGA. Ethanol was used to dissolve captopril and to disperse DMSO, as DMSO is not miscible with chloroform. Finally DMSO was used to increase the boiling point to the solution to avoid any possible cloggage in the dispenser. The ratios of captopril to the polymer were 30/70 and 50/50 (w/w), whereas the concentration of the polymer was 20mg/ml.

Hydrochlorothiazide

Solutions of hydrochlorothiazide with PLGA were prepared by dissolving them into a mixture of acetone, and DMSO (93/7). Both HCT and PLGA are soluble in acetone. DMSO was used to increase the boiling point of the solution to avoid clogging the dispenser.

6.6.2.2 Dispensing of solutions

The solutions were dispensed using either by a or a microarrays printer. When the samples were deposited by using pipette, the solutions were contained 20mg/ml PLGA in both the case of captopril and HCT. 2µl of solution was deposited on each spot of the microarray.

When the samples were deposited by means of the microarray printer the solutions were contained 10mg/ml PLGA. Captopril solution was sprayed without PLGA,

whereas HCT was sprayed with PLGA and Pluronic F-127 in a ratio of 50/45/5 HCT/PLGA/Pluronic.

Microarrays were formed using an ink-jet printer (*i*) (SciflexarrayerS5, Scienion). 10 ml of wash solution (Acetone) was flushed through the system at 60 µl/s. Nozzle was then connected to the system and flushed with a further 2 ml of acetone at 10 µl/s. The nozzle used was a 90 µm hydrophobic nozzle. Printing conditions were 15ºC base temperature, 22ºC air temperature, 34% humidity, 509 Hz frequency, 164 V pulse and 64 µs pulse width. The number of spots was 16×49, where 300 droplets were deposited on each spot.

6.6.2.3 Atomic Force Microscopy

AFM analysis was performed in tapping mode using a Dimension 3000 (Nanoscope IIIa controller, Veeco, CA). Tap300 cantilevers were used (Budget Sensors, Sofia, Bulgaria). SPIP software (Image Metrology, Denmark) was used to analyse the images.

6.6.2.4 Confocal Raman

Confocal Raman studies were performed using a Jobin-Yvon/Horiba micro-Raman spectrometer, by means of red laser with 632nm wavelength and 600 1/nm grating. The spectrometer is equipped with an Olympus microscope BX41.

Raman spectra were obtained using red laser with 632nm wavelength and 600 1/nm grating. The acquisition time was 8sec with 5 repetitions.

Confocal Raman mapping has been applied to captopril/PLGA, HCT/PLGA and HCT/PLGA/Pluronic mixtures. The sample profiling at step increment in these case were performed on 12µm in x- and y- directions with 3 sec exposure time with 2 repetitions. Raman data were collected through a 100× objective. The data analysis was carried out in the NGLabSpec software. After acquisition multivariate analysis was carried out using routines from the software. Eigenvalues and PCA when it was necessary were carried out by means of Solo+MIA software (Eigenvector, USA).

6.6.2.5 Dissolution study of the microarray

The dissolution rate of the microarrays was measured using a beaker shaken with a shaking stage. Each sample was placed in SGF solution without enzyme in a

concentration of 0.035 mg/ml. The SGF solution was prepared by dissolving 0.05M NaCl in deionised water and adjusted it at pH 1.5 with HCl. At predetermined time intervals, samples of 1ml were withdrawn from the dissolution medium, filtered through 0.2µm syringe filter and assayed using the HPLC method for the drug.

The investigation of the dissolution profile of Capozide^{TM} tablets was performed in a USP paddle apparatus 2 at a paddle rotation speed 50rpm at room temperature in 900ml SGF solution without enzyme.

6.6.2.6 HPLC analysis

The chromatographic system was an HP agilet 1050. The chromatographic column was a C_8 gemini analytical column (100mm x 4.6mm I.D., particle size 5µm). The mobile phase consisted of acetonitrile and 0.1% phosphate buffer (25/75 v/v). The mobile phase was determined so that both captopril and HCT was able to be detected simultaneously (Figure 6.2) and also because captopril exhibits the maximum stability on pH below 4 [134].

The mobile phase was also filtered with 0.2µm autofilter. The autosampler was set up to make 20µl injections, every 6mins. The flow rate of the mobile phase was 1ml/min and the detection was at 218nm at 40°C.

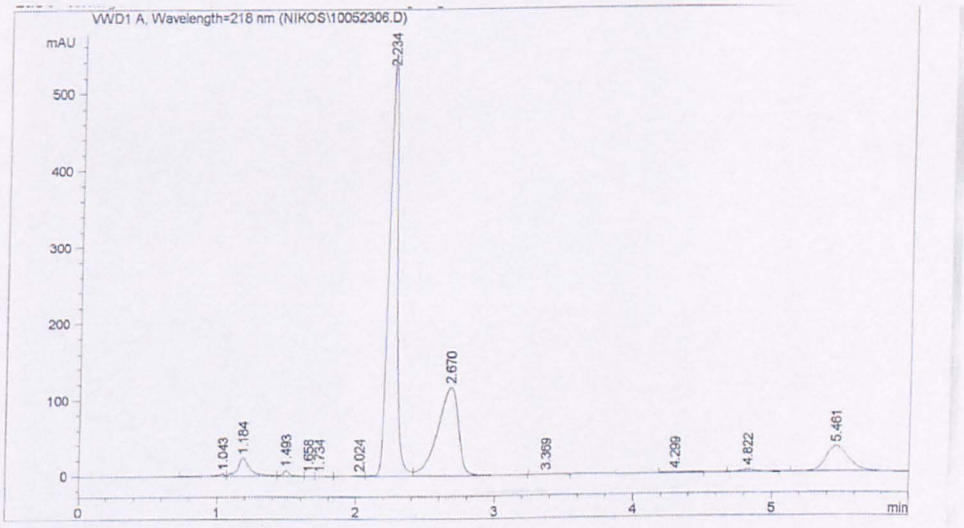

Figure 6.2: Representative chromatogram of the of the tablet. The large peak at 2.23 minutes corresponds to the HCT and the samller peak at 2.67 corresponds to captopril.

6.7 Results

6.7.1 Atomic Force Microscopy

6.7.1.1 Captopril

The product obtained when captopril and PLGA of different ratios were deposited using pipette is illustrated in Figure 6.3. When PLGA was sprayed alone the deposited material appeared amorphous and homogenous (Figure 6.3a). However, the addition of captopril resulted in the formation of small circular features on the surface and an inhomogeneous mixture (Figure 6.3b,c). These features are likely to be captopril exposed on the surface.

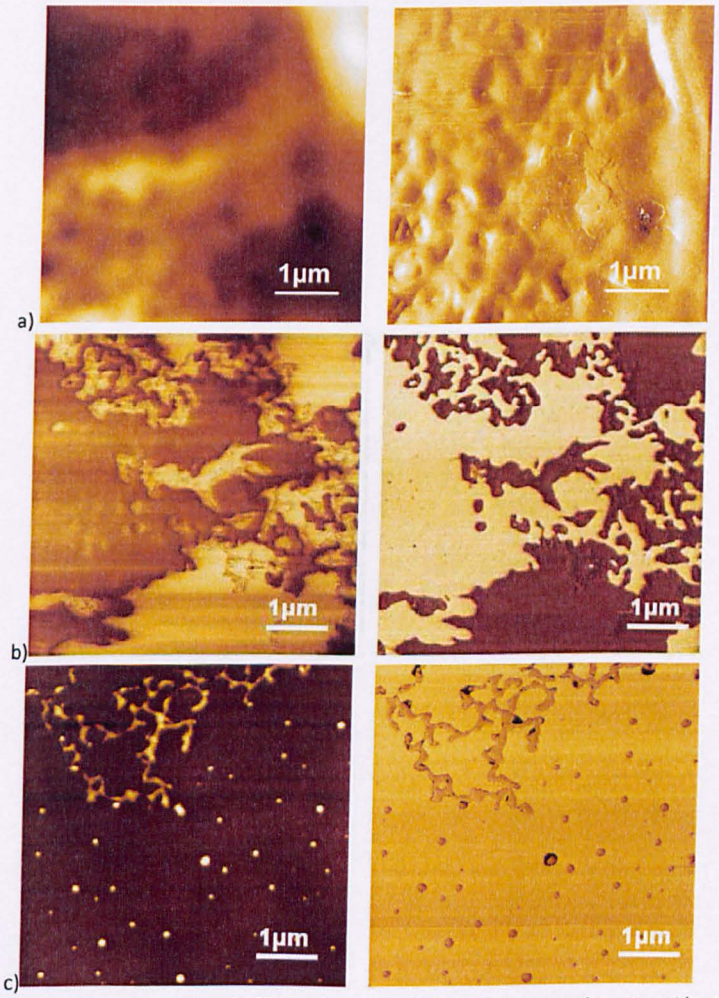

Figure 6.3: Topographic (left) and phase (right) AFM images of Captopril/PLGA mixtures of a) 50/50, b)30/70 and c) after the dissolution of 30/70 captopril/PLGA mixture for 10sec in water.

6.7.1.2 Hydrochlorothiazide

AFM images of the mixture of HCT with PLGA prepared by pipetting and by the microarray printer are illustrated in Figure 6.4. In all the cases the phase images show that there can be phase separation between the two components. The addition of pluronic resulted to a phase separated mixture (Figure 6.4c). The product occurred by using the microarray printer appeared homogenous without phase separation and with no sign of crystallization (Figure 6.4d).

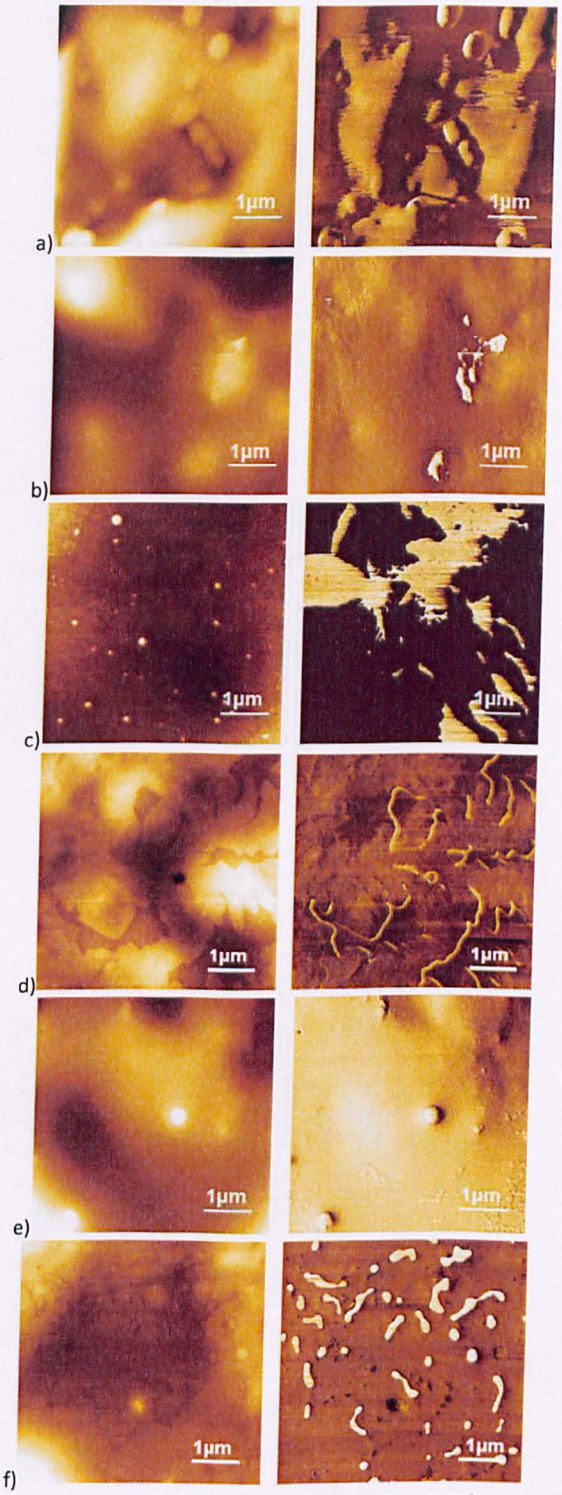

Figure 6.4: Topographic (left) and phase (right) AFM images of a) HCT/PLGA = 50/50 produced by pipette b)HCT/PLGA = 30/70 produced by pipette, c)HCT/PLGA =20/80 produced by pipette, d)PLGA/Pluronic = 90/10 produced by pipette, e) HCT/PLGA/Pluronic = 50/47/3 produced by microarray printer f) HCT/PLGA/Pluronic = 20/75/5 produced by pipette.

6.7.2 Raman Mapping

The spectra of pure captopril, PLGA, HCT, Pluronic and substrate are illustrated in Figure 6.5 Figure 6.6. In the mixture of captopril/PLGA the characteristic peaks that can be used to distinguish the two compounds from the mixture are the two carbonyl peaks of captopril at 1619cm^{-1} and 1728cm^{-1} and the carbonyl peak of PLGA at 1768cm^{-1}. Also, good markers can be the peak at 920cm^{-1} corresponding to the ring breathing of captopril and the peak of PLGA at 1130cm^{-1} corresponding to the asymmetric vibration of C-O-C groups of PLGA.

In terms of the mixture of HCT/PLGA and HCT/PLGA/Pluronic, the compounds could be distinguished from the peak at 1768cm^{-1} for PLGA, 1600cm^{-1} for HCT and 847cm^{-1} or 1478cm^{-1} for pluronic.

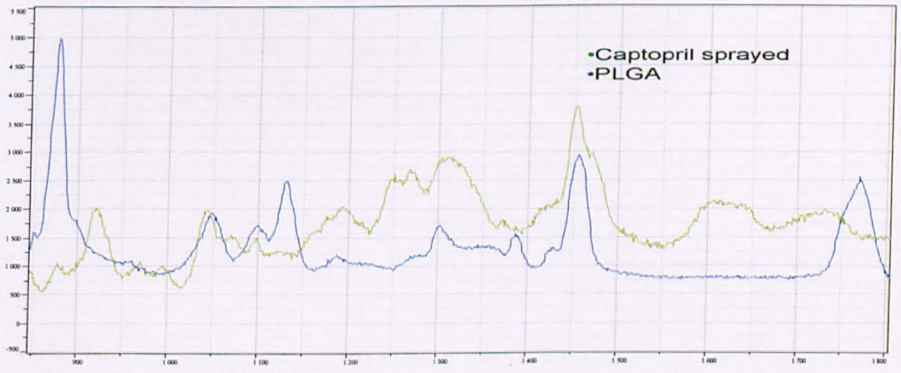

Figure 6.5: Raman spectra of Captopril sprayed and PLGA in the area of 850 – 1800cm^{-1}.

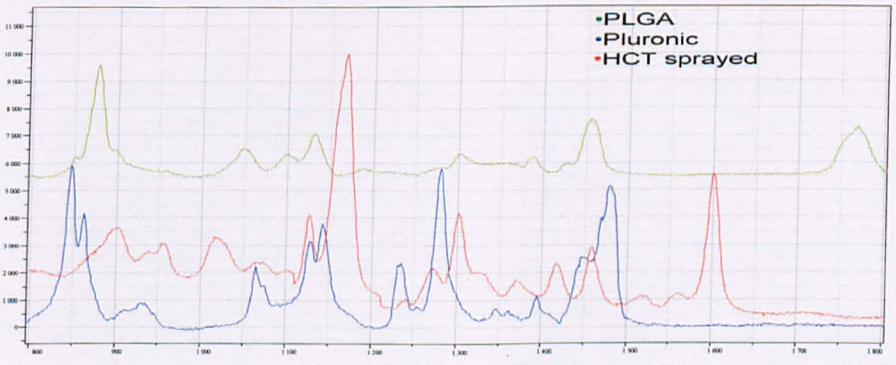

Figure 6.6: Raman spectra of sprayed HCT, PLGA and Pluronic in the area of 850 – 1800cm^{-1}

6.7.2.1 Captopril

Figure 6.7 shows the Eigenvalues for each principal component. It is observed that the Eigenvalues were reduced dramatically after the first factor and were almost zero after the third factor which indicates that the contribution of more than three factors is limited. Hence, the chemical map of the product has been created by using two principal components (PCs).

From the model spectra in Figure 6.7b, it is clear that the red spectra corresponds to areas with a higher concentration of captopril, as the characteristic peaks of PLGA are less intense and moreover the carbonyl peak of PLGA covered by the carbonyl peak of captopril.

Also, in Figure 6.7c the optical microscope image is illustrated with the rectangular box are the data limits for the chemical image. From these two images, it is clear that there is a correlation of the topographic figures in the optical microscope image with the chemical data in the chemical image.

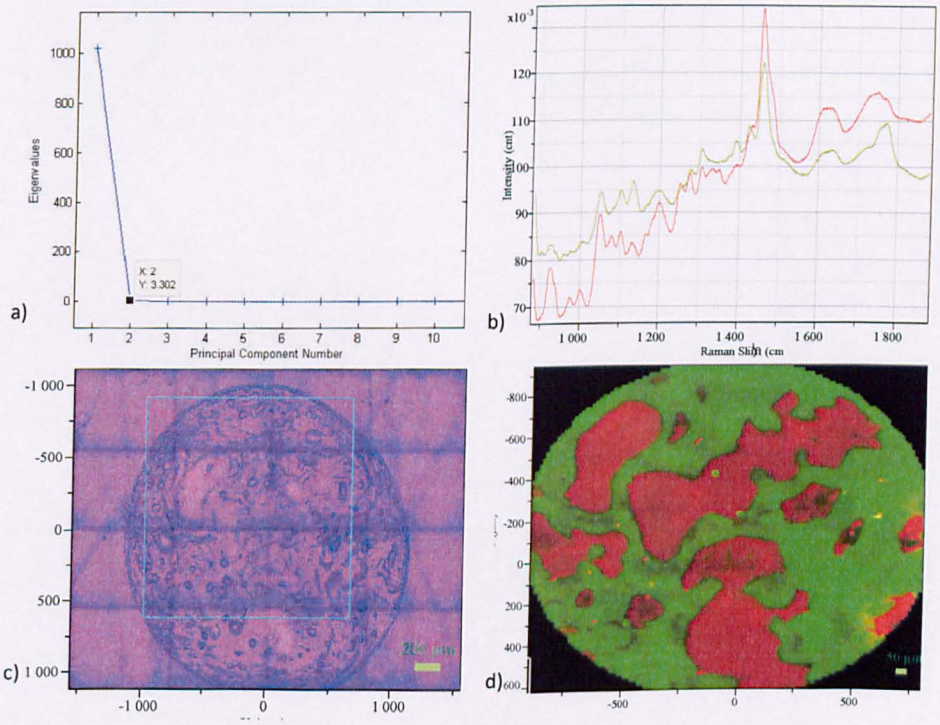

Figure 6.7: a) eigenvalues plot versus Principal Components numbers, b) model spectra used to create the chemical map, c)optical microscope image of deposition of Captopril/PLGA=50/50 mixture, d) Chemical image of the Captopril/PLGA = 50/50 mixture.

6.7.2.2 Microarray (HCT/PLGA/Pluronic = 50/47/3)

As shown from the eigenvalue plot versus the PC numbers, PCA analysis suggests using 3 factors to create the chemical image of the sample. However, in this case four PCs have been found to be more suitable, as by using this number of factors an additional chemical characteristic of the product appeared model spectra (blue spectra). The two most characteristic peaks of the Raman spectra of the samples are the NH_2 bending vibration of HCT corresponded by the strong peak at 1597cm^{-1} and the carbonyl peak of PLGA corresponds to the peak at 1758cm^{-1}.

The yellow and the red spectra are separated based only on their intensity as they look qualitively similar. However, the areas corresponding to the yellow spectra are more concentrated in the polymer, than the areas corresponding to red spectra, since the ratio of the characteristic peak of HCT to the peak of PLGA are less than in red API. The purple area contains the API only, whereas in terms of the green spectra, it has the less intensity and the peaks are not so clear. The most interesting spectra is the blue. In the blue spectra, the carbonyl peak has moved towards lower wavenumbers which indicate hydrogen bonding of the carbonyl peak of the PLGA. This hydrogen bonding can occur between the carbonyl group of PLGA and either the NH groups of HCT or the OH groups of pluronic as discussed in chapter 3.

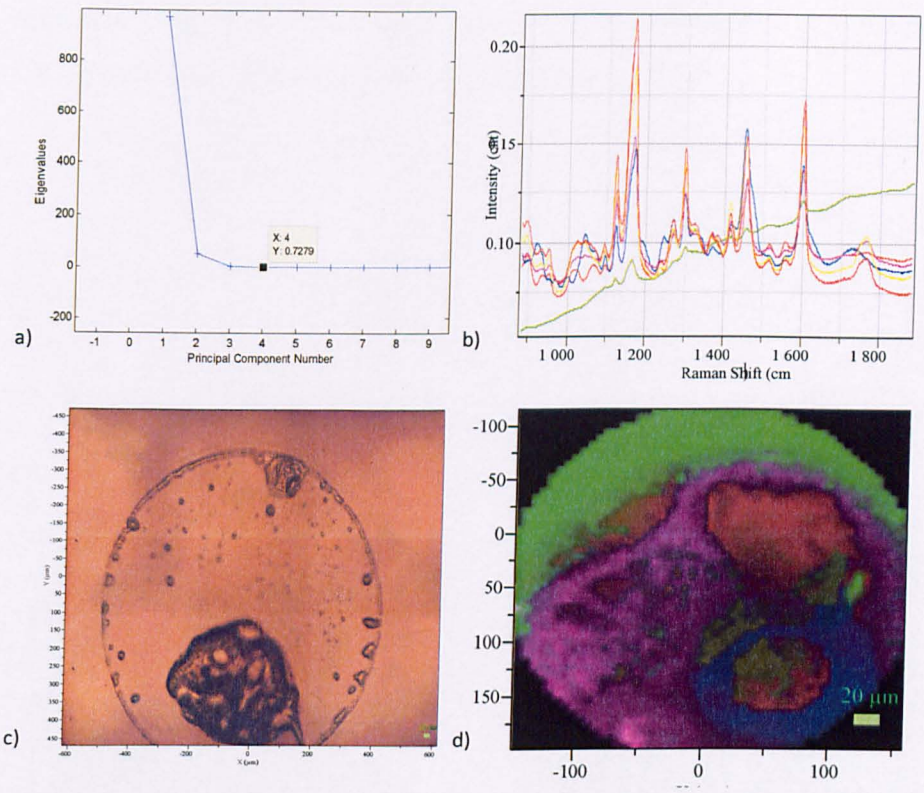

Figure 6.8: a) eigenvalues plot versus PCs numbers of the HCT/PLGA/Pluronic = 50/47/3 mixture produced by the microarray printer b) model spectra used to create the chemical map. The green spectrum corresponds to the background, the pink one corresponds to areas with pure API, the red and yellow spectra correspond to areas with HCT/PLGA mixture and the blue spectrum correspond to areas where the HCT interacts with PLGA, c)optical microscope image of deposited product d) Chemical image of the mixture.

6.7.2.3 Pippete produced formualtions

PLGA/Pluronic = 90/10

The eigenvalues plot versus the PC numbers for the PLGA/Pluronic mixture show that the first PC is enough to show the obtained spectra. This is proved by the model spectra used to plot the chemical map as it is clear that the model spectra are separated based on the intensity of the peaks. However, due to their low detection signal the peaks of pluronic were not revealed. Finally, the optical microscope image shows that the product is evenly distributed along the substrate.

To reveal the position of pluronic, by using the Solo+MIA software, PCA was employed. Peaks of pluronic appeared in the 8th PC whereas the previous were PCs found to contain peaks from PLGA. As a representative PC of this kind, the 2nd PC is

illustrated in Figure 6.10. The chemical image of pluronic seems to be more reliable than this method because it is nicely reproduced in the 8th PC.

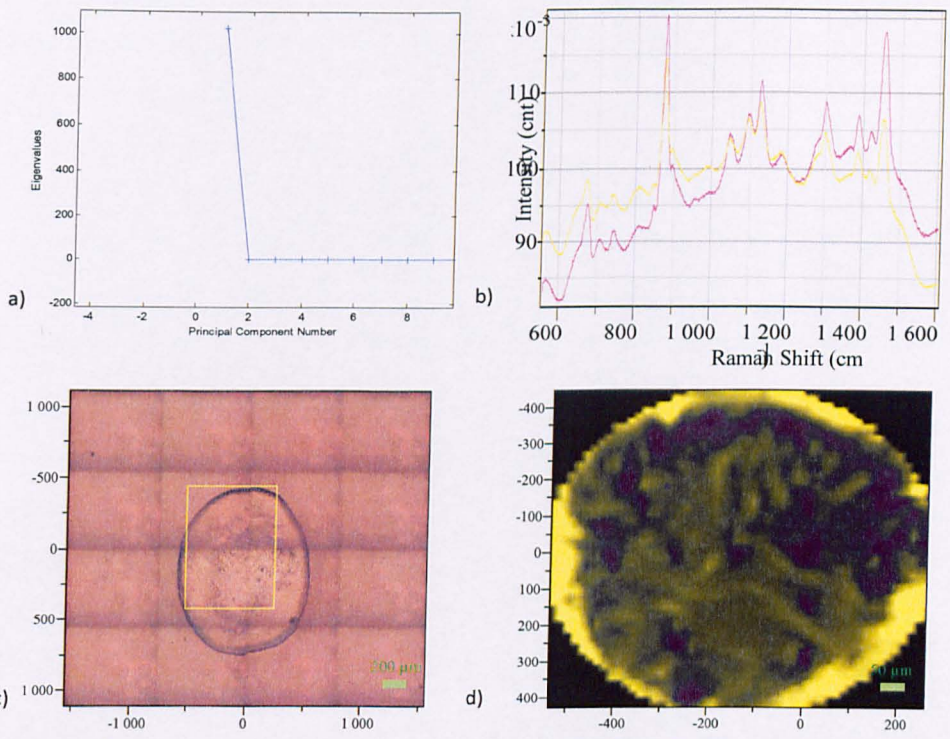

Figure 6.9: a) eigenvalues plot versus PCs numbers of the HCT/PLGA = 20/80 mixture produced by the microarray printer b) model spectra used to create the chemical map, c) optical microscope image of deposited product d) Chemical image of the mixture.

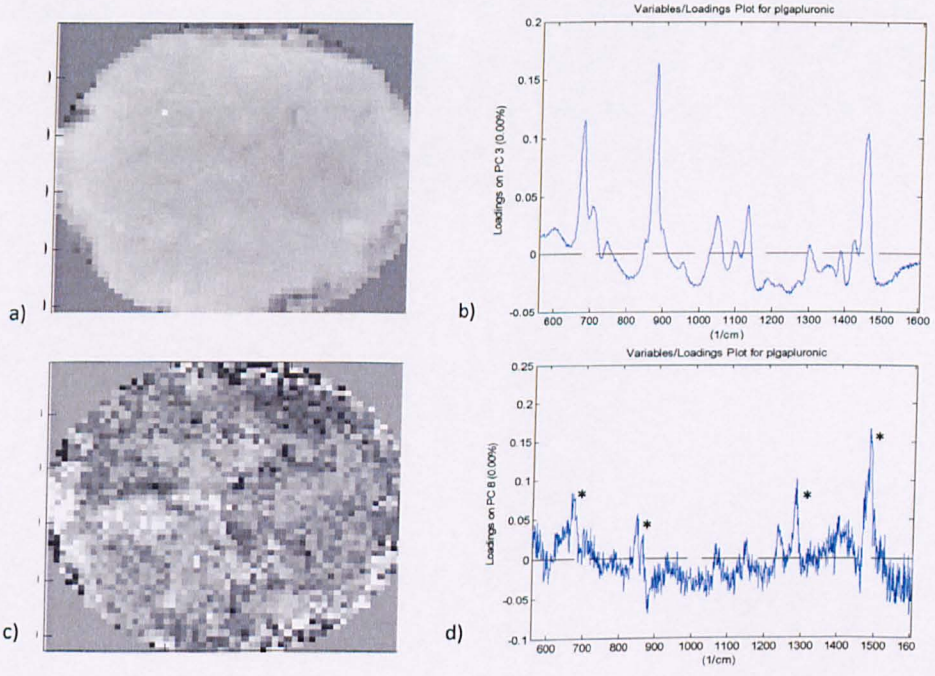

Figure 6.10: a) Chemical image of PC2, b) spectrum of PC2, c) chemical image of PC8, d) spectrum of PC8. The asterisks are the characteristic peaks of pluronic.

HCT/PLGA = 20/80

In Figure 6.11a the Eigenvalues plot with the principal components is illustrated. From this plot, it is clear that the factors that can contribute to the obtained spectra are the first three. Figure 6.11c shows the area of the spot that was mapped. The chemical map has been created by separating the spectra in to three principal components. Hence, the areas corresponding to red model spectrum are areas contain only HCT since the characteristics peaks of PLGA such as the carbonyl group at 1760cm^{-1} are missing in model spectra. The green and blue area contain both HCT and PLGA as the model spectra corresponding to these contain the characteristic peaks of HCT and the characteristic peak of PLGA at 1760cm^{-1} (Figure 6.11b).

However, the use of four factors produced the most accurate map of the product. This was confirmed when a spectrum was taken in a random position in the yellow area in the sample (Figure 6.11d). From Figure 6.11g the spectrum at this position fits better to the yellow model spectra which does not contain PLGA peaks rather than the green spectrum of the model with three factors which contain peaks of the PLGA.

Finally, based on this analysis, and in combination with the optical microscope image (Figure 6.11c), it is clear that the API is gathered in the centre of the product. Specifically, the yellow and purple model spectra are related to the spectrum of pure HCT in areas where the API is highly concentrated. Finally, the optical microscope image shows that most of the material was gathered at the edge the spot. The chemical image along with the optical microscope image shows that PLGA moves tends to gathered at the edge of the spot.

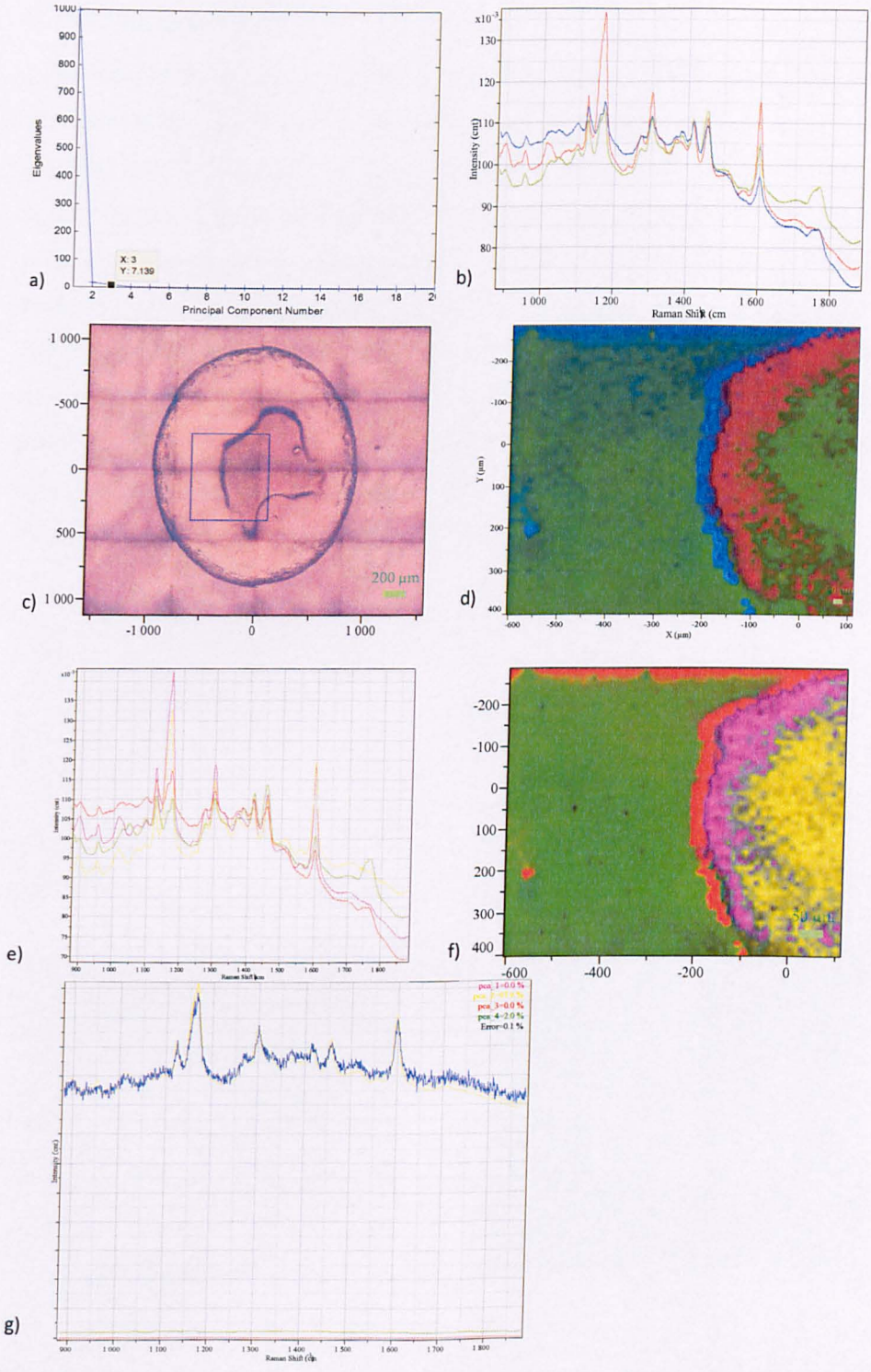

Figure 6.11: a) Eigenvalues plot versus PCs numbers of the HCT/PLGA = 20/80 mixture produced by the microarray printer b) 3 model spectra used to create the chemical map. The red spectrum corresponds areas with pure HCT, whereas the green and the blue correspond to areas with HCT/PLGA mixture c)optical microscope image of deposited product d) Chemical image of the mixture based on 3 factors, e) 4 model spectra used to create the chemical map, f) Chemical image of the mixture based on 4 factors, g) a spectrum taken in a random point at yellow area.

HCT/PLGA/Pluronic = 20/75/5

In the case of the mixture of HCT/PLGA/Pluronic mixture the PCA analysis showed that two factors contribute to the spectra obtained (Figure 6.12a). Hence, the chemical map of the spot has been separated in to two PCs. Both components contain peaks of both HCT and PLGA. Unfortunately, Raman was not able to distinguish the pluronic's characteristic peak due to its low concentration and because most of the pluronic peaks are overlapped from those from PLGA and HCT. The red model spectra express areas which contain the less material. Also it is interesting to notice the two shoulders at the 1720cm^{-1} and at the 1780cm^{-1} in the green spectrum. However, the peak at 1720cm^{-1} it is most likely noise which was picked up by the multivariate analysis. Also, the optical microscope image shows that the compounds have been distributed evenly during the evaporation.

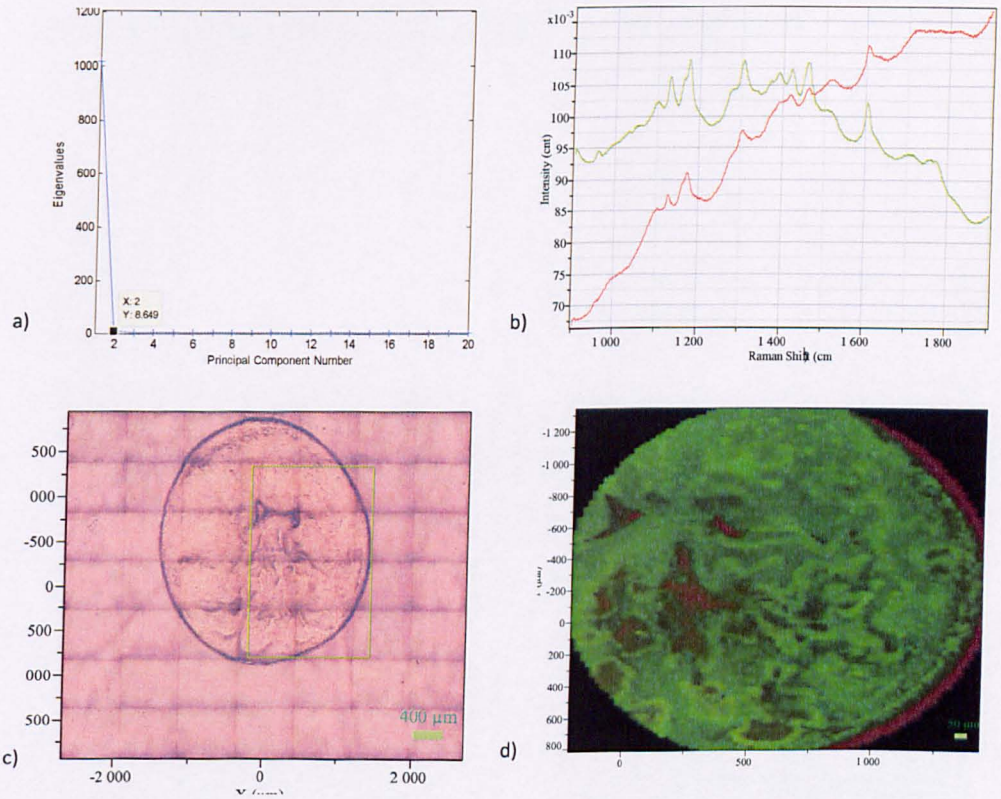

Figure 6.12: Eigenvalues plot versus PCs numbers of the HCT/PLGA/pluronic = 20/75/5 mixture produced by the microarray printer b) 3 model spectra used to create the chemical map, c)optical microscope image of deposited product d) Chemical image of the mixture.

HCT/PLGA = 50/50

The Eigenvalues plots versus the number of principal components are illustrated in Figure 6.13a. According to this plot, three factors contribute to the obtained spectra mostly. Figure 6.13b and c illustrate the chemical map of the spot and the three components used to plot the chemical image. The green spectrum corresponds to areas with low quantity of materials or to areas where the laser beam lost its focus. The red spectra correspond to areas which consist of HCT only whereas the blue spectra contain both PLGA and HCT as the characteristics peaks of HCT and PLGA coexist.

Finally, the chemical and optical microscope image shows that the centre of the product is occupied by HCT whereas PLGA has been moved to the edge where most of the deposited material has been gathered to the edges. Similarly the optical microscope image shows that most of the deposited material was gathered to the edge. ,

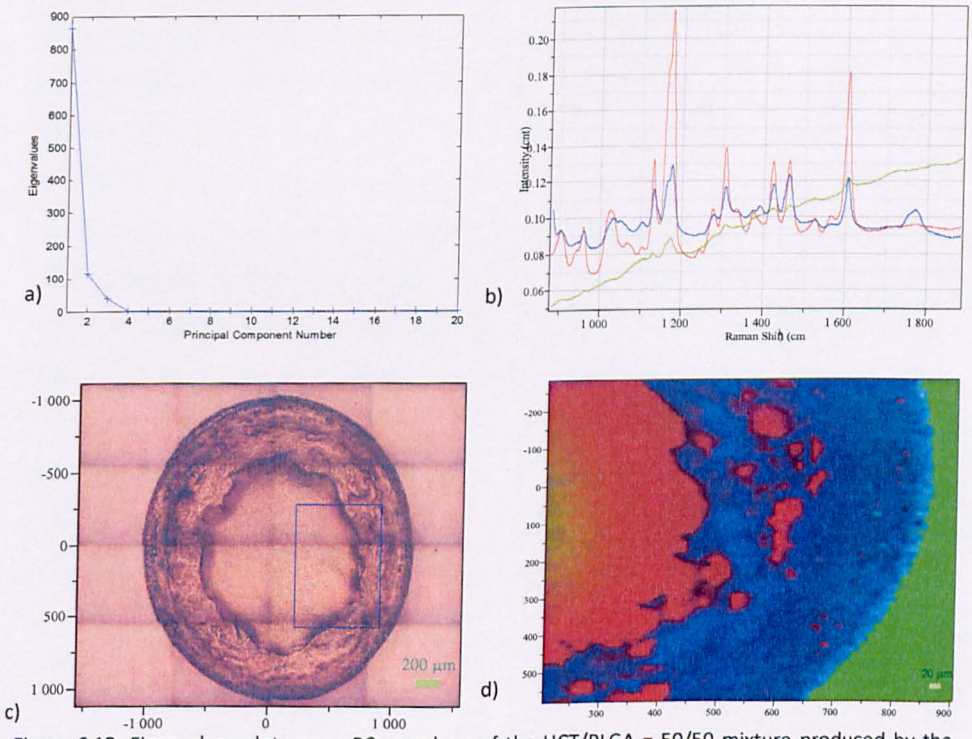

Figure 6.13: Eigenvalues plot versus PCs numbers of the HCT/PLGA = 50/50 mixture produced by the microarray printer b) 3 model spectra used to create the chemical map. The green spectrum correspond to the background, whereas the blue and the red correspond to areas with HCT/PLGA and pure HCT respectively c)optical microscope image of deposited product d) Chemical image of the mixture.

6.7.3 Raman spectra

6.7.3.1 Hydrochlorothiazide

To investigate the physicochemical nature of the hydorchlorothiazide, Raman spectra of the products were taken at two random places at the centre and the edge of the samples.

The most important groups in the mixture of HCT and PLGA are the NH groups and the SO groups of HCT and the carbonyl group of PLGA. The NH groups occurred at the area between 3100–3700cm^{-1}, whereas the SO groups are assigned to peaks at 1300cm^{-1} corresponding to the asymmetric vibration and at 1165 cm^{-1} corresponding to the symmetric vibration of the group in question. Finally the carbonyl group of PLGA occurs at 1765 cm^{-1}.

From the Figure 6.14, 6.15, Figure 6.16 and Figure 6.17c, it is clear in all samples that the broadness of the amino peaks of HCT compared with the powder indicates an amorphous nature of the product. Also, in the mixtures HCT/PLGA 20/80 and HCT/PLGA/Pluronic the peak assigned to the symmetric vibration of SO group has moved slightly to higher wavenumbers from 1164cm^{-1} to 1174cm^{-1} in the case of HCT/PLGA = 20/80 and to 1172 cm^{-1} when pluronic is added. In the case of the HCT/PLGA 50/50 the SO peaks of the spectrum obtained from the edge and the centre of the product, are in the same position. Nevertheless, they both have been shifted slightly to higher wavenumbers than the sprayed HCT from 1166cm^{-1} to 1171cm^{-1}. In the mixture produced by the microarray Finally, the carbonyl group of PLGA remains in the same position with the carbonyl group of the unprocessed PLGA. In terms of the amino groups, the broadness of the peaks makes the analysis difficult. However in all the cases they seem to remain in the same position. However, in the case of HCT/PLGA 50/50 both the peaks corresponding to the amino groups looks to have been moved to lower wavenumbers.

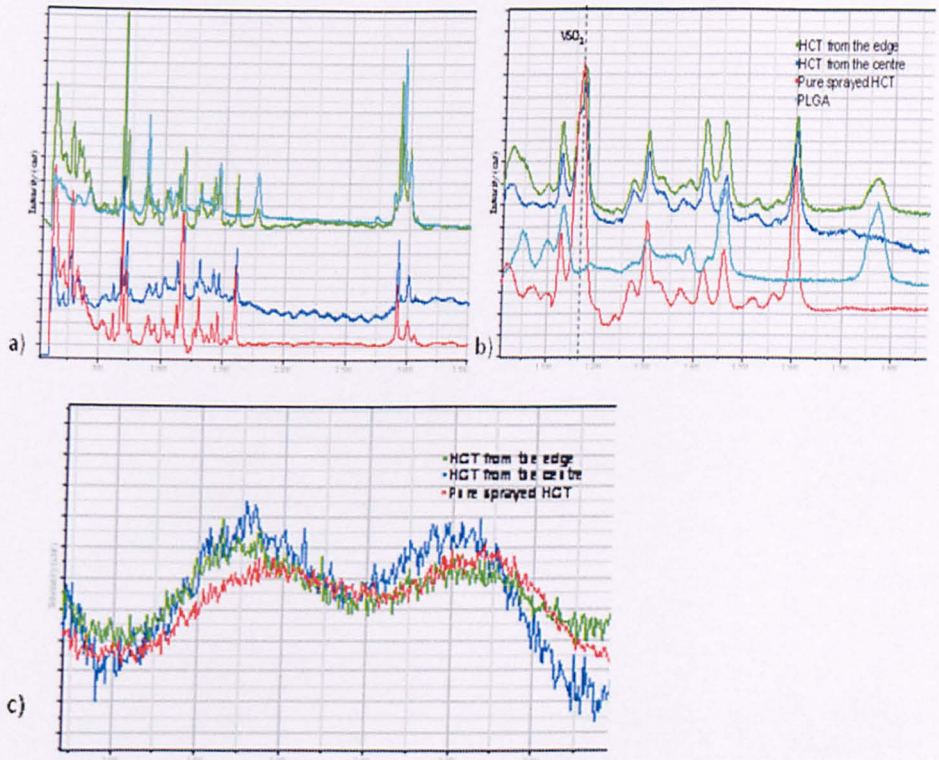

Figure 6.14: Raman spectra of HCT/PLGA 50/50 taken from the edge, from the centre, pure HCT and PLGA with zoom at the area of b) SO vibrations and c) amino groups.

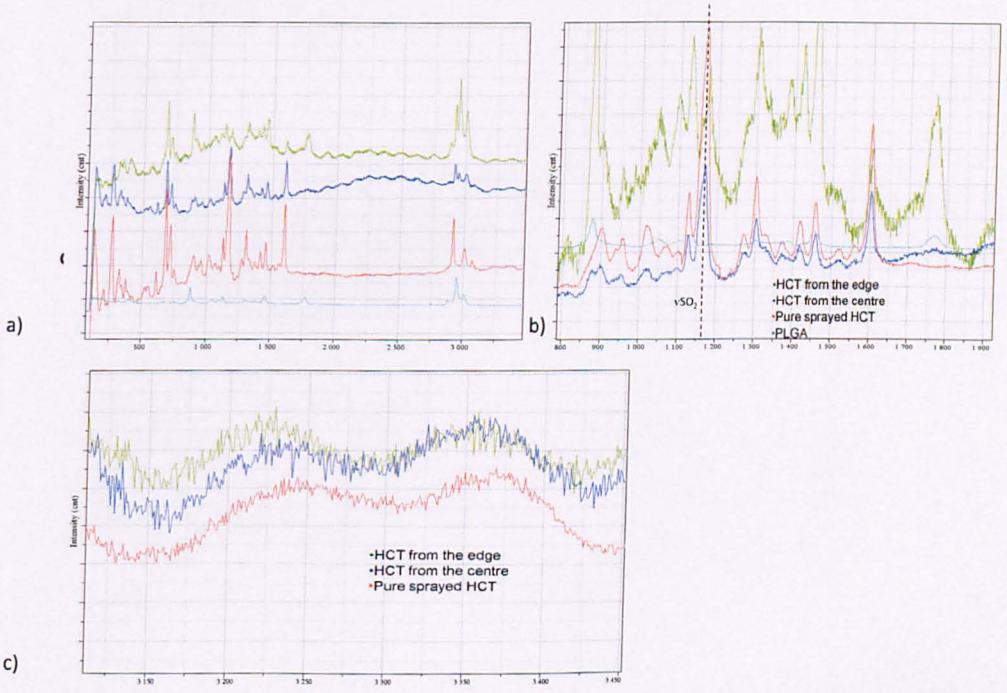

Figure 6.15: Raman spectra of HCT/PLGA 20/80 taken from the edge, from the centre, pure HCT and PLGA with zoom at the area of b) SO vibrations and c) amino groups.

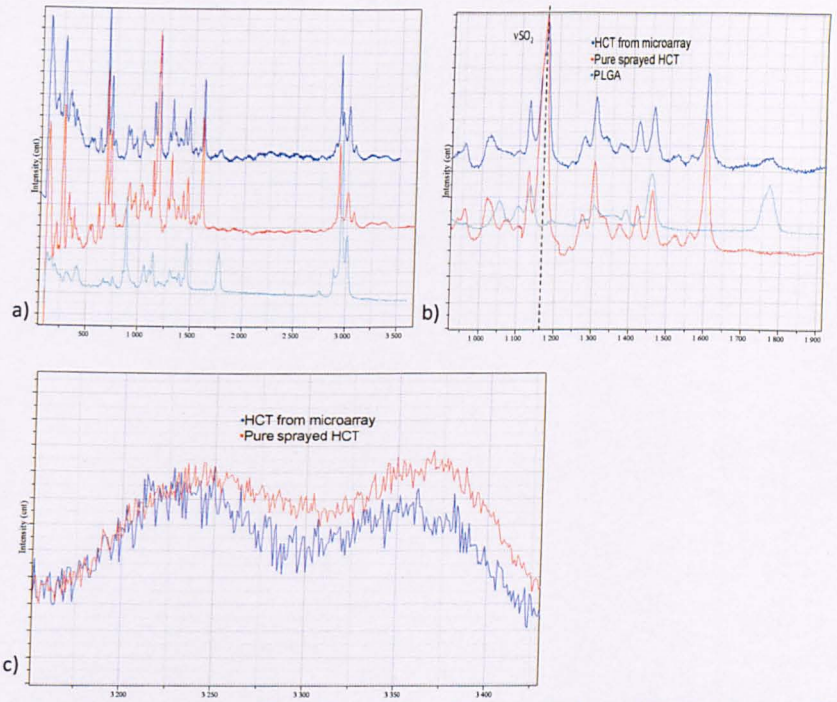

Figure 6.16: Raman spectra of HCT/PLGA a) 50/50, b) 30/70, c) 20/80, d)HCT/PLGA/Pluroic = 20/75/5, e) product from the microarray printer with zoom at the area of II) SO vibrations and III) amino groups.

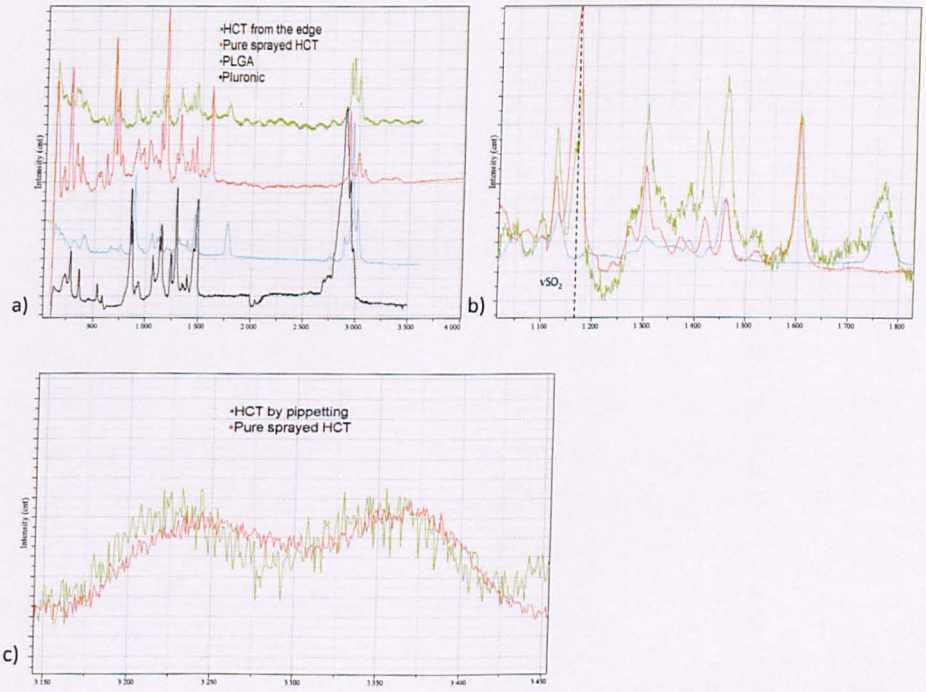

Figure 6.17: Raman spectra of HCT/PLGA a) 50/50, b) 30/70, c) 20/80, d)HCT/PLGA/Pluroic = 20/75/5, e) product from the microarray printer with zoom at the area of II)SO vibrations and III) amino groups..

6.7.3.2 Captopril

In the captopril powder the C=O stretching vibration of the carboxylic group of captopril is assigned at 1745 cm^{-1} and the C=O stretching vibration of the amide group at 1603 cm^{-1} and at 1583cm^{-1}. In the sprayed drug the former peak has been shifted to 1727 cm^{-1} whereas the latter has been shifted to 1616 cm^{-1}. Moreover, due to the broadness of the peak, it is not clear if both the peaks of the amide of the crystalline pwoder have been shifted.

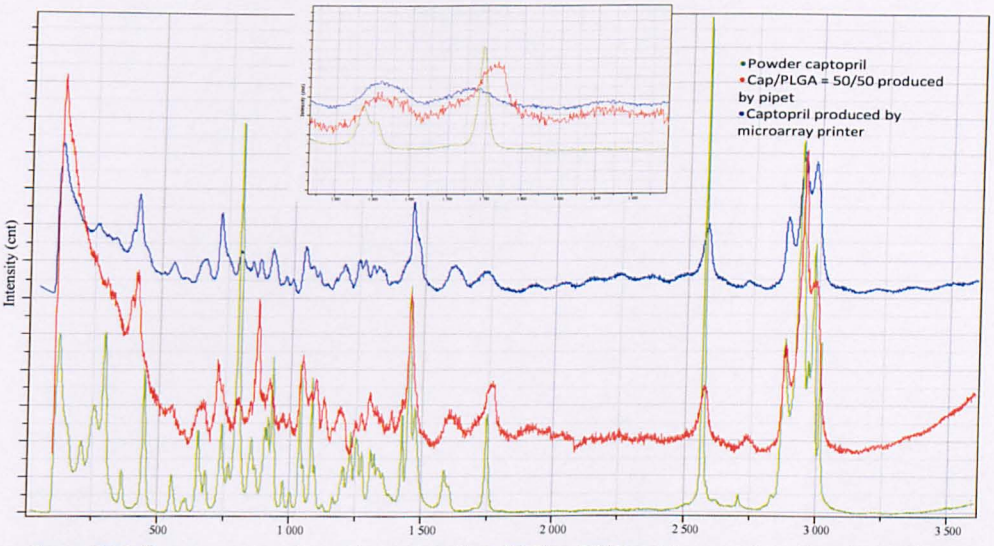

Figure 6.18: Raman spectra of powder captopril, Ca/PLGA = 50/50 mixture produced by pipet and pure captopril produced by the microarray printer with zoom in the carboxylic region.

6.7.4 Dissolution studies

Figure 6.19 shows the effect that PLGA has on the dissolution rate of captopril. When captopril was immersed in blank SGF, it is dissolved completely in less than three minutes. The addition of PLGA results in a more extended release of the API. Increasing the concentration of PLGA 70% in the mixture causes the captopril to be released more slowly, where even after 3hrs the drug has released 60% only of the drug. In the mixture of equal concentrations of API and PLGA there is an initial burst release of the API and after the fifth minute the drug is released in an extended manner where it is released completely after 3hrs.

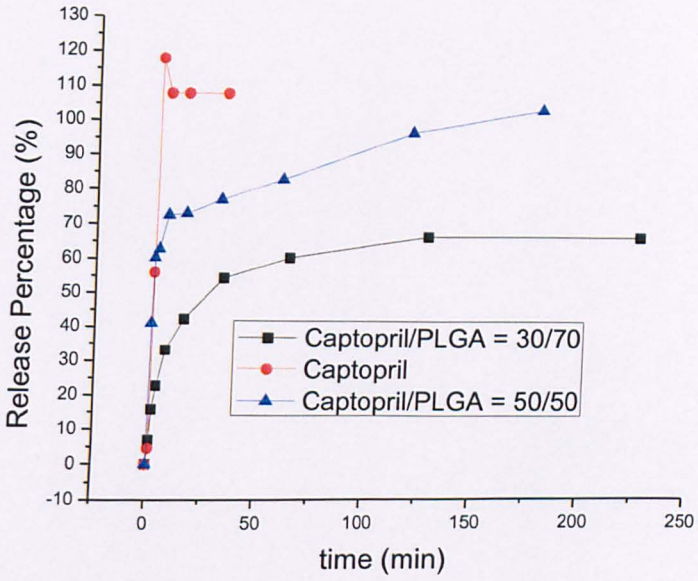

Figure 6.19: Dissolution profile of Captopril, Captopril/PLGA 30/70 and Captopril/PLGA 50/50.

The influence of PLGA in the release of API is illustrated in the Figure 6.21. Pure HCT is dissolved rapidly in the blank SGF. The utilization of PLGA in the mixture results in an extended release of the API. Hence, at the lower concentration of the API the drug is released with the slowest rate where after two hours only 20% has been released in the medium. Increasing the concentration of API in the mixture, results in an increased dissolution rate. However, even after two hours the API being released is 70% of the initial loading.

The addition of Pluronic results in a much more rapid release of the API. Hence, both when the API consists the 30% and when the API consists of the 20% it is released completely after the 40 minutes.

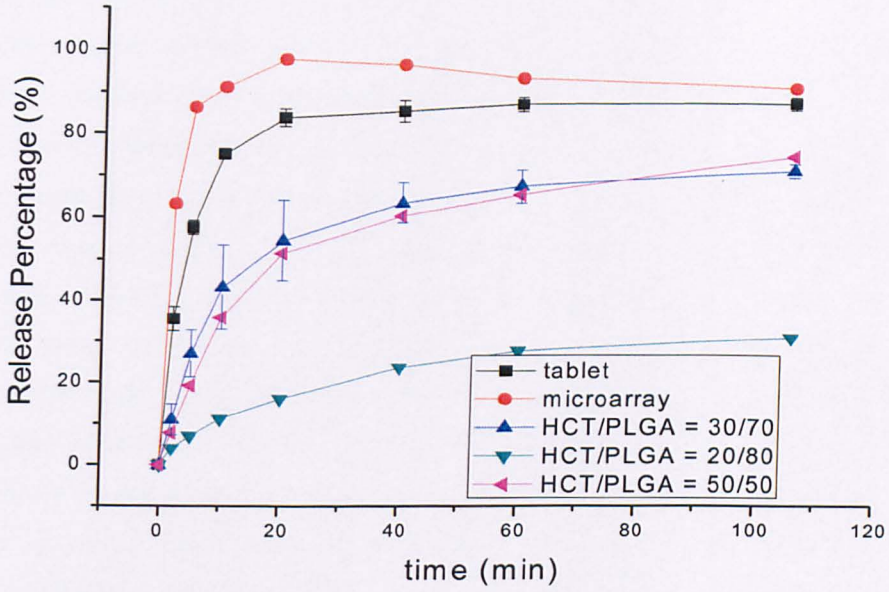

Figure 6.20: comparison the dissolution profiles of HCT from the Capozide tablet, HCT/PLGA/Pluronic = 50/75/5 produced by the microarray printer and HCT/PLGA = 20/80, 30/70, 50/50 mixtures produced by pipetting.

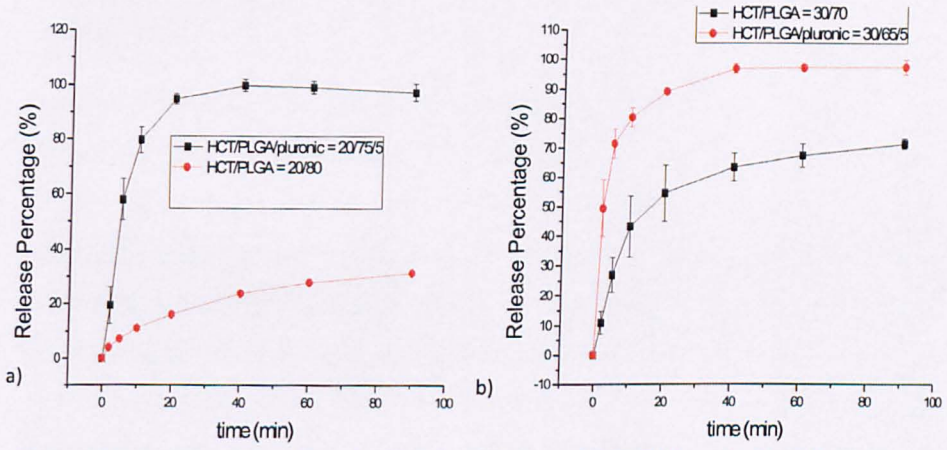

Figure 6.21: a) dissolution profiles of HCT/PLGA 20/80 and HCT/PLGA/Pluronic 20/75/5, b) dissolution profiles of HCT/PLGA 30/70 and 30/65/5.

6.8 Discussion

AFM data showed phase separation for both the mixtures of captopril and HCT with PLGA. For captopril/PLGA the phase separation appears as small dots on the surface of the polymer matrix. This can be realised when after its dissolution in water, the dots were replaced by small depressions indicating that the captopril was dissolved.

In the mixtures of HCT/PLGA the two compounds are phase separated. This phenomenon was observed by AFM also when the mixtures were prepared using the piezo- dispenser from GeSim (chapter 3.12). However, it is worth noticing that the phase separated portion of the sample is a low percentage of the whole sample. The observed phase also is consistant with the burst effect in the dissolution studies for both captopril and the HCT, since the API which is phase separated will dissolve rapidly and then dispersed in the polymer in a more gradual manner. It is also interesting that the samples with pluronic produced by pipetting exhibited phase separation and those produced by the microarray printer were homogenous. The reason for this may come from technical issues regarding taking AFM images. More specifically, the shape of product produced by the microarray printer contains lots of curved surfaces which make the imaging with AFM more difficult. Therefore, it is likely that the phase separation occurred in the areas where AFM could not work. Also, the mixture of pluronic and PLGA produced a non-homogenous mixture. This is consistent with previous results where the use of 2% of pluronic resulted in a homogenous product whereas 50% of pluronic caused a phase separation on the surface [216].

The chemical map of the samples were processed using direct classical least square (DCLS) based on the algorithms of the NGLabspec. In order to choose the number of factors that contribute to the plot of chemical mapping, the Eigenvalues of each principal component was analysed. As in the previous chapters the PC Eigenvalues sharply decrease after the first PC. Based on this behaviour, it can be concluded that it is quite likely that two components exists which is plausible like in chapter 3 there is no pure polymer areas. The factors which have been used to plot the chemical image have been chosen in such a way that the model spectra will reveal all the necessary chemical information. However, in the sample containing mixture of HCT PLGA and Pluronic, Pluronic was not able to be detected due to its low detectable signal and because its strongest peaks were covered by the peaks of HCT and PLGA. However in the case of the PLGA/pluronic mixture, PCA was able to reveal pluronic. The interesting and the unexpected result was that a clear pattern of the peaks of pluronic appeared in the 8th PC very far away from the first PC which was suggested by the Eigenvalues versus PC numbers plot. By using DCLS from the NGLabspec software, it is likely that the small shoulder at 849cm^{-1} belongs to the strong pluronic

peak. However, the spectrum of the pure PLGA has a small peak on this wavenumber and as the concentration of PLGA is 9 times higher it may belong to the PLGA. Hence, by using the MIA software and PCA analysis it was able to reveal the whole pattern of the pluronic.

Raman mapping revealed that the samples prepared by both the microarray printer and depositing with pipette have different physicochemical properties at their surfaces. The samples HCT/PLGA prepared by the microarray device are phase separated, a phenomenon which has been first introduced in chapter 3 in the samples prepared by the GeSim dispenser. Samples prepared by depositing the solution with pipette are phase separated to a much greater extent. The main reason for this is the slower kinetics of drying of the larger droplets. Due to this some of the drug is deposited in the centre whereas the polymer tends to move at the edge taking along the remaining drug forming a mixture where in some areas it is not homogenous according to the AFM results.. The justification of the spot formation like in the samples represented in chapter 3 can be based on the different solubility of the compounds has in the solvents. More specifically in the mixtures of HCT/PLGA, the HCT is soluble in acetone but not in DMSO, and hence it will precipitate before the ring is formed, since DMSO will be the last to evaporate inducing the coffee ring formation of PLGA.

The addition of pluronic results to a more uniform product where all the compounds are equally distributed. This is maybe due to the interactions between the pluronic and PLGA via hydrogen bonding of the ether groups of pluronic with the hydroxyl groups of PLGA [205]. When pluronic is added, the solvent system consists of acetone, ethanol and DMSO. Pluronic is not soluble in DMSO [177] and therefore it will precipitate together with the HCT, which is slightly soluble in ethanol, without forming the coffee ring formation. PLGA will be the last to precipitate where pluronic can hold the PLGA molecules closer.

Finally, Raman studies of the samples produced by pippetting and by inkjet printing gave results similar to the product produced by the GeSim dispenser in chapter 3. Specifically, Raman studies showed a shift towards lower wavenumbers and a shift of the symmetric vibration of SO group of HCT indicating disruption of the hydrogen bonding between the SO groups and the amino groups among the HCT molecules

and formation of hydrogen bonding between the amino groups of HCT and the carbonyl groups of PLGA. A more thorough analysis of the phenomenon is described in the chapter 3. where it was observed in the samples produced by the GeSim dispenser. Nevertheless, as in that chapter the carbonyl peak of PLGA remain in the same position with the unprocessed material. This may happen due to the limited number of carbonyl ions which take part in the hydrogen bonding formation and hence the peak shift that may occur is covered by the broad and strong peak of the inert carbonyl groups. Finally, it is important to mention that a second peak appeared next to the carbonyl peak of PLGA in the spectra used to create the chemical map of the samples results from noise from the instrument and not a carbonyl peak shift as the most detailed Raman spectra in Figure 6.17 showed since by using higher acquisition time this figure has been remove.

In terms of captopril, the Raman studies showed that the printed API is in that cis-form as the carbonyl peak at 1642cm^{-1} appeared at higher wavenumbers whereas the peak of the carbonyl peak at 1700 appeared in lower wavenumbers from the powder Captopril. This was also confirmed by the product produced with the GeSim dispenser in chapter 3 where a detailed analysis of the phenomenon is represented.

The last step to investigate any drug formulation is to study the release of the APIs from it. Both captopril and hydrochlorothiazide are freely soluble in the medium used. PLGA was chosen to create a polymer matrix which can control drug release. PLGA has been widely used to control the release of freely soluble drugs [206, 217-219]. The mechanisms involved the release of the drug from polymeric matrixes are swelling, diffusion and degradation. However, in our case since the dissolution duration lasts for only 2hrs and PLGA (85:15) requires days in order to be degraded; hence, the main release mechanism of the APIs from the polymer is likely to be diffusion. Also, it is interesting to notice that both in the case of captopril/PLGA and HCT/PLGA when 30/70 is used the release rate is similar even though it would be expected that HCT would be released at a slower rate. More specifically, HCT as a base will be protonated in the acidic environment. Moreover, PLGA exhibits free carboxylic groups which would demonstrate electrostatic interactions with the protonated HCT, inhibiting the diffusion of the API. In contrast, captopril as an acid will be deprotonated and exist as negative ions. Hence electrostatic interactions

between the API and the polymer cannot exist. The fact that both the HCT and Captopril follow the same dissolution profile indicates that these interactions do not affect the diffusion of the drug from the polymer. Also, the reason why only 60% of both the APIs are released must be due to fact that the polymer covers the rest of the API. The rest of the drug will be dissolved when the polymer starts being eroded where the medium will be inserted into its structure dissolving the drug. The prolonged release of the 20/80 HCT/PLGA mixture may be attributed to the formation of a more homogenous and intimate mixture with the drug and the polymer.

In order to achieve a complete release of the API as in the commercial tablets, Pluronic- f127 was attempted to incorporate with the polymer. From Figure 6.21, it is clear that the Pluronic has a significant effect on the release of the API. The addition of Pluronic results in a more rapid release of the entire API within 40mins. In terms of the mechanism that governs the release, it could be expected a priori that the hydrophilic poloxamer would quickly leach out from the PLGA leaving pores which allow the medium to dissolve the API mixed within the polymer.

To investigate the release API from the formulation the zero order, first order, Higuchi and Korsmeyer – Peppas model were applied. The suitability of each model to describe the mechanism of the drug release was based on the calculation of the R^2 for the formulations. From the table 6.1 , most of the formulations follow the data fitting of the Korsmeyer – Peppas model. More specifically, in terms of hydrochlorothiazide mixtures, data fitting for HCT/PLGA 20/80 gives a high r^2 value of 0.99. The n value is equal to 0.55 which indicates a non-Fickian release. The mixture of HCT/PLGA 30/70 seems to be closer to the non-Fickian Higuchi model with R^2 = 0.933. The release of the HCT/PLGA 50/50 does not seem to follow any of the proposed models as the R^2 value is low in all the cases. From the mixtures of HCT/PLGA/Pluronic only the 30/65/5 was able to correlate with the proposed models. This mixture seems to follow the Peppas model with n value equal to 0.216.

In the case of captopril mixtures, for a better fitting with the proposed models the first two time points have been excluded. During this time period the API which is phase separated is burst from the formulation. Figure 6.24 shows that the release of

captopril follows the Peppas model having R^2 value equal to 0.94 in both the cases. The n values are equal to 0.35 and 0.116 which indicates a Fickian release model.

It has been suggested that when the n exponent is less than 0.5 is due to drug diffusion partially through a swollen matrix and water filled pores in the formulations [220]. This looks to be valid in the formulations presented in this chapter. As it has been shown before from the AFM and Raman microscopy the samples are phase separated. Hence in these cases, the phase separated drug which is exposed to the medium was dissolved first, leaving big pores which due to the small sizes of each spot, compared to medium, filled with the solution following a Fickian diffusion.

Besides the good fitting of some formulations with selected models, no complete description could be found in current models. Especially the samples with pluronic where the drug is released completely in less that 20mins was not able to fit to any of the model. Therefore, the obtaining of more values below 20mins is necessary to correlate the drug release with the models. However, the limitations of the models can justify any deviation of the release profile from them. In the Higuchi model, the device geometry must be a thin film with negligible edge effects, the size of the drug particles should be much smaller than the thickness of the film, the carrier material should not swell or dissolve and perfect sink conditions should prevail. In our systems most of the aforementioned prerequisites can be fulfilled as the spots can be considered thin films to an extent but clearly not completely.

In terms of the Korsmeyer – Peppas model the release is modelled to occur in a one-dimensional manner and the system width–thickness or length–thickness relation must be at least 10, as well as assumptions about constant diffusivities of a drug with a polymer, constant dimensions of a device during an *in vitro* release test, one-dimensional diffusional behaviour, and perfect sink conditions in an *in vitro* release test. Finally, these models a better fit is obtained when apparatus I or II are used for the dissolution test. In our case the dissolution test was carried out on a shaking stage which may affect the final results.

	zero order	1st order	Higuchi	Korsmeyer-Peppas
HCT/PLGA = 50/50	0.75	0.42	0.88	0.9
HCT/PLGA = 30/70	0.64	0.48	0.93	0.86
HCT/PLGA = 20/80	0.87	0.68	0.99	0.99
HCT/PLGA/Pluronic = 30/65/5	0.41	0.3	0.75	0.9
HCT/PLGA/Pluronic = 20/75/5	0.56	0.3	0.84	0.77
Captopril/PLGA = 50/50	0.9	0.39	0.86	0.94
Captopril/PLGA = 30/70	0.53	0.84	0.79	0.94

Table 6.1: r^2 fitting of the various release models for Captopril/PLGA and HCT/PLGA mixtures.

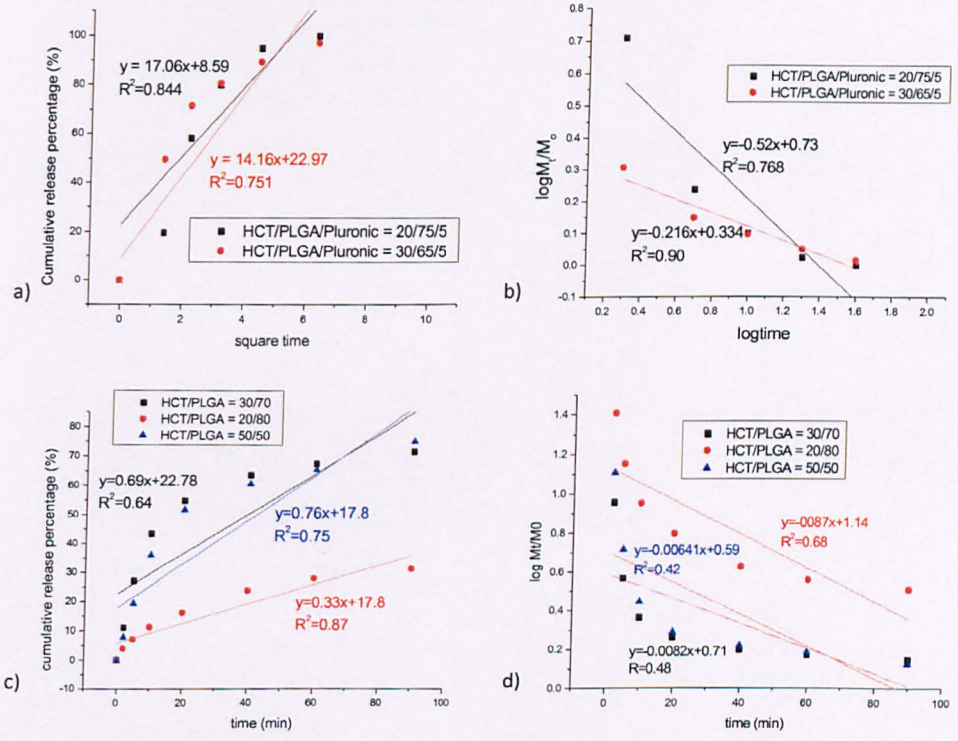

Figure 6.22: a) Higuchi, b) Korsmeyer-Peppas c)zero order, d) first order for mechanism of drug release for the mixtures HCT/PLGA/pluronic at ratio of 20/80, 30/70, 50/50 prepared by pippetting deposition.

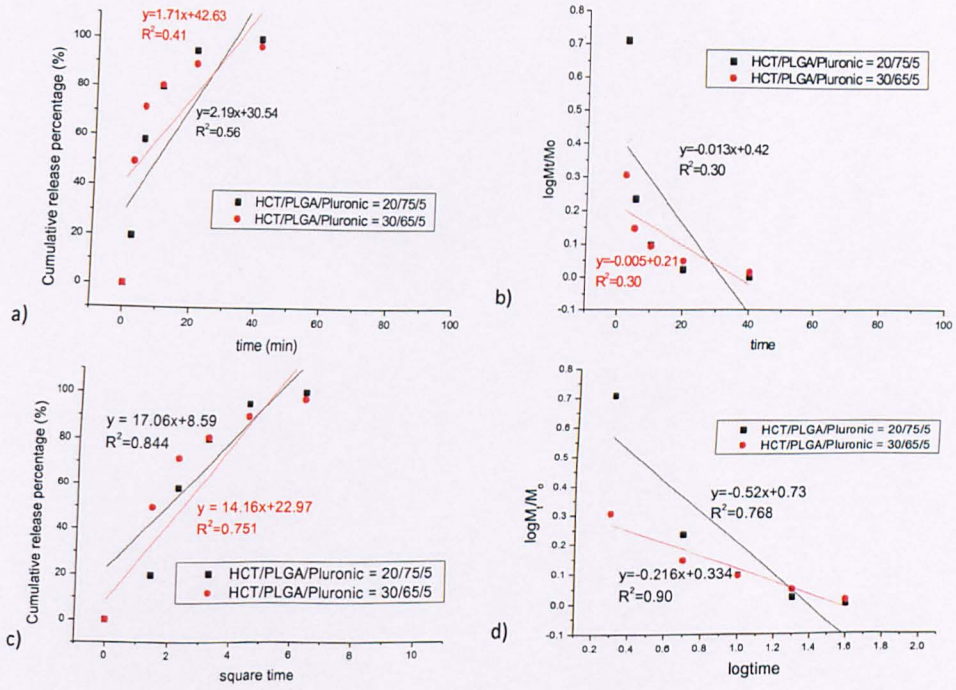

Figure 6.23: a) Higuchi, b) Korsmeyer-Peppas c)zero order, d) first order for mechanism of drug release for the mixtures HCT/PLGA/pluronic at ratio of 20/80, 30/70, 50/50 prepared by pippetting deposition.

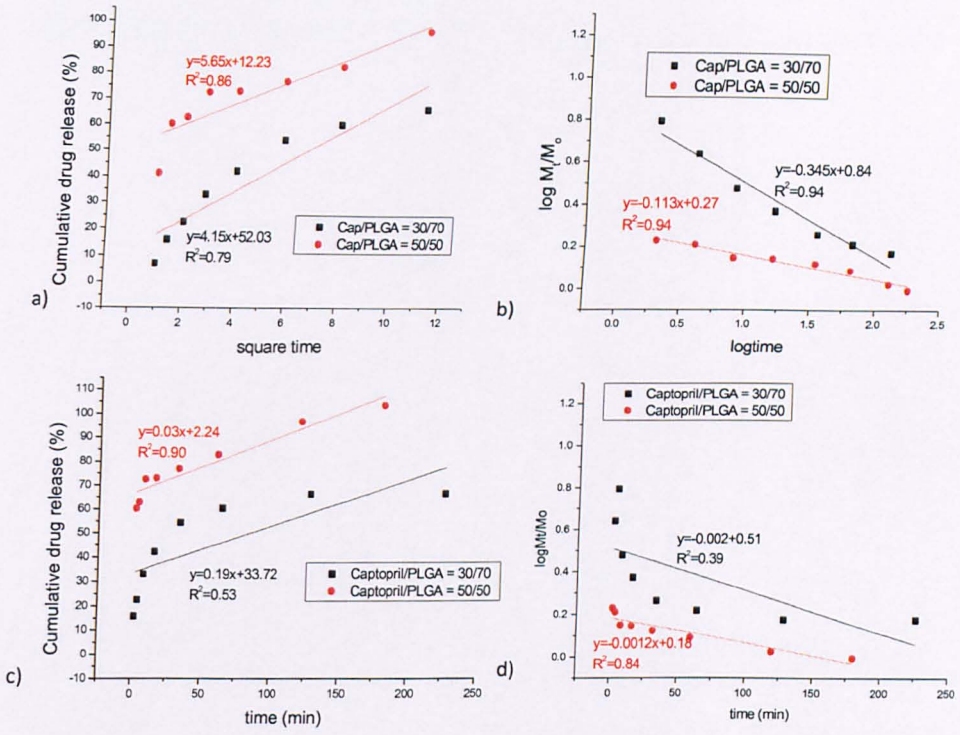

Figure 6.24: a) Higuchi, b) Korsmeyer-Peppas c)zero order, d) first order for mechanism of drug release for the mixtures Captopril/PLGA at ratio of 30/70, and 50/50 prepared by pippetting deposition.

6.9 Conclusions

In this chapter, a successful extended release formulation was prepared using Captopril and Hydrochlorothiazide as APIs. Captopril and HCT were printed along with PLGA which has been used as polymeric matrix to control the release of the APIs. AFM and confocal Raman mapping revealed phase separation for both the mixtures of Captopril/PLGA and HCT/PLGA. Also PCA was proved a powerful technique to reveal the location of pluronic which was not able to be observed using algorithms from the NGLabspec.

It was found that pluronics increase the dissolution rate of the HCT significantly. Finally, the mechanism of the release of the drug from the polymeric matrix was investigated by applying the four most common mathematical models which can better, whereas in the case of Captopril there is a Fickian drug release as the describe the drug release from monolithic polymeric matrixes. It was found that in the case of

HCT/PLGA = 30/70 the Higuchi release kinetic described the system Korsmeyer – Peppas showed and HCT/PLGA = 20/80 a non fickian drug release is happening.

7. Conclusions – Future work

This aim of the thesis was to prove inkjet printing can be used to produce drug formulation product. In order to confirm this, solid dispersion formulations and controlled release drug formulation were attempted to be produced. Hence, in chapter 3, APIs with excipients were successfully printed and characterized. Single droplet and multiple droplets of mixtures of felodipine and PVP, captopril with PLGA and hydrochlorothiazide with PVP and PLGA were sprayed onto hydrophobic substrates. The characterization of felodipine/PVP and HCT/PVP mixtures showed that an intimate mixture of the components. However, when PLGA was used both captopril and HCT were phase separated with the polymer.

In chapter 4, the release of felodipine from a single spot was investigated. By using the intensity of the characteristics Raman bands of felodipine and PVP, it was shown, that the release of the API is directly dependent on the felodipine's concentration in the mixture where when felodipine is in its lowest concentration is dissolved completely. However, more investigation needs to be done regarding the effect of the concentration of the solute in the release of the API. It has been found that by using less concentrated solutions, the API releases quicker which may be either due to the increase of surface area. Also for the same reason, the use of a hydrophilic surface must be investigated.

In chapter 5, a proper therapeutic dosage form of felodipine was attempted. For this purpose microarrays of felodipine/PVP mixtures were produced and characterised. Although each individual spot gave similar AFM, SThM and Raman results, the drug was not be able to be released in blank FASSIF solution. In contrast, the dissolution test in the FASSIF solution with enzyme results to an immediate release of the API.

In chapter 6, the application of inkjet printing was attempted to get extended by producing a therapy composed of two APIs; captopril and hydrochlorothiazide. As captopril and HCT is freely soluble to the dissolution medium, PLGA was used to control the release of the API. When the solution was deposited by pipette, the API was released from the formulation in a controlled manner. Yet the deposition of solution by the microarray printer results to an immediate release of the API which can be due to the total increase of surface area as the spots produced by the microarray printer are much smaller.

Even though, this work showed that inkjet printing is a promising drug formulation method, there still lot of room for development in this area. First of all, an appropriate substrate to print for the deposition of the solution is fundamental to apply. This substrate must be biocompatible which could protect the drug from the environment allowing it to release in the desired area. Such substrate can be a tablet into which the solution will be ejected. Also the porosity of the substrate is of fundamental importance. A porous material would allow the solute to be absorbed modifying the release of the API or it would be possible that the solvent would not be able to evaporate completely.

Also apart from using a polymer matrix, another approach which could be apply to control the release of the API is to coat it with a polymer which would also could protect it to release in undesirable areas, by using two different solutions a microarray printer could print the solution containing the API at first and subsequently the solutions containing the coating material.

To summarise all the above, it can be concluded that inkjet printing due to its high flexibility to produce drugs with tailored properties can gain the interest of pharmaceutical industries. The proper technology exists and it is continuously developed to handle solutions difficult to be printed, such as viscous solutions. Hewlett Packard (HP) has already patented an inkjet device which could produce drug formulation [221]. Moreover, recently, Crospon has licensed a 'smart' drug delivery skin patch technology from HP Labs that uses inkjet printing technology to deliver drugs under the skin [222]. These two facts may be the evidence that the commercial availability of a device which produces real tailored medicine is not far away.

Appendix I

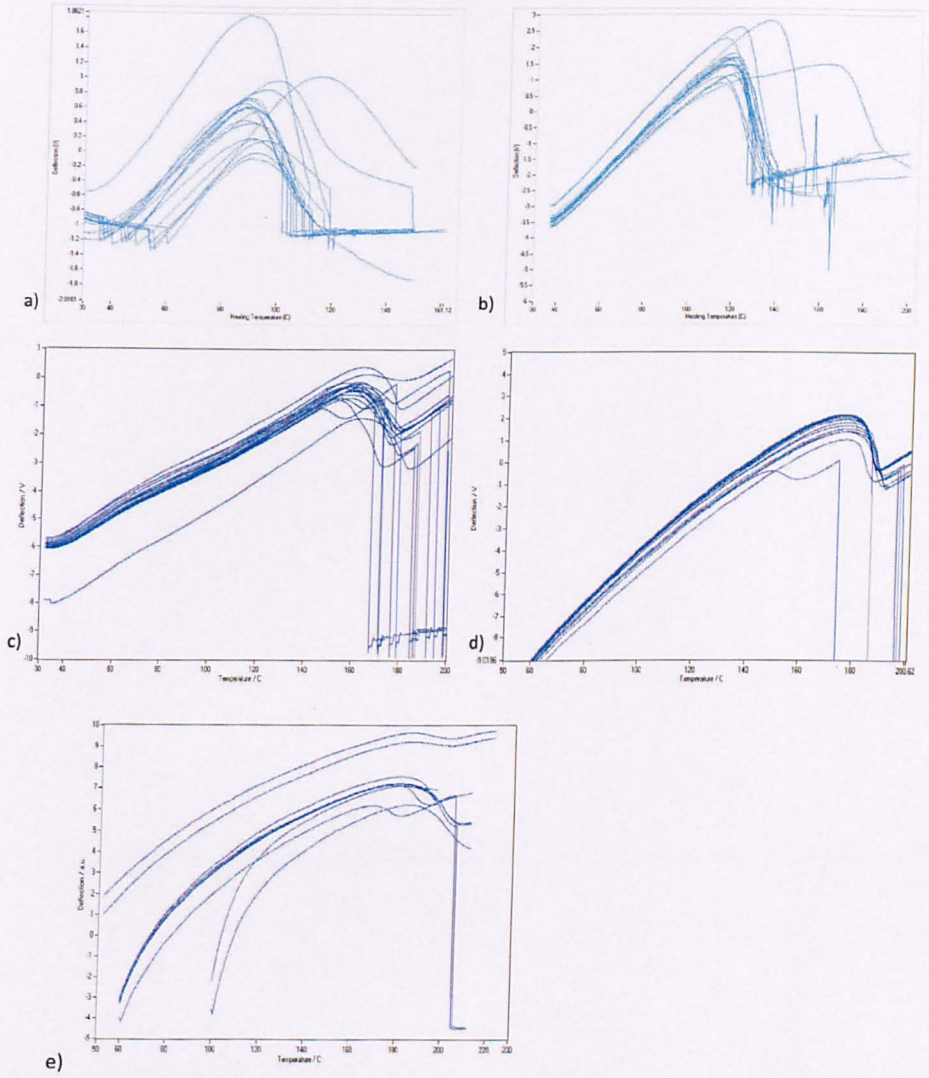

Figure 0.1: NTA graphs of felodipine/PVP ratios of a) 2/1, b) 1/1, c) 1/2, d)1/5, e) 1/10.

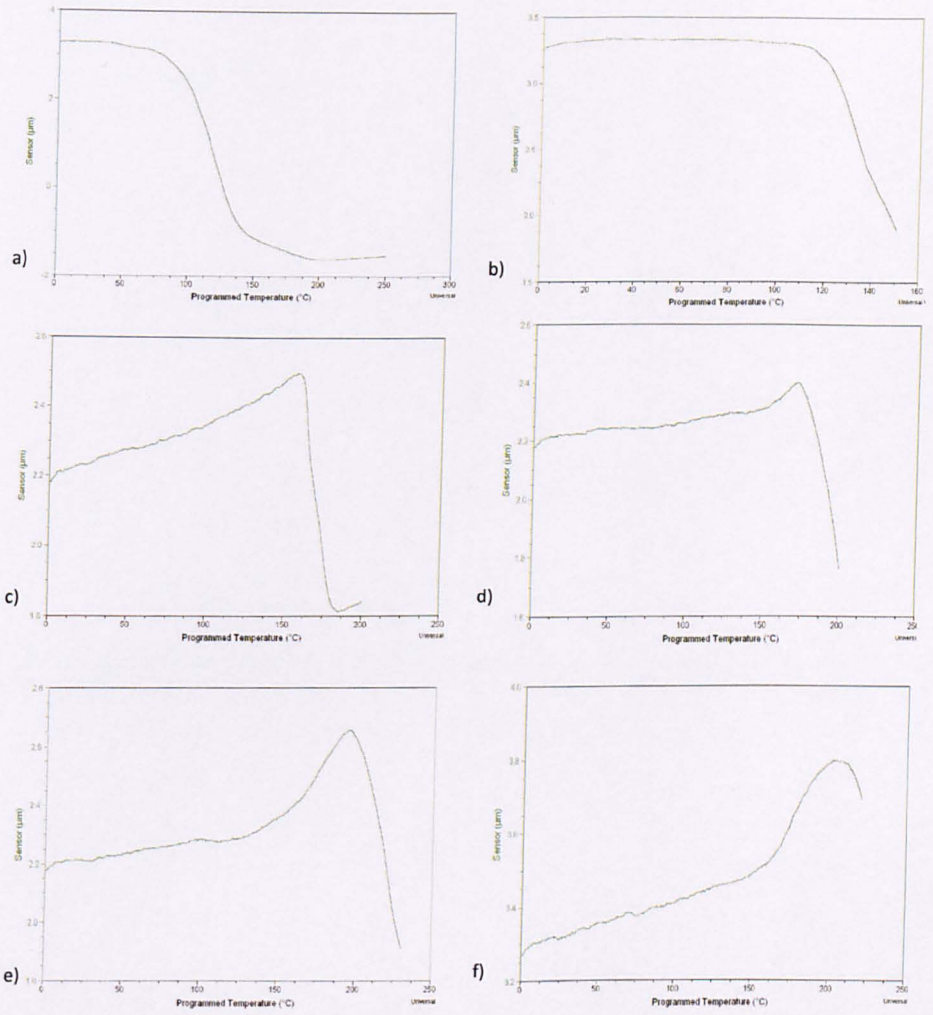

Figure 0.2: SThM graphs of felodipine/PVP ratios of a) 2/1, b) 1/1, c) 1/2, d)1/5, e) 1/10, f) sprayed PVP.

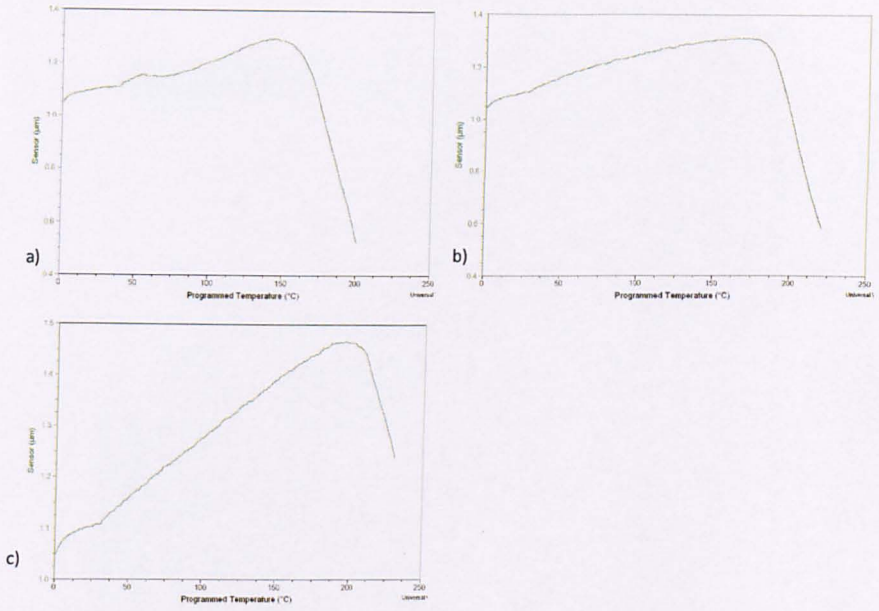

Figure 0.3: SThM graphs of felodipine/PVP mixture produced by the microarray printer of ratio of a) 1/2, b)1/5, c) 1/10.

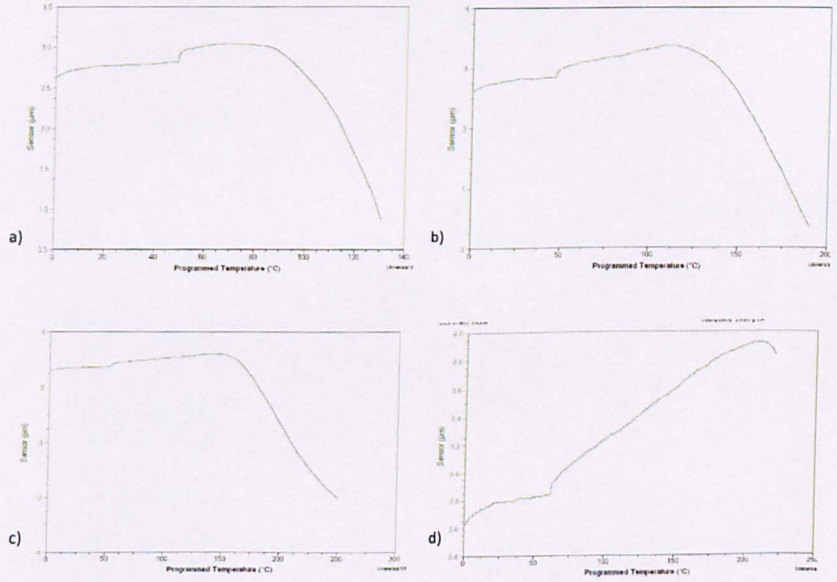

Figure 0.4: SThM graphs of HCT/PVP of ratios a) 2/1, b) 1/1, c) 1/2, d)1/5.

Appendix II

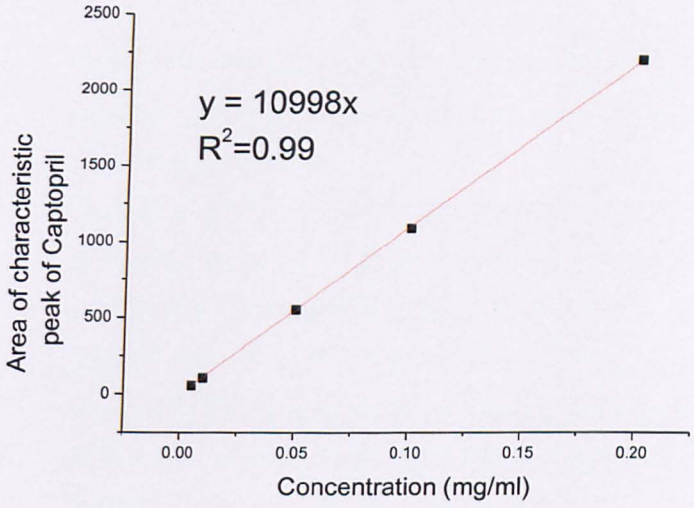

Figure 5: Callibration curve of Captopril for the HPLC dissolution experiments.

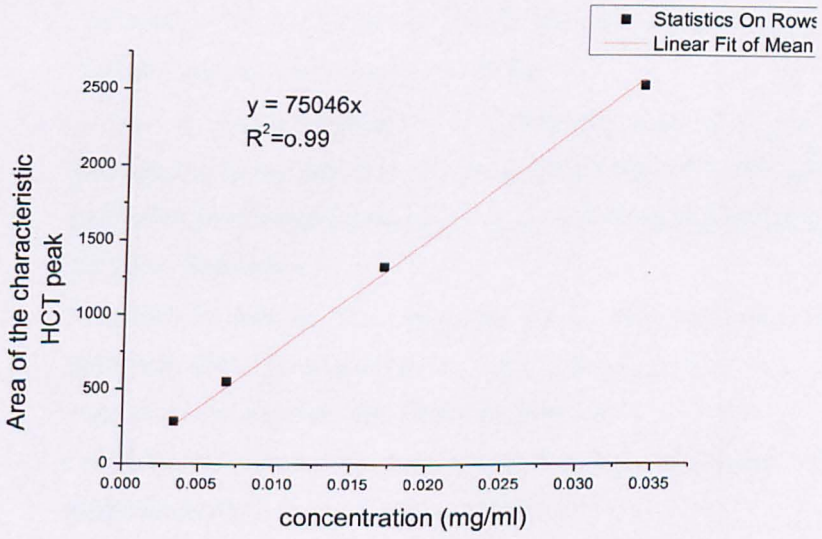

Figure6: Callibration curve of HCT for the HPLC dissolution experiments.

References

1. Sastry S.V., Nyshadham J.R., and Fix J.A., *Recent technological advances in oral drug delivery - a review.* Pharmaceutical Science & Technology Today, 2000. **3**(4): p. 138-145.
2. Jivra, M., Martini L.G., and Thomson C.M., *An overview of the different excipients useful for the direct compression of tablets.* Pharmaceutical Science & Technology Today, 2000. **3**(2): p. 58-63.
3. Jayesh P. and Rane M., *Tablet Formulation Design And Manufacture: Oral Immediate Release Application.* **Pharma Times**, 2009. **41**(4): p. 21 - 29.
4. Gibson M., *PHARMACEUTICAL PREFORMULATION AND FORMULATION: A Practical Guide from Candidate Drug Selection to Commercial Dosage Form.* 2004: CRC Press.
5. Zhang G.G.Z., et al., *Phase transformation considerations during process development and manufacture of solid oral dosage forms.* Advanced Drug Delivery Reviews, 2004. **56**(3): p. 371-390.
6. Li W., et al., *Determination of polymorph conversion of an active pharmaceutical ingredient in wet granulation using NIR calibration models generated from the premix blends.* Journal of Pharmaceutical Sciences, 2005. **94**(12): p. 2800-2806.
7. Wikström H., Marsac P.J., and Taylor L.S., *In-line monitoring of hydrate formation during wet granulation using Raman spectroscopy.* Journal of Pharmaceutical Sciences, 2005. **94**(1): p. 209-219.
8. Armstrong N.A., *Direct compression characteristics of granulated Lactitol.* pharmaceutical Technology, 1998. **22**: p. 84-92.
9. Cooley P.W., Wallace D.B., and Antohe B.V. *Applications of ink-jet printing technology to BioMEMS and microfluidic systems.* in *SPIE Concference on Microfluidics and BioMEMS.* 2001: Mastrangelo, Carlos, H. Becker, Holger

10. Lemmo A.V., Rose D.J., and Tisone T.C., *Inkjet dispensing technology: applications in drug discovery.* Current Opinion in Biotechnology, 1998. **9**(6): p. 615-617.

11. Rose D., *Microdispensing technologies in drug discovery.* Drug Discovery Today, 1999. **4**(9): p. 411-419.

12. Bauer J., et al., *Ritonavir: An Extraordinary Example of Conformational Polymorphism.* Pharmaceutical Research, 2001. **18**(6): p. 859-866.

13. Price R., et al., *The influence of relative humidity on particulate interactions in carrier-based dry powder inhaler formulations.* International Journal of Pharmaceutics, 2002. **246**(1-2): p. 47-59.

14. Surana R., et al., *Determination of Glass Transition Temperature and in Situ Study of the Plasticizing Effect of Water by Inverse Gas Chromatography.* Pharmaceutical Research, 2003. **20**(10): p. 1647-1654.

15. Taylor L.S. and Zografi G., *Sugar-polymer hydrogen bond interactions in lyophilized amorphous mixtures.* Journal of Pharmaceutical Sciences, 1998. **87**(12): p. 1615-1621.

16. Sumie Y. and Stella V.J., *Stability of Drugs and Dosage Forms.* 2002, Kluwer Academic Publishers. p. 263.

17. Desai D.S., et al., *Povidone- and poloxamer-mediated degradation of hydrochlorothiazide in an antihypertensive combination tablet product.* International Journal of Pharmaceutics, 1996. **142**(1): p. 61-66.

18. Tønnesen H.H., *Formulation and stability testing of photolabile drugs.* International Journal of Pharmaceutics, 2001. **225**(1-2): p. 1-14.

19. Ipatova O.M., et al., *Bioavailability of oral drugs and the methods for its improvement.* Biochemistry (Moscow) Supplement Series B: Biomedical Chemistry, 2010. **4**(1): p. 82-94.

20. Leuner C. and Dressman J., *Improving drug solubility for oral delivery using solid dispersions.* European Journal of Pharmaceutics and Biopharmaceutics, 2000. **50**(1): p. 47-60.

21. Grau M.J., Kayser O., and Müller R.H., *Nanosuspensions of poorly soluble drugs -- reproducibility of small scale production.* International Journal of Pharmaceutics, 2000. **196**(2): p. 155-159.

22. Bruno C. Hancock, G.Z., *Characteristics and significance of the amorphous state in pharmaceutical systems.* Journal of Pharmaceutical Sciences, 1997. **86**(1): p. 1-12.

23. Varshosaz J., et al., *Dissolution enhancement of gliclazide using in situ micronization by solvent change method.* Powder Technology, 2008. **187**(3): p. 222-230.

24. Vogt M., Kunath K., and Dressman J.B., *Dissolution enhancement of fenofibrate by micronization, cogrinding and spray-drying: Comparison with commercial preparations.* European Journal of Pharmaceutics and Biopharmaceutics, 2008. **68**(2): p. 283-288.

25. Liversidge G.G. and Cundy K.C., *Particle size reduction for improvement of oral bioavailability of hydrophobic drugs: I. Absolute oral bioavailability of nanocrystalline danazol in beagle dogs.* International Journal of Pharmaceutics, 1995. **125**(1): p. 91-97.

26. Jounela A.J., Pentikäinen P.J., and Sothmann A., *Effect of particle size on the bioavailability of digoxin.* European Journal of Clinical Pharmacology, 1975. **8**(5): p. 365-370.

27. Hörter D. and Dressman J.B., *Influence of physicochemical properties on dissolution of drugs in the gastrointestinal tract.* Advanced Drug Delivery Reviews, 2001. **46**(1-3): p. 75-87.

28. Sekiguchi K. and Obi N., *Studies on absorption of eutectic mixtures. I. Acomparison of the behavior of eutectic mixtures of sulphathiazole and that ofordinary sulphathiazole in man.* Chemical & Pharmaceutical Bulletin, 1961. **9**: p. 866-872.

29. Serajuddin A.T.M., *Solid dispersion of poorly water-soluble drugs: Early promises, subsequent problems, and recent breakthroughs.* Journal of Pharmaceutical Sciences, 1999. **88**(10): p. 1058-1066.

30. Yamashita K., et al., *Establishment of new preparation method for solid dispersion formulation of tacrolimus.* International Journal of Pharmaceutics, 2003. **267**(1-2): p. 79-91.

31. Papageorgiou, G., et al., *Effect of physical state and particle size distribution on dissolution enhancement of nimodipine/PEG solid dispersions prepared by*

melt mixing and solvent evaporation. The AAPS Journal, 2006. **8**(4): p. E623-E631.

32. Bhole P.G. and Patil V.R., *Enhancement of water solubility of felodipine by preparing solid dispersion using poly-ethylene glycol 6000 and poly-vinyl alcohol.* Asian Journal of Pharmaceutics, 2009. **3**(3): p. 240-244.

33. Ozeki T., Yuasa H., and Kanaya Y., *Application of the solid dispersion method to the controlled release of medicine. IX. Difference in the release of flurbiprofen from solid dispersions with poly(ethylene oxide) and hydroxypropylcellulose and the interaction between medicine and polymers.* International Journal of Pharmaceutics, 1997. **155**(2): p. 209-217.

34. Hajime K. and Taylor L.S., *Influence of different polymers on the crystallization tendency of molecularly dispersed amorphous felodipine.* Journal of Pharmaceutical Sciences, 2006. **95**(12): p. 2692-2705.

35. Khougaz K. and Clas S.-D., *Crystallization inhibition in solid dispersions of MK-0591 and poly(vinylpyrrolidone) polymers.* JOURNAL OF PHARMACEUTICAL SCIENCES, 2000. **89**(10): p. 1325-1334.

36. Rumondor A., Stanford L., and Taylor L., *Effects of Polymer Type and Storage Relative Humidity on the Kinetics of Felodipine Crystallization from Amorphous Solid Dispersions.* Pharmaceutical Research, 2009. **26**(12): p. 2599-2606.

37. Matsumoto T. and Zografi G., *Physical Properties of Solid Molecular Dispersions of Indomethacin with Poly(vinylpyrrolidone) and Poly(vinylpyrrolidone-co-vinyl-acetate) in Relation to Indomethacin Crystallization.* Pharmaceutical Research, 1999. **16**(11): p. 1722-1728.

38. Van den Mooter G., et al., *Physical stabilisation of amorphous ketoconazole in solid dispersions with polyvinylpyrrolidone K25.* European Journal of Pharmaceutical Sciences, 2001. **12**(3): p. 261-269.

39. Rumondor A.C.F., et al., *Phase Behavior of Poly(vinylpyrrolidone) Containing Amorphous Solid Dispersions in the Presence of Moisture.* Molecular Pharmaceutics, 2009. **6**(5): p. 1492-1505.

40. Damian F., et al., *Physical stability of solid dispersions of the antiviral agent UC-781 with PEG 6000, Gelucire® 44/14 and PVP K30.* International Journal of Pharmaceutics, 2002. **244**(1-2): p. 87-98.

41. Saers E.S., Nyström C., and Aldén M., *Physicochemical aspects of drug release. XVI. The effect of storage on drug dissolution from solid dispersions and the influence of cooling rate and incorporation of surfactant.* International Journal of Pharmaceutics, 1993. **90**(2): p. 105-118.

42. Hassan M.A., et al., *Characterization of famotidine polymorphic forms.* International Journal of Pharmaceutics, 1997. **149**(2): p. 227-232.

43. Siepmann J. and Siepmann F., *Mathematical modeling of drug delivery.* International Journal of Pharmaceutics, 2008. **364**(2): p. 328-343.

44. Costa P. and Sousa Lobo J.M., *Modeling and comparison of dissolution profiles.* European Journal of Pharmaceutical Sciences, 2001. **13**(2): p. 123-133.

45. Colombo P., *Swelling-controlled release in hydrogel matrices for oral route.* Advanced Drug Delivery Reviews, 1993. **11**(1-2): p. 37-57.

46. Hamidi M., Azadi A., and Rafiei P., *Hydrogel nanoparticles in drug delivery.* Advanced Drug Delivery Reviews, 2008. **60**(15): p. 1638-1649.

47. Varelas C.G., Dixon D.G., and Steiner C.A., *Zero-order release from biphasic polymer hydrogels.* Journal of Controlled Release, 1995. **34**(3): p. 185-192.

48. Siepmann J. and Göpferich A., *Mathematical modeling of bioerodible, polymeric drug delivery systems.* Advanced Drug Delivery Reviews, 2001. **48**(2-3): p. 229-247.

49. Uhrich K.E., et al., *Polymeric Systems for Controlled Drug Release.* Chemical Reviews, 1999. **99**(11): p. 3181-3198.

50. Verma R.K., Krishna D.M., and Garg S., *Formulation aspects in the development of osmotically controlled oral drug delivery systems.* Journal of Controlled Release, 2002. **79**(1-3): p. 7-27.

51. Santus G. and Baker R.W., *Osmotic drug delivery: a review of the patent literature.* Journal of Controlled Release, 1995. **35**(1): p. 1-21.

52. Lecomte F., et al., *Blends of enteric and GIT-insoluble polymers used for film coating: physicochemical characterization and drug release patterns.* Journal of Controlled Release, 2003. **89**(3): p. 457-471.

53. Fekete R., et al., *Structural Characteristics and Permeability of Ethyl Cellulose Films Containing Different Plasticizers.* Macromolecular Symposia, 2006. **239**(1): p. 105-113.

54. Chan, L.W., Ong K.T., and Heng P.W.S., *Novel Film Modifiers to Alter the Physical Properties of Composite Ethylcellulose Films.* Pharmaceutical Research, 2005. **22**(3): p. 476-489.

55. Hjärtstam J. and Hjertberg T., *Swelling of pellets coated with a composite film containing ethyl cellulose and hydroxypropyl methylcellulose.* International Journal of Pharmaceutics, 1998. **161**(1): p. 23-28.

56. Frohoff-Hülsmann M.A., Schmitz A., and Lippold B.C., *Aqueous ethyl cellulose dispersions containing plasticizers of different water solubility and hydroxypropyl methylcellulose as coating material for diffusion pellets: I. Drug release rates from coated pellets.* International Journal of Pharmaceutics, 1999. **177**(1): p. 69-82.

57. Damgé C., Maincent P., and Ubrich N., *Oral delivery of insulin associated to polymeric nanoparticles in diabetic rats.* Journal of Controlled Release, 2007. **117**(2): p. 163-170.

58. Mohanraj VJ and Chen Y., *Nanoparticles – A Review* Tropical Journal of Pharmaceutical Research, 2006. **5**(1): p. 561-573.

59. Cooley P.W., Wallace D.B., and Antohe B.V. *Applications of ink-jet printing technology to BioMEMS and microfluidic systems.* in *SPIE Concference on Microfluidics and BioMEMS.* 2001: Microfluidics and BioMEMS, Carlos H. Mastrangelo; Holger Becker; Eds.

60. Gans B.-J.d., et al., *Ink-jet Printing Polymers and Polymer Libraries Using Micropipettes.* Macromolecular Rapid Communications, 2004. **25**(1): p. 292-296.

61. Sanaur S., et al., *Jet-printed electrodes and semiconducting oligomers for elaboration of organic thin-film transistors.* Organic Electronics, 2006. **7**(5): p. 423-427.

62. Levi B.G., *New Printing Technologies Raise Hopes for Cheap Plastic Electronics* physics today, 2001. **54**(2): p. 20-22.

63. Martin G.D. and et al., *Inkjet printing - the physics of manipulating liquid jets and drops.* Journal of Physics: Conference Series, 2008. **105**(1): p. 012001.

64. Hue P. Le, *Progress and Trends in Ink-jet Printing Technology.* Journal of Imaging Science and Technology, 1998. **42**(1): p. 49-62.

65. Brunahl, J. and Grishin A.M., *Piezoelectric shear mode drop-on-demand inkjet actuator.* Sensors and Actuators A: Physical, 2002. **101**(3): p. 371-382.

66. Jan de Gans B., Duineveld C., P , and Schubert S., *Inkjet Printing of Polymers: State of the Art and Future Developments.* Advanced Materials, 2004. **16**(3): p. 203-213.

67. Rahman K., et al., *Simulation of droplet generation through electrostatic forces.* Journal of Mechanical Science and Technology, 2010. **24**(1): p. 307-310.

68. Ellson R.N. *NANOLITER AND PICOLITER LIQUID HANDLING FOR LIFE SCIENCE APPLICATIONS* in *Nanotech and Biotech Convergence Conference* 2003.

69. Schiaffino S. and Sonin A.A., *Molten droplet deposition and solidification at low Weber numbers.* Physics of Fluids, 1997. **9**(11): p. 3172-3187.

70. Jang D., Kim D., and Moon J., *Influence of Fluid Physical Properties on Ink-Jet Printability.* Langmuir, 2009. **25**(5): p. 2629-2635.

71. Yang A.S., Cheng C.H., and Lin C.T., *Investigation of Droplet-Ejection Characteristics for a Piezoelectric Inkjet Printhead.* Proceedings of the Institution of Mechanical Engineers, Part C: Journal of Mechanical Engineering Science, 2006. **220**(4): p. 435-445.

72. Reis N., Ainsley C., and Derby B., *Ink-jet delivery of particle suspensions by piezoelectric droplet ejectors.* Journal of Applied Physics, 2005. **97**(9): p. 6.

73. Okamoto T., Suzuki T., and N. Y., *Microarray fabrication with covalent attachment of DNA using Bubble Jet technology.* Nature Biotechnology, 2000. **18**: p. 438-441.

74. Gbureck U., et al., *Direct Printing of Bioceramic Implants with Spatially Localized Angiogenic Factors.* Advanced Materials, 2007. **19**(6): p. 795-800.

75. Tarcha P., et al., *The Application of Ink-Jet Technology for the Coating and Loading of Drug-Eluting Stents.* Annals of Biomedical Engineering, 2007. **35**(10): p. 1791-1799.

76. Peter A. Melundez, et al., *Thermal inkjet application in the preparation of oral dosage forms: Dispensing of prednisolone solutions and polymorphic characterization by solid-state spectroscopic techniques.* Journal of Pharmaceutical Sciences, 2007. **9999**(9999): p. n/a.

77. Stephan Hauschild, et al., *Direct Preparation and Loading of Lipid and Polymer Vesicles Using Inkjets.* Small, 2005. **1**(12): p. 1177-1180.

78. RadulescuD., Schade N., and Wawro D. *Uniform Paclitaxel-Loaded Biodegradable Microspheres Manufactured by Ink-Jet Technology.* in *Proc., Recent A dv. in Drug Delivery Sys.* March 2003.

79. Xie J., et al., *Encapsulation of protein drugs in biodegradable microparticles by co-axial electrospray.* Journal of Colloid and Interface Science, 2008. **317**(2): p. 469-476.

80. Chan K.L.A. and Kazarian S.G., *Fourier Transform Infrared Imaging for High-Throughput Analysis of Pharmaceutical Formulations.* Journal of Combinatorial Chemistry, 2005. **7**(2): p. 185-189.

81. Wu B.M., et al., *Solid free-form fabrication of drug delivery devices.* Journal of Controlled Release, 1996. **40**(1-2): p. 77-87.

82. Sachs E., et al., *Three dimensional printing. Rapid Tooling and prototypes directly from a CAD model.* Journal of engineering for industry, 1992. **114**(4): p. 481-488.

83. biodot, *Manual of sciFLEXARRAYER S5 & S11*, biodot, Editor.

84. Lal R. and John S.A., *Biological applications of atomic force microscopy.* Am J Physiol Cell Physiol, 1994. **266**(1): p. C1-21.

85. Geisse N.A., *AFM and combined optical techniques.* Materials Today. **12**(7-8): p. 40-45.

86. Jalili, N. and Laxminarayana K., *A review of atomic force microscopy imaging systems: application to molecular metrology and biological sciences.* Mechatronics, 2004. **14**(8): p. 907-945.

87. Overney R.M, et al., *friction measurements on phase-separated thin films with a modified atomic force microscopé.* nature, 1992. **359**: p. 133 - 135.

88. Galuska A.A., Poulter R.R., and McElrath K.O., *Force Modulation AFM of Elastomer Blends: Morphology, Fillers and Cross-linking.* Surface and Interface Analysis, 1997. **25**(6): p. 418-429.

89. Yamanaka K. and Nakano S., *Quantitative elasticity evaluation by contact resonance in an atomic force microscope.* Applied Physics A: Materials Science & Processing, 1998. **66**(0): p. S313-S317.

90. Magonov S.N., Elings V., and Whangbo M.H., *Phase imaging and stiffness in tapping-mode atomic force microscopy.* Surface Science, 1997. **375**(2-3): p. L385-L391.

91. Sitterberg J., et al., *Utilising atomic force microscopy for the characterisation of nanoscale drug delivery systems.* European Journal of Pharmaceutics and Biopharmaceutics, 2010. **74**(1): p. 2-13.

92. Danesh A., et al., *The Discrimination of Drug Polymorphic Forms from Single Crystals Using Atomic Force Microscopy.* Pharmaceutical Research, 2000. **17**(7): p. 887-890.

93. Shen E., et al., *Microphase separation in bioerodible copolymers for drug delivery.* Biomaterials, 2001. **22**(3): p. 201-210.

94. Begat P., et al., *The effect of mechanical processing on surface stability of pharmaceutical powders: Visualization by atomic force microscopy.* Journal of Pharmaceutical Sciences, 2003. **92**(3): p. 611-620.

95. Mu L. and Feng S.S., *A novel controlled release formulation for the anticancer drug paclitaxel (Taxol®): PLGA nanoparticles containing vitamin E TPGS.* Journal of Controlled Release, 2003. **86**(1): p. 33-48.

96. Sant S., Nadeau V., and Hildgen P., *Effect of porosity on the release kinetics of propafenone-loaded PEG-g-PLA nanoparticles.* Journal of Controlled Release, 2005. **107**(2): p. 203-214.

97. Berg M.C., et al., *Controlled Drug Release from Porous Polyelectrolyte Multilayers.* Biomacromolecules, 2005. **7**(1): p. 357-364.

98. Davies M., et al., *Characterization of Drug Particle Surface Energetics and Young's Modulus by Atomic Force Microscopy and Inverse Gas Chromatography.* Pharmaceutical Research, 2005. **22**(7): p. 1158-1166.

99. Traini D., et al., *The Use of AFM and Surface Energy Measurements to Investigate Drug-Canister Material Interactions in a Model Pressurized Metered Dose Inhaler Formulation.* Aerosol Science and Technology, 2006. **40**(4): p. 227 - 236.

100. Fischer H., *Thermal Probe Surface Treatment of a Bulk Polymer: Does a Surface Layer with a Lower Glass Transition Than the Bulk Exist?* Macromolecules, 2002. **35**(9): p. 3592-3595.

101. Price D.M., et al., *Micro-thermal analysis: scanning thermal microscopy and localised thermal analysis.* International Journal of Pharmaceutics, 1999. **192**(1): p. 85-96.

102. Sanders G.H.W., et al., *Discrimination of polymorphic forms of a drug product by localized thermal analysis.* Journal of Microscopy, 2000. **198**(2): p. 77-81.

103. Royall P.G., Craig D.Q.M., and Grandy D.B., *The use of micro-thermal analysis as a means of in situ characterisation of a pharmaceutical tablet coat.* Thermochimica Acta, 2001. **380**(2): p. 165-173.

104. Zhang J., et al., *Nanoscale thermal analysis of pharmaceutical solid dispersions.* International Journal of Pharmaceutics, 2009. **380**(1-2): p. 170-173.

105. Six K., et al., *Identification of Phase Separation in Solid Dispersions of Itraconazole and Eudragit® E100 Using Microthermal Analysis.* Pharmaceutical Research, 2003. **20**(1): p. 135-138.

106. Intruments, A., *ThermaLever™ Probes: Probes for sub-100nm Localized Thermal Analysis*, in *Data sheet*, A. Instruments, Editor.

107. John C. Lindon, George E. Tranter, and Holmes J.L., *Encyclopedia of Spectroscopy and Spectrometry.* Vol. 1. 2000: Academic Press. 2581.

108. Zhang L., Henson M.J., and Sekulic S.S., *Multivariate data analysis for Raman imaging of a model pharmaceutical tablet.* Analytica Chimica Acta, 2005. **545**(2): p. 262-278.

109. Widjaja E. and Seah R.K.H., *Application of Raman microscopy and band-target entropy minimization to identify minor components in model pharmaceutical tablets.* Journal of Pharmaceutical and Biomedical Analysis, 2008. **46**(2): p. 274-281.

110. Wang J.H., et al., *Application of modified alternating least squares regression to spectroscopic image analysis.* Analytica Chimica Acta, 2003. **476**(1): p. 93-109.

111. Sasic´ S.et al., *Raman line mapping as a fast method for analyzing pharmaceutical bead formulations.* Analyst, 2005. **2005**: p. 1530-1536.

112. Sasic S., et al., *A comparison of Raman chemical images produced by univariate and multivariate data processing-a simulation with an example from pharmaceutical practice.* Analyst, 2004. **129**(11): p. 1001-1007.

113. Šašić S., *Raman Mapping of Low-Content API Pharmaceutical Formulations. I. Mapping of Alprazolam in Alprazolam/Xanax Tablets.* Pharmaceutical Research, 2007. **24**(1): p. 58-65.

114. Clark D., Scaronascaroni S., and cacute, *Chemical images: Technical approaches and issues.* Cytometry Part A, 2006. **69A**(8): p. 815-824.

115. Breitenbach J., Schrof W., and Neumann J., *Confocal Raman-Spectroscopy: Analytical Approach to Solid Dispersions and Mapping of Drugs.* Pharmaceutical Research, 1999. **16**(7): p. 1109-1113.

116. Sasic S. and Clark D.A., *Defining a Strategy for Chemical Imaging of Industrial Pharmaceutical Samples on Raman Line-Mapping and Global Illumination Instruments.* Appl. Spectrosc., 2006. **60**(5): p. 494-502.

117. Lewis E. Neil, Schoppelrei J., and Le E., *Near-infrared Chemical Imaging and the PAT Initiative* in *The role of spectroscopy in process analytical technologies*. 2005, Spectroscopy. p. 28 - 34.

118. Batonneau Y., et al., *Polarization Effects of Confocal Raman Microspectrometry of Crystal Powders Using Interactive Self-Modeling Analysis.* The Journal of Physical Chemistry B, 2003. **107**(7): p. 1502-1513.

119. Gendrin C., Roggo Y., and Collet C., *Pharmaceutical applications of vibrational chemical imaging and chemometrics: A review.* Journal of Pharmaceutical and Biomedical Analysis, 2008. **48**(3): p. 533-553.

120. Teberekidis V.I. and Sigalas M.P., *Theoretical study of hydrogen bond interactions of felodipine with polyvinylpyrrolidone and polyethyleneglycol.* Journal of Molecular Structure: THEOCHEM, 2007. **803**(1-3): p. 29-38.

121. Marsac P., Konno H., and Taylor L., *A Comparison of the Physical Stability of Amorphous Felodipine and Nifedipine Systems.* Pharmaceutical Research, 2006. **23**(10): p. 2306-2316.

122. Marsac J. P., Shamblin L. S., and L. T.S., *Theoretical and Practical Approaches for Prediction of Drug–Polymer Miscibility and Solubility.* Pharmaceutical Research, 2006. **23**(16): p. 2417-2426.

123. Konno H. and Taylor L., *Ability of Different Polymers to Inhibit the Crystallization of Amorphous Felodipine in the Presence of Moisture.* Pharmaceutical Research, 2008. **25**(4): p. 969-978.

124. Konno H., et al., *Effect of polymer type on the dissolution profile of amorphous solid dispersions containing felodipine.* European Journal of Pharmaceutics and Biopharmaceutics, 2008. **70**(2): p. 493-499.

125. Kim E.J., et al., *Preparation of a solid dispersion of felodipine using a solvent wetting method.* European Journal of Pharmaceutics and Biopharmaceutics, 2006. **64**(2): p. 200-205.

126. Karavas E., et al., *Effect of hydrogen bonding interactions on the release mechanism of felodipine from nanodispersions with polyvinylpyrrolidone.* European Journal of Pharmaceutics and Biopharmaceutics, 2006. **63**(2): p. 103-114.

127. Karavas E., et al., *Miscibility Behavior and Formation Mechanism of Stabilized Felodipine-Polyvinylpyrrolidone Amorphous Solid Dispersions.* Drug Development & Industrial Pharmacy, 2005. **31**(6): p. 473-489.

128. Karavas E., et al., *Combining SEM, TEM, and micro-Raman techniques to differentiate between the amorphous molecular level dispersions and nanodispersions of a poorly water-soluble drug within a polymer matrix.* International Journal of Pharmaceutics, 2007. **340**(1-2): p. 76-83.

129. Karavas E., Georgarakis E., and Bikiaris D., *Felodipine nanodispersions as active core for predictable pulsatile chronotherapeutics using PVP/HPMC blends as coating layer.* International Journal of Pharmaceutics, 2006. **313**(1-2): p. 189-197.

130. A Bossini et al., *Felodipine ER formulation in the treatment of mild hypertension: efficacy and tolerability vs placebo.* Br J Clin Pharmacol, 1990. **30**(4): p. 567-571.

131. E Blychert K.W., B Edgar, K Lidman, *Plasma concentration profiles and antihypertensive effect of conventional and extended-release felodipine tablets.* Br J Clin Pharmacol., 1990. **29**(1): p. 39 - 45.

132. Karavas E., et al., *Investigation of the release mechanism of a sparingly water-soluble drug from solid dispersions in hydrophilic carriers based on physical state of drug, particle size distribution and drug-polymer*

interactions. European Journal of Pharmaceutics and Biopharmaceutics, 2007. **66**(3): p. 334-347.

133. Savolainen M., et al., *Evaluation of polar lipid-hydrophilic polymer microparticles.* International Journal of Pharmaceutics, 2003. **262**(1-2): p. 47-62.

134. Timmins P., Jackson I.M., and Wang Y.-c.J., *Factors affecting captopril stability in aqueous solution.* International Journal of Pharmaceutics, 1982. **11**(4): p. 329-336.

135. Matharu R.S. and Sanghavi N.M., *Novel drug delivery system for captopril.* Drug Development and Industrial Pharmacy, 1992. **18**(14): p. 1567-1574.

136. Seta Y., et al., *Design and preparation of captopril sustained-release dosage forms and their biopharmaceutical properties.* International Journal of Pharmaceutics, 1988. **41**(3): p. 245-254.

137. Abu T. M. Serajudin and Fakes M.G., *Sustained release formulation containing captopril and method,* U.S. patent, Editor. 1995, Bristol - Myers Squibb company.

138. Robert A., Yatinda M. Joshi, and Nemichand B. Jain, *CAPTOPRIL FORMULATION PROVIDING INCREASED DURATION OF ACTIVITY.* 1992, E. R. Squibb & Sons, Inc., Princeton.

139. Ho H.O., Wang H.-Y., and Sheu M.-T., *The evaluation of granulated excipients as matrix material for controlled delivery of captopril.* Journal of Controlled Release, 1997. **49**(2-3): p. 243-251.

140. Vervaet C. and Remon J.P., *Bioavailability of Hydrochlorothiazide from Pellets, Made by Extrusion/ Spheronisation, Containing Polyethylene Glycol 400 as a Dissolution Enhancer.* Pharmaceutical Research, 1997. **14**(11): p. 1644-1646.

141. Corrigan OI, Timoney RF, and MJ. W., *The influence of polyvinylpyrrolidone on the solution and bioavailability of hydrochlorothiazide.* journal of pharmacy and pharmacology, 1976. **28**(9): p. 703 - 706

142. Wood L.A., *Glass transition temperatures of copolymers.* Journal of Polymer Science, 1958. **28**(117): p. 319-330.

143. Tajber L., Corrigan O.I., and Healy A.M., *Physicochemical evaluation of PVP-thiazide diuretic interactions in co-spray-dried composites--analysis of glass*

transition composition relationships. European Journal of Pharmaceutical Sciences, 2005. **24**(5): p. 553-563.

144. Tsukruk V.V., Gorbunov V.V., and Fuchigami N., *Microthermal analysis of polymeric materials.* Thermochimica Acta, 2002. **395**(1-2): p. 151-158.

145. Nelson B.A. and King W.P., *Measuring material softening with nanoscale spatial resolution using heated silicon probes.* Review of Scientific Instruments, 2007. **78**(2): p. 023702.

146. Daniela A. and Grant D.J.W., *Hydrogen Bonding in Sulfonamides.* JOURNAL OF PHARMACEUTICAL SCIENCES, 2001. **90**(12): p. 2058 - 2077.

147. Hu H. and Larson R.G., *Marangoni Effect Reverses Coffee-Ring Depositions.* The Journal of Physical Chemistry B, 2006. **110**(14): p. 7090-7094.

148. Robert D. Deegan, et al., *Contact line deposits in an evaporating drop.* Physical Review E, 2000. **62**(1): p. 756-765.

149. Deegan R.D., et al., *Capillary flow as the cause of ring stains from dried liquid drops.* Nature, 1997. **389**(6653): p. 827-829.

150. de Gans, B.J. and Schubert U.S., *Inkjet Printing of Well-Defined Polymer Dots and Arrays.* Langmuir, 2004. **20**(18): p. 7789-7793.

151. Tekin E., de Gans B.-J., and Schubert U.S., *Ink-jet printing of polymers - from single dots to thin film libraries.* Journal of Materials Chemistry, 2004. **14**(17): p. 2627-2632.

152. Nicolaides E., et al., *Forecasting the In Vivo Performance of Four Low Solubility Drugs from Their In Vitro Dissolution Data.* Pharmaceutical Research, 1999. **16**(12): p. 1876-1882.

153. Thorsett E.D., et al., *Conformationally restricted inhibitors of angiotensin-converting enzyme. Synthesis and computations.* Journal of Medicinal Chemistry, 1986. **29**(2): p. 251-260.

154. Mariappan S.V.S. and Rabenstein D.L., *Kinetics and thermodynamics of cis-trans isomerization of captopril and related compounds.* The Journal of Organic Chemistry, 1992. **57**(24): p. 6675-6678.

155. Rabenstein D.L. and Isab A.A., *Conformational and acid-base equilibriums of captopril in aqueous solution.* Analytical Chemistry, 1982. **54**(3): p. 526-529.

156. Simona C., Simona C. P., and Chis V., *CAPTOPRIL ADSORPTION TO SILVER NANOSTRUCTURES.* ROMANIAN J. BIOPHYS, 2007. **17**(3): p. 195-203.

157. Gupta A., et al., *Development and application of a validated HPLC method for the analysis of dissolution samples of gabapentin drug products.* Journal of Pharmaceutical and Biomedical Analysis, 2008. **46**(1): p. 181-186.

158. Bueno Rolim C.M., et al., *Development and validation of an RP-HPLC method for the dissolution studies of bisoprolol in pharmaceutical dosage forms.* Journal of Liquid Chromatography and Related Technologies, 2005. **28**(3): p. 477-486.

159. Chen X.P., Guo T.X., and Guo Q.D., *A HPLC method for the determination of dissolution of naltrexone hydrochloride tablets.* Chinese Pharmaceutical Journal, 2001. **36**(9): p. 619-620.

160. Tinke A.P., et al., *A new approach in the prediction of the dissolution behavior of suspended particles by means of their particle size distribution.* Journal of Pharmaceutical and Biomedical Analysis, 2005. **39**(5): p. 900-907.

161. Xie J., Jun Chen Tan, and Wang C.-H., *Biodegradable films developed by electrospray deposition for sustained drug delivery.* Journal of Pharmaceutical Sciences, 2007. **97**(8): p. 3109 - 22.

162. McGinity J.and Felton L.A., *Aqueous Polymeric Coatings for Pharmaceutical Dosage Forms*. 3 ed. Vol. 176. 2008: Informa Healthcare USA Inc.

163. Siepmann F., et al., *How to adjust desired drug release patterns from ethylcellulose-coated dosage forms.* Journal of Controlled Release, 2007. **119**(2): p. 182-189.

164. Rowe R.C., *The effect of the molecular weight of ethyl cellulose on the drug release properties of mixed films of ethyl cellulose and hydroxypropylmethylcellulose.* International Journal of Pharmaceutics, 1986. **29**(1): p. 37-41.

165. Mazurek S. and Szostak R., *Quantitative determination of captopril and prednisolone in tablets by FT-Raman spectroscopy.* Journal of Pharmaceutical and Biomedical Analysis, 2006. **40**(5): p. 1225-1230.

166. Ryder A.G., O'Connor G.M., and Glynn T.J., *Quantitative analysis of cocaine in solid mixtures using Raman spectroscopy and chemometric methods.* Journal of Raman Spectroscopy, 2000. **31**(3): p. 221-227.

167. Giles J.H., Gilmore D.A., and Denton M.B., *Quantitative analysis using Raman spectroscopy without spectral standardization.* Journal of Raman Spectroscopy, 1999. **30**(9): p. 767-771.

168. Sato-Berrú R.Y., et al., *Quantitative NIR Raman analysis in liquid mixtures.* Spectrochimica Acta Part A: Molecular and Biomolecular Spectroscopy, 2004. **60**(10): p. 2225-2229.

169. Schweinsberg D.P. and West Y.D., *Quantitative FT Raman analysis of two component systems.* Spectrochimica Acta Part A: Molecular and Biomolecular Spectroscopy, 1997. **53**(1): p. 25-34.

170. Smith E and Dent G., *Modern Raman Spectroscopy – A Practical Approach*, ed. J.W.S. Ltd.

171. Marsac P.J., et al., *Effect of temperature and moisture on the miscibility of amorphous dispersions of felodipine and poly(vinyl pyrrolidone).* Journal of Pharmaceutical Sciences, 2010. **99**(1): p. 169-185.

172. Sethia S. and Squillante E., *Solid dispersion of carbamazepine in PVP K30 by conventional solvent evaporation and supercritical methods.* International Journal of Pharmaceutics, 2004. **272**(1-2): p. 1-10.

173. Shah J., et al., *Enhancement of dissolution rate of valdecoxib by solid dispersions technique with PVP K 30 & PEG 4000: preparation and in vitro evaluation.* Journal of Inclusion Phenomena and Macrocyclic Chemistry, 2009. **63**(1): p. 69-75.

174. Barzegar-Jalali, M., et al., *Cogrinding as an approach to enhance dissolution rate of a poorly water-soluble drug (gliclazide).* Powder Technology, 2010. **197**(3): p. 150-158.

175. Taylor L.S. and Zografi G., *Spectroscopic Characterization of Interactions Between PVP and Indomethacin in Amorphous Molecular Dispersions.* Pharmaceutical Research, 1997. **14**(12): p. 1691-1698.

176. Karavas E., et al., *Effect of hydrogen bonding interactions on the release mechanism of felodipine from nanodispersions with polyvinylpyrrolidone.* European Journal of Pharmaceutical Sciences, 2006. **63**(2): p. 103-114.

177. *Dimethyl Sulfoxide (DMSO) Solubility Data*, in *bulletin*, L.L.C. Gaylord Chemical Company, Editor. 2007.

178. *felodipine* in catalog Sigma - Aldrich.

179. Gommans H.H., et al., *Fibers of aligned single-walled carbon nanotubes: Polarized Raman spectroscopy.* Journal of Applied Physics, 2000. **88**(5): p. 2509-2514.

180. Lagerwall J., et al., *Nanotube Alignment Using Lyotropic Liquid Crystals.* Advanced Materials, 2007. **19**(3): p. 359-364.

181. Huang X., et al., *Cancer Cells Assemble and Align Gold Nanorods Conjugated to Antibodies to Produce Highly Enhanced, Sharp, and Polarized Surface Raman Spectra: A Potential Cancer Diagnostic Marker.* Nano Letters, 2007. **7**(6): p. 1591-1597.

182. Bubert H.and Jenett H., *Surface and Thin Film Analysis: A Compendium of Principles, Instrumentation, and Applications.* 2002.

183. Lourdin D., et al., *Influence of equilibrium relative humidity and plasticizer concentration on the water content and glass transition of starch materials.* Polymer, 1997. **38**(21): p. 5401-5406.

184. Vogt M., Kunath K., and Dressman J.B., *Dissolution improvement of four poorly water soluble drugs by cogrinding with commonly used excipients.* European Journal of Pharmaceutics and Biopharmaceutics, 2008. **68**(2): p. 330-337.

185. Jinno J.i., et al., *Effect of particle size reduction on dissolution and oral absorption of a poorly water-soluble drug, cilostazol, in beagle dogs.* Journal of Controlled Release, 2006. **111**(1-2): p. 56-64.

186. Mosharraf M. and Nyström C., *The effect of particle size and shape on the surface specific dissolution rate of microsized practically insoluble drugs.* International Journal of Pharmaceutics, 1995. **122**(1-2): p. 35-47.

187. Sica, D.A., *Fixed-Dose Combination Antihypertensive Drugs: Do They Have a Role in Rational Therapy?* Drugs, 1994. **48**(1): p. 16-24.

188. Neutel J.M., *The role of combination therapy in the management of hypertension.* Nephrol. Dial. Transplant., 2006. **21**(6): p. 1469-1473.

189. Ambrosioni E., Borghi C., and Costa F.V., *Captopril and hydrochlorothiazide: rationale for their combination.* British journal of clinical pharmacology, 1987. **23**: p. 43-50.

190. WEINBERGER M.H., *Comparison of Captopril AND Hydrochlorothiazide alone and in combination in mild to mederate essential hypertension.* Br J Clin Pharmacol., 1982. **14**: p. 127-131.

191. Hao W., et al., *Collagen I Gel Can Facilitate Homogenous Bone Formation of Adipose-Derived Stem Cells in PLGA-β-TCP Scaffold.* Cells Tissues Organs, 2008. **187**(2): p. 89-102.

192. Hasirci V., et al., *PLGA bone plates reinforced with crosslinked PPF.* Journal of Materials Science: Materials in Medicine, 2002. **13**(2): p. 159-167.

193. Edwards D.A., et al., *Large Porous Particles for Pulmonary Drug Delivery.* Science, 1997. **276**(5320): p. 1868-1872.

194. Kim D.H. and Martin D.C., *Sustained release of dexamethasone from hydrophilic matrices using PLGA nanoparticles for neural drug delivery.* Biomaterials, 2006. **27**(15): p. 3031-3037.

195. Anderson J.M. and Shive M.S., *Biodegradation and biocompatibility of PLA and PLGA microspheres.* Advanced Drug Delivery Reviews, 1997. **28**(1): p. 5-24.

196. Jain R.A., *The manufacturing techniques of various drug loaded biodegradable poly(lactide-co-glycolide) (PLGA) devices.* Biomaterials, 2000. **21**(23): p. 2475-2490.

197. Li J.K., Wang N., and Wu X.S., *A novel biodegradable system based on gelatin nanoparticles and poly(lactic-co-glycolic acid) microspheres for protein and peptide drug delivery.* Journal of Pharmaceutical Sciences, 1997. **86**(8): p. 891-895.

198. Neeraj M., et al., *Biodegradable Polymer Based Particulate Carrier(s) for the Delivery of Proteins and Peptides.* Anti-Inflammatory & Anti-Allergy Agents in Medicinal Chemistry, 2008. **7**: p. 240 - 251.

199. Takeuchi H., Yamamoto H., and Kawashima Y., *Mucoadhesive nanoparticulate systems for peptide drug delivery.* Advanced Drug Delivery Reviews, 2001. **47**(1): p. 39-54.

200. Bivas-Benita M., et al., *PLGA-PEI nanoparticles for gene delivery to pulmonary epithelium.* European Journal of Pharmaceutics and Biopharmaceutics, 2004. **58**(1): p. 1-6.

201. Hans M.L. and Lowman A.M., *Biodegradable nanoparticles for drug delivery and targeting.* Current Opinion in Solid State and Materials Science, 2002. **6**(4): p. 319-327.

202. Reed A.M. and Gilding D.K., *Biodegradable polymers for use in surgery -- poly(glycolic)/poly(lactic acid) homo and copolymers: 2. In vitro degradation.* Polymer, 1981. **22**(4): p. 494-498.

203. Kabanov A.V., Batrakova E.V., and Alakhov V.Y., *Pluronic® block copolymers as novel polymer therapeutics for drug and gene delivery.* Journal of Controlled Release, 2002. **82**(2-3): p. 189-212.

204. Yadav K.S., et al., *Long circulating nanoparticles of etoposide using PLGA-MPEG and PLGA-pluronic block copolymers: characterization, drug-release, blood-clearance, and biodistribution studies.* Drug Development Research, 2010. **71**(4): p. 228-239.

205. Tobío M., et al., *A Novel System Based on a Poloxamer/ PLGA Blend as a Tetanus Toxoid Delivery Vehicle.* Pharmaceutical Research, 1999. **16**(5): p. 682-688.

206. Wang Y., et al., *Pluronic F127 gel effectively controls the burst release of drug from PLGA microspheres.* Pharmazie, 2006. **61**(4): p. 367-368.

207. Siepmann J. and Peppas N.A., *Modeling of drug release from delivery systems based on hydroxypropyl methylcellulose (HPMC).* Advanced Drug Delivery Reviews, 2001. **48**(2-3): p. 139-157.

208. Higuchi T., *Mechanism of sustained-action medication. Theoretical analysis of rate of release of solid drugs dispersed in solid matrices.* Journal of Pharmaceutical Sciences, 1963. **52**(12): p. 1145-1149.

209. Freitas M.N. and Marchetti J.M., *Nimesulide PLA microspheres as a potential sustained release system for the treatment of inflammatory diseases.* International Journal of Pharmaceutics, 2005. **295**(1-2): p. 201-211.

210. Serra L., Doménech J., and Peppas N.A., *Drug transport mechanisms and release kinetics from molecularly designed poly(acrylic acid-g-ethylene glycol) hydrogels.* Biomaterials, 2006. **27**(31): p. 5440-5451.

211. Bravo S.A., M.C. Lamas, and Salomon C.J., *In-vitro studies of diclofenac sodium controlled-release from biopolymeric hydrophilic matrices.* J Pharm Pharmaceut Sci, 2002. **5**(3): p. 213 - 219.

212. Kalia Y.N. and Guy R.H., *Modeling transdermal drug release.* Advanced Drug Delivery Reviews, 2001. **48**(2-3): p. 159-172.

213. Mario G. and Grassi G., *Mathematical Modelling and Controlled Drug Delivery: Matrix Systems.* Current Drug Delivery, 2005. **2**(1): p. 97 - 116.

214. Yan G., et al., *Preparation and Evaluation of a Sustained-Release Formulation of Nifedipine HPMC Tablets.* Drug Development and Industrial Pharmacy, 2000. **26**(6): p. 681-686.

215. Ritger P.L. and Peppas N.A., *A simple equation for description of solute release I. Fickian and non-fickian release from non-swellable devices in the form of slabs, spheres, cylinders or discs.* Journal of Controlled Release, 1987. **5**(1): p. 23-36.

216. Vasita R., et al., *Surface hydrophilization of electrospun PLGA micro-/nano-fibers by blending with Pluronic® F-108.* Polymer, 2010. **51**(16): p. 3706-3714.

217. Ito F., et al., *Control of drug loading efficiency and drug release behavior in preparation of hydrophilic-drug-containing monodisperse PLGA microspheres.* Journal of Materials Science: Materials in Medicine, 2010. **21**(5): p. 1563-1571.

218. Nikkola L., Viitanen P., and Ashammakhi N., *Temporal control of drug release from biodegradable polymer: Multicomponent diclofenac sodium releasing PLGA 80/20 rod.* Journal of Biomedical Materials Research - Part B Applied Biomaterials, 2009. **89**(2): p. 518-526.

219. Tang Z.G., Rhodes N.P., and Hunt J.A., *Control of the domain microstructures of PLGA and PCL binary systems: Importance of morphology in controlled drug release.* Chemical Engineering Research and Design, 2007. **85**(7 A): p. 1044-1050.

220. Joshi G.V., et al., *Montmorillonite intercalated with vitamin B1 as drug carrier.* Applied Clay Science, 2009. **45**(4): p. 248-253.

221. Vitello C.J., et al., *INKJET DISPENSER FOR AUTOMATED DRUG ADMINISTRATION IN A HOSPITAL MANAGEMENT SYSTEM,* in *World Intellectual Property Organisation*, L.P. HEWLETT-PACKARD DEVELOPMENT COMPANY, Editor. 2006.

222. Wilkinson, M. *Crospon to make drug delivery smarter.* 2007; Available from: http://www.in-pharmatechnologist.com/Materials-Formulation/Crospon-to-make-drug-delivery-smarter.